Innovation Center of Molecular Diagnostics,
Beijing University of Chemical Technology

Volume 3 · Issue 1
February 2026

Innovative Medicines & Omics

ISSN: 3060-8910 (Print)
ISSN: 3060-8740 (Online)

ACCSCIENCE PUBLISHING

ACCSCIENCE PUBLISHING

Innovative Medicines & Omics

Print ISSN: 3060-8910
Online ISSN: 3060-8740

Innovative Medicines & Omics (IMO) aims to publish high-quality articles related to the discovery and development of innovative medicines through omics research in the field of human and animal health, for all the major therapeutic areas. The journal includes a variety of omics layers, such as genomics, proteomics, epigenomics metabolomics, lipidomics, peptidomics, metagenomics, microbiome, pharmacogenomics, toxicogenomics, etc., with the focus on disease etiology, prevention, treatment, prognosis and monitoring.

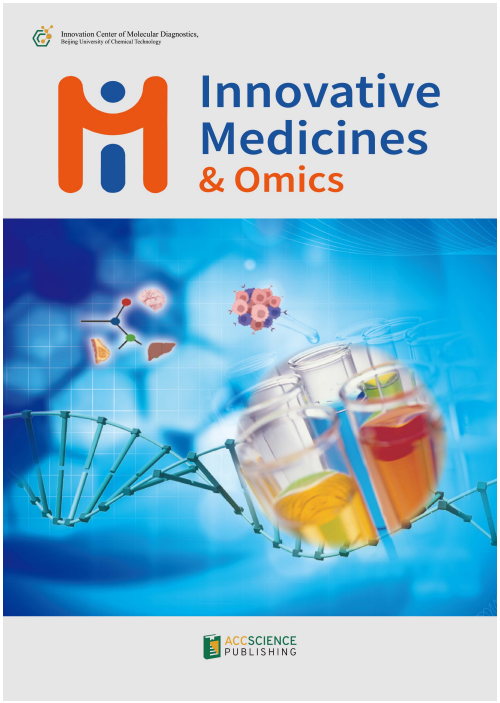

About the Publisher

AccScience Publishing is a publishing company based in Singapore. We publish a range of high-quality, open-access, peer-reviewed journals and books from a broad spectrum of disciplines.

Contact Us

Managing Editor
imo.office@accscience.sg

AccScience Publishing
9 Raffles Place, Republic Plaza 1 #06-00 Singapore 048619.

Volume 3 • Issue 1 • February 2026
ISSN 3060-8910 (print) ISSN 3060-8740 (online)

INNOVATIVE MEDICINES & OMICS

ACCSCIENCE PUBLISHING

Access Science Without Barriers

INNOVATIVE MEDICINES & OMICS

ISSN: 3060-8910 (print)
ISSN: 3060-8740 (online)

Editorial and Production Credits

Publisher: AccScience Publishing
Managing Editor: Ting Li
Production Editor: Sharmila Velapasamy
Article Layout and Typeset: Sinjore Technologies (India)

For all advertising queries, contact imo.office@accscience.sg.

Supplementary file

Supplementary files of articles can be obtained at https://accscience.com/journal/IMO/3/1.

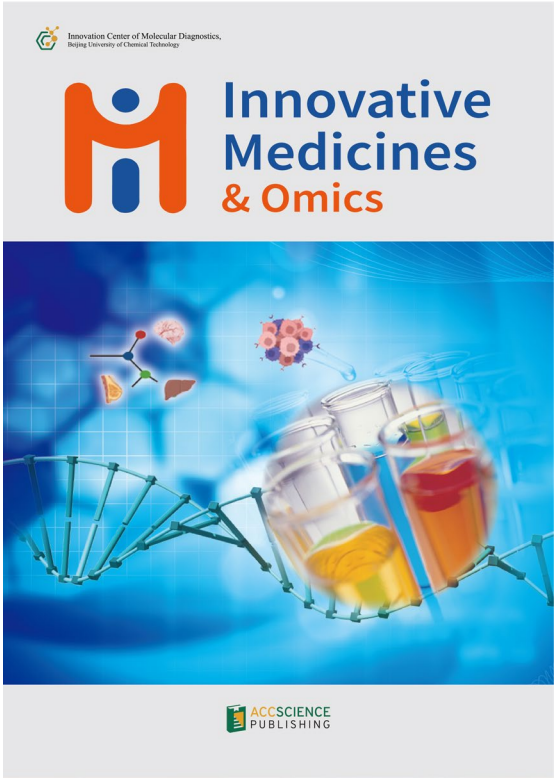

Disclaimer

AccScience Publishing is not liable to the statements, perspectives, and opinions contained in the publications. The appearance of advertisements in the journal shall not be construed as a warranty, endorsement, or approval of the products or services advertised and/or the safety thereof. AccScience Publishing disclaims responsibility for any injury to persons or property resulting from any ideas or products referred to in the publications or advertisements. AccScience Publishing remains neutral with regard to jurisdictional claims in published maps and institutional affiliations.

Innovative Medicines & Omics

Editorial Board

*Editorial Board Members as of February 23, 2026

ACCSCIENCE PUBLISHING

Volume 3 | Issue 1 | February 2026 | Page 1 – 76 |

Innovative Medicines & Omics

https://accscience.com/journal/IMO

CONTENTS

ACCSCIENCE PUBLISHING

Innovative Medicines & Omics

REVIEW ARTICLE

Carbohydrate polymer derivatives as gastrointestinal pH-responsive oral drug delivery systems: A review

Diego E. Boldrini[1,2]*

[1]Pilot Plant of Chemical Engineering, National University of The South, National Scientific and Technical Research Council, Bahía Blanca, Buenos Aires, Argentina

[2]Department of Chemical Engineering, National University of The South, Bahía Blanca, Buenos Aires, Argentina

Abstract

PH-responsive carbohydrate polymers have gained significant attention as promising candidates for next-generation oral drug delivery systems. This review focuses on the use of pH-sensitive carbohydrate polymers as a platform for controlled drug delivery. The unique ability of these polymers to undergo a conformational or structural change in response to specific pH ranges makes them ideal for targeted drug release. The gastrointestinal tract, with its distinct pH environments ranging from the highly acidic stomach to the neutral small intestine, presents a perfect scenario for these intelligent delivery systems. The design principles of these systems, including the chemical modification of natural carbohydrate polymers and the synthesis of new pH-sensitive materials, are explored. Furthermore, this review summarizes recent advancements and challenges in the application of carbohydrate polymers for oral drug delivery, particularly in enhancing drug bioavailability, protecting acid-labile drugs, and enabling site-specific release in the colon. The review concludes by highlighting the immense potential of these biocompatible and biodegradable materials in developing advanced, patient-friendly pharmaceutical formulations. In addition, the primary limitations of these materials are discussed with respect to enzymatic degradation, scaling up, cost-effectiveness, and regulatory approval.

Keywords: Carbohydrate polymer derivatives; Drug delivery systems; pH-sensitivity

***Corresponding author:**
Diego E. Boldrini
(dboldrini@plapiqui.edu.ar)

Citation: Boldrini DE. Carbohydrate polymer derivatives as gastrointestinal pH-responsive oral drug delivery systems: A review. *Innov Med Omics*. 2026;3(1):1-14. doi: 10.36922/IMO025390049

Received: September 24, 2025

Revised: November 13, 2025

Accepted: December 9, 2025

Published online: December 23, 2025

1. Introduction

The field of drug delivery has seen a paradigm shift from conventional formulations to sophisticated systems that can precisely control the release of therapeutic agents. This evolution is driven by the need to enhance drug efficacy, minimize side effects, and improve patient compliance. Among the various materials explored for this purpose, carbohydrate polymers have emerged as a highly promising class of biomaterials. Their unique properties, including biocompatibility, biodegradability, and a wide array of functional groups, make them ideal for designing advanced drug delivery systems.[1] Carbohydrate polymers, also known as polysaccharides, are naturally abundant and structurally diverse macromolecules that play crucial roles in biological systems. Their inherent non-toxicity and lack of immunogenicity make them exceptionally

well-suited for biomedical applications. Unlike synthetic polymers, which can sometimes pose concerns regarding long-term toxicity and environmental impact, these natural polymers are recognized by the body, leading to predictable degradation into non-toxic byproducts. This biological compatibility allows for their use in various routes of administration, including oral.[2] Furthermore, the presence of numerous hydroxyl groups on their backbone provides multiple sites for chemical modification. This versatility allows for the fine-tuning of their physical and chemical properties, such as solubility, swelling behavior, and hydrophobicity, to achieve a desired release profile. This has led to the development of a new class of materials known as stimulus-responsive polymers. These smart polymers are highly sensitive to their environment, designed to detect subtle physicochemical shifts and react by self-assembling or drastically altering their properties. This inherent responsiveness makes them an excellent tool for controlled drug delivery, where a specific trigger can release a therapeutic agent from the carrier.[3] Stimuli used for drug release can be classified as either internal (endogenous) or external (exogenous). Internal stimuli are those that occur naturally within the human body, such as changes in pH, the presence of enzymes, specific biomolecules, or the redox microenvironment. External stimuli, on the other hand, are applied artificially, including physical cues such as light, magnetic or electric fields, and temperature. In particular, temperature is a physical stimulus that can be both internal and external.[4] Among the various strategies, systems that respond to pH changes have garnered considerable attention. The human body presents a diverse range of pH environments, from the highly acidic stomach to the near-neutral small intestine and the slightly alkaline colon. These natural pH gradients provide an ideal trigger for smart delivery systems. By designing carriers that are stable at one pH and dissolve or swell at another, it is possible to protect drugs from harsh environments, enable site-specific release in the gastrointestinal tract (GIT), and improve the bioavailability of sensitive compounds. Consequently, pH-responsive systems are at the forefront of research for oral drug delivery, offering a powerful approach to optimize therapeutic outcomes.[5-8] In summary, the sophisticated design of pH-responsive carbohydrate polymer derivatives offers a powerful solution to overcome the challenges associated with oral drug delivery. By leveraging the body's natural pH gradients, these systems can protect labile drugs from specific environments in the GIT, ensuring targeted release at the desired site of absorption, thereby improving therapeutic outcomes and patient compliance. As the industry shifts toward personalized medicine and biologics, these systems provide adaptive platforms that can respond to pathological microenvironments, such as the acidic pH characteristic of tumor tissues or inflamed regions, thereby enhancing therapeutic efficacy while minimizing systemic side effects. Furthermore, their natural origin aligns with the growing demand for sustainable and biobased materials in pharmaceutical manufacturing. Despite significant progress in the development of pH-responsive carbohydrate-based drug delivery systems, several limitations still hinder their translation into clinical use. The inherent variability of physiological pH along the GIT and between patients often leads to inconsistent release profiles and limited site-specific targeting.[9] Furthermore, the structural heterogeneity of natural polysaccharides, such as chitosan, pectin, and alginate, results in batch-to-batch variations in molecular weight, degree of substitution, and charge density, which complicate reproducibility and large-scale manufacturing.[2] Another major challenge lies in the stability of these systems under physiological conditions, where enzymatic degradation and ionic strength can alter polymer conformation and drug-polymer interactions, affecting release kinetics.[10] From a regulatory standpoint, carbohydrate-based matrices are often classified as combination products, subject to dual evaluation under pharmaceutical and medical device frameworks, which significantly prolongs approval timelines.[11,12] In addition, the lack of harmonized protocols for assessing *in vitro–in vivo* correlation in pH-responsive formulations further limits the predictive power of pre-clinical data and their clinical translation.[13] Addressing these issues requires standardized characterization methods, advanced modeling of release mechanisms, and coordinated regulatory guidance tailored to stimuli-responsive biomaterials. This review provides a comprehensive overview of the design principles, synthesis methods, and key mechanisms of these innovative GIT drug delivery systems. We also discuss recent advancements, limitations, and future perspectives of these biocompatible materials in the development of next-generation oral pharmaceuticals. The structure of this manuscript is designed to provide a comprehensive and logically organized discussion of pH-responsive carbohydrate-based drug delivery systems. Section 2 describes the pH gradient along the GIT, emphasizing its physiological relevance for the design of site-specific drug delivery platforms. Section 3 outlines the regulatory framework governing pH-sensitive and polysaccharide-based delivery systems, referencing key international guidelines, such as International Council for Harmonisation of Technical Requirements for Pharmaceuticals for Human Use (ICH) Q8–Q10, International Organization for Standardization (ISO) 10993, U.S. Food and Drug Administration (FDA), and

European Medicines Agency (EMA) recommendations for nanomaterials and combination products. Section 4 summarizes the fundamental characteristics of pH-responsive polymers, focusing on their ionization behavior, network dynamics, and physicochemical parameters that influence drug release. Section 5 presents a detailed analysis of carbohydrate polymer derivatives as pH-responsive gastric drug delivery systems, subdivided into four mechanistic categories: Swelling-controlled systems (Section 5.1), dissolution-controlled systems (Section 5.2), drug–polymer interactions (Section 5.3), and combined mechanisms (Section 5.4), highlighting their structure–function relationships and release kinetics. Section 6 discusses the broader implications of the findings, integrating molecular mechanisms with translational and clinical perspectives. Finally, Section 7 provides the concluding remarks, summarizing key insights, realistic challenges, and future directions for advancing carbohydrate-based smart delivery technologies toward clinical application.

2. pH gradient along the human GIT

The human GIT (Figure 1) is a highly dynamic and heterogeneous environment, characterized by distinct regions with significant pH variations. This natural pH gradient is a key physiological factor that is widely exploited in the design of smart drug delivery systems.

The oral route begins from the mouth, where the pH is around 6.8–7.0, and the transit time is negligible. After that, the stomach is a highly acidic environment, with a pH typically between 1.2 and 2.0. With a transit time of 3–4 h, the stomach's condition can protect against pathogens but also degrade acid-sensitive drugs. As gastric contents move into the small intestine, they are progressively neutralized by pancreatic secretions, with the pH gradually increasing from approximately 6.0 in the duodenum to around 7.4 in the ileum. This region is the primary site for drug absorption. Finally, the material reaches the large intestine (colon), which maintains a slightly acidic to near-neutral pH, generally in the range of 6.0–6.7, influenced by the metabolic activity of the resident microbiota. This unique physiological sequence of pH changes provides an ideal trigger for controlling the release of therapeutic agents at a specific site along the GIT.[19] Table 1 summarizes the pH gradient and transit time along the human GIT.[20-22]

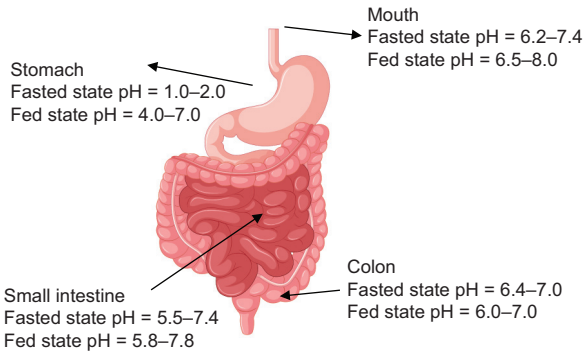

Figure 1. Schematic representation of the human gastrointestinal tract showing the typical pH gradient (fed and fasted states)[14-18]

The values reported in Table 1 represent average physiological conditions of the human GIT. It is important to note that these parameters can vary considerably due to physiological variability associated with the fasted/fed state, age, disease status, co-medications, antacid use, and the presence of *Helicobacter pylori*.[15,23,24] These variations are particularly relevant for the design and *in vitro* evaluation of pH-responsive drug delivery systems, as they directly influence polymer ionization, swelling-dissolution kinetics, and site-specific drug release behavior. Therefore, when interpreting the data in Table 1, it should be understood that the listed values correspond to mean estimates and should be contextualized within the expected physiological variability observed *in vivo*. In the particular case of the broad range reported for colonic transit time (6–70 h), it is worth mentioning that the variability well reflects the documented interindividual and physiological differences. Specifically, the shorter values correspond to healthy adults under normal or accelerated motility conditions, whereas the longer durations are associated with slower transit, often observed in older individuals or those with constipation.[25]

3. Regulatory framework

Despite the rapid progress of pH-responsive carbohydrate-based drug delivery systems at the pre-clinical level, their translation into clinical applications remains limited due to stringent regulatory and practical constraints.[2,26-29] To enter clinical evaluation, such systems must comply with international standards, such as ICH Q8-Q10 (pharmaceutical development and quality systems), ISO 10993 (biological evaluation of medical devices), and the FDA's Guidance for Industry on Nanotechnology in 2022, which emphasizes safety, reproducibility, and quality-

Table 1. pH gradient and transit time along the human gastrointestinal tract

Organ	pH	Transit time (h)
Mouth	6.8–7.0	Negligible
Stomach	1.2–2.0	3–4
Small intestine	6.0–7.4	2–6
Large intestine (colon)	6.0–6.7	6–70

by-design principles. Clinical trials for nanocarriers or bioresponsive polymers must follow Good Manufacturing Practice (GMP) and Good Clinical Practice standards, with extensive documentation on pharmacokinetics, biodegradation, immunogenicity, and long-term toxicity. However, a major challenge arises from the inherent variability of natural carbohydrate sources and the lack of harmonized protocols for characterizing their pH sensitivity, stability, and release kinetics under physiological conditions. Moreover, both EMA and FDA currently evaluate bioresponsive systems on a case-by-case basis, leading to uncertain regulatory pathways. Overcoming these barriers demands standardized analytical frameworks, cross-disciplinary collaboration, and early regulatory engagement to ensure that innovative biopolymer-based systems meet safety and efficacy criteria suitable for clinical translation.[30-34]

4. Characteristics of pH-responsive polymers

Drug delivery systems designed to release their payload in response to a specific pH often incorporate ionizable groups into the carrier's structure. These groups are essential because their protonation or deprotonation alters the polymer's hydrophobicity, thereby triggering a change in system behavior.[35,36]

These polymers contain either acidic or basic functional groups that can donate or accept protons depending on the pH of their environment. For instance, acidic (anionic) polymers feature ionizable acidic side chains, such as carboxylic (–COOH), sulfonic, or phosphonic acids. Conversely, basic (cationic) polymers are characterized by basic groups, such as amines, which can be located in the main chain or as side groups. The ionization of these functional groups in response to pH creates a net charge on the polymer chains, thereby altering their interactions.[37,38] This process is schematically represented in Figure 2, which illustrates how the state of an acidic or basic polymer changes based on the degree of ionization of its groups.

The ionization process is what enables swelling in cross-linked systems or dissolution in other polymer matrices. For acidic polymers, the chains repel one another when the surrounding pH is greater than the polymer pKa, while they attract each other at pH values below the pKa. Conversely, for a basic polymer, the chains attract each other at pH values above the pKb but repel at pH values below the pKb. In both scenarios, the ionization of the functional groups generates a net charge on the polymer chains, leading to their mutual repulsion and a subsequent change in the material structure. In addition to these mechanisms, drug release can occur in systems that involve

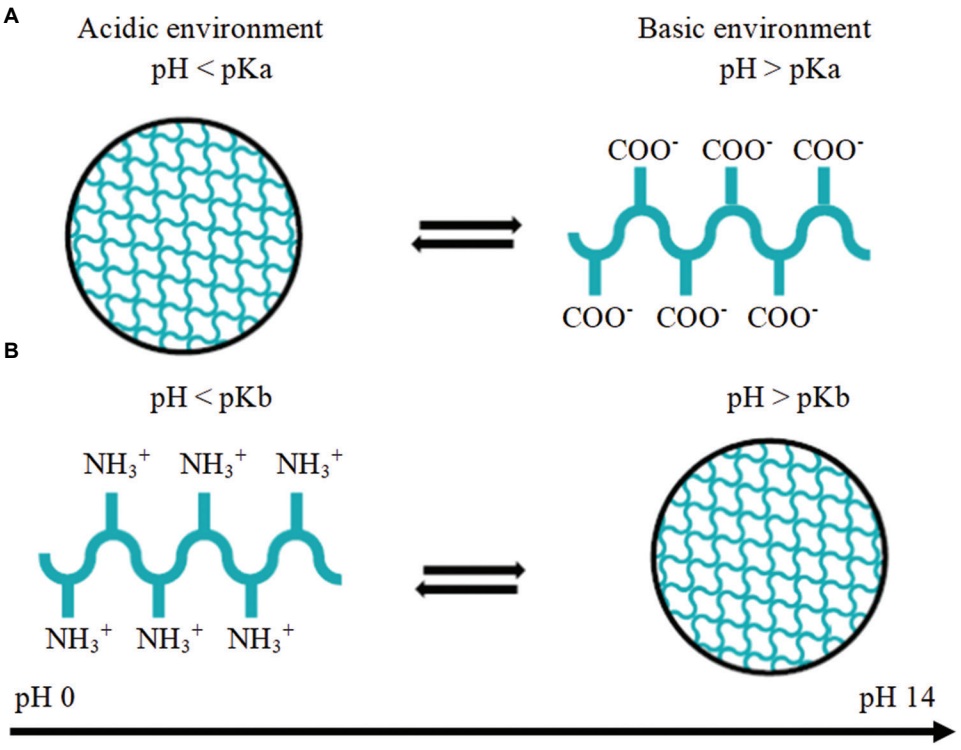

Figure 2. The state of the polymeric chain based on the ionization degree. (A) Acidic polymeric chain. (B) Basic polymeric chain. Image created by the authors.

an interaction between the drug and the polymer. In this case, the hydrogen bond between the drug and the polymer is influenced by the environmental pH because the drug can exist in protonated, neutral, or deprotonated forms. On the other hand, in some systems, these release mechanisms may be combined.[4] Determining the effective pKa of ionizable groups within polymeric networks is essential for predicting their pH-responsive behavior. In carbohydrate-based systems, several complementary methods are employed. Potentiometric titration is the most common approach, in which titration curves of polymer solutions or hydrogels are recorded, and inflection points correspond to the apparent pKa values. Ultraviolet–visible spectroscopy can also monitor protonation–deprotonation equilibria through absorbance or band-shift changes, offering insight into specific functional groups. In cases where direct titration is hindered by low solubility or crosslinking, model monomeric compounds (e.g., glucosamine and galacturonic acid) are often used to estimate intrinsic pKa values, later corrected for polymeric effects. The apparent pKa in polymer matrices often deviates from that of corresponding small molecules due to the microenvironmental effects of the polymer network. Factors such as electrostatic interactions, polymer chain density, hydration degree, and dielectric constant alter proton activity around ionizable sites. For example, strong intramolecular hydrogen bonding or dense crosslinking can restrict solvent access, thereby increasing the apparent pKa, whereas high hydration and charge repulsion may decrease it. These effects must be considered when designing pH-responsive carbohydrate carriers, as they directly influence the onset of swelling or dissolution under physiological conditions.[39-41]

A prime commercial example of a pH-responsive polymer family is the Eudragit® series, a non-biodegradable, poly(methacrylate)-based copolymer.[42] Their basic chemical structure, shown in Figure 3, can be modified to achieve different functionalities.

For instance, a product sensitive to acidic pH, such as Eudragit E, has tertiary amine groups as side chains

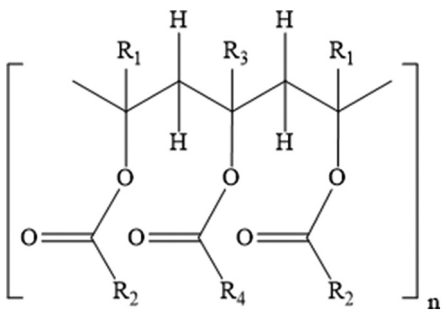

Figure 3. Basic structure of the Eudragit® compounds

(R_2 = $CH_2CH_2N(CH_3)_2$) and methyl or butyl esters (R_4 = CH_3 or C_4H_9), whereas for a product sensitive to basic pH (Eudragit L or S), the side chains contain carboxylic acid groups (R_2 = H) and methyl esters (R_4 = CH_3). Furthermore, a pH-independent material that swells and is permeable can be created by incorporating hydrophilic quaternary ammonium groups (R_4 = $CH_2CH_2N(CH_3)_3^+Cl^-$), as is the case with Eudragit RL and RS. This specific modification allows for water uptake, which gives the polymer its swelling and permeability properties. While Eudragit copolymers are among the most established pH-responsive materials in oral dosage forms, they are non-biodegradable polymethacrylates. Upon administration, these polymers resist enzymatic and microbial degradation and are excreted largely unchanged in feces. From a regulatory perspective, Eudragit grades (e.g., L100, S100, and EPO) are classified as pharmaceutically safe excipients and are included in both the FDA Inactive Ingredient Databases and the European Pharmacopoeia monographs.[43,44] However, their lack of biodegradability raises increasing concerns regarding long-term environmental persistence and residual accumulation, particularly in high-dosage or chronic therapies. In contrast, natural polysaccharides, such as alginate, chitosan, and pectin, are enzymatically and microbially degradable, providing a sustainable and biocompatible alternative with favorable regulatory perception in current green-pharma initiatives.[45] From a processing standpoint, synthetic polymers, such as Eudragit, exhibit excellent compatibility with manufacturing techniques, including hot-melt extrusion and three-dimensional (3D) printing, due to their defined thermal stability and rheological behavior.[44] In contrast, carbohydrate-based polymers (e.g., chitosan, alginate, and starch derivatives) often exhibit limited processability due to a narrow processing window between their glass transition temperature and the onset of thermal degradation temperature. Consequently, adapting carbohydrate matrices for hot-melt extrusion or 3D printing often requires chemical modification or processing under solvent-assisted or low-temperature conditions to maintain functionality and achieve consistent drug release behavior.[46] These differences are crucial for translating pH-responsive formulations into scalable manufacturing processes.

In summary, the acid-base dissociation constant (pKa or pKb) of a polymer's functional groups is a critical determinant of its pH-responsiveness and thus its suitability for gastrointestinal drug delivery. In pH-sensitive carbohydrate-based systems, ionizable groups, such as –COOH group, amino group, and hydroxyl group, undergo protonation–deprotonation equilibria depending on the luminal pH. The design principle involves matching the polymer's pKa to the target region's pH within the GIT: for

instance, polymers with pKa values around 4.0–5.0 (e.g., alginate, chitosan-citrate) respond to the acidic-to-neutral transition of the small intestine, whereas polymers with pKa around 6.5–7.0 (e.g., carboxymethyl cellulose and pectin derivatives) activate in the colonic environment. When the environmental pH exceeds the polymer's pKa, ionization induces electrostatic repulsion and osmotic swelling, facilitating drug diffusion or polymer erosion. Conversely, in pH below pKa, the polymer remains collapsed and less permeable, protecting the drug in acidic media, such as the stomach. Therefore, rational pKa selection enables spatially controlled release and optimization of swelling-dissolution kinetics in carbohydrate-based matrices.[13,47,48]

5. Carbohydrate polymer derivatives as pH-responsive gastric drug delivery systems

The pH-responsive drug delivery systems based on carbohydrate polymers can exhibit distinct release mechanisms, including swelling-controlled, dissolution-controlled, or a combination of both, depending on the polymer structure, crosslinking density, and environmental pH. In swelling-controlled systems, drug release is primarily governed by the diffusion of the therapeutic agent through a hydrated polymer matrix, where the rate of swelling dictates the release kinetics, often following Fickian or anomalous diffusion behavior. Conversely, dissolution-controlled systems rely on the gradual solubilization or erosion of the polymer network under specific pH conditions; this mechanism typically results in zero-order or erosion-controlled kinetics, allowing sustained and predictable release profiles. The combination of swelling and dissolution mechanisms introduces complex, often biphasic kinetics, an initial diffusion-driven burst phase followed by a slow degradation-dependent release, offering fine-tuned control over therapeutic delivery. The interplay between these processes can be modulated by adjusting polymer composition and degree of crosslinking, or by incorporating pH-labile linkages, enabling the design of systems optimized for site-specific and time-dependent drug release under physiological or pathological pH gradients.[9]

It should be noted that the behavior of pH-responsive carbohydrate-based systems is highly dependent on several experimental variables, including buffer composition, ionic strength, temperature, and the degree of crosslinking. However, such parameters are not uniformly reported across studies. Consequently, the data summarized in Tables 2-5 represent the most commonly reported pH conditions (typically pH 1.2 for gastric and pH 6.8–7.4 for intestinal media) and reflect generalized qualitative trends rather than standardized quantitative comparisons. Experimental details, such as media composition or United States Pharmacopeia apparatus type, are mentioned only when explicitly provided in the original publications. This approach ensures internal consistency and avoids introducing sporadically available methodological data.

In general terms, for drugs with limited solubility but good chemical stability, swelling-controlled matrices are preferred because gradual water uptake supports diffusion-driven release. Conversely, drugs that are highly soluble or unstable in gastric conditions benefit from dissolution-controlled carriers or polymer–drug ionic complexes. The combination approach is suitable when dual responsiveness (swelling and erosion) is required to balance protection and release kinetics. Patient-related factors, such as gastric pH variability, fed or fasted state, and co-medications, should also be considered, as they may significantly shift the effective pH triggers and hence the performance of these delivery systems.

5.1. Swelling-controlled systems

Cross-linked carbohydrate polymers represent a highly promising class of biomaterials for the development of pH-sensitive drug delivery systems. By crosslinking natural polymers, a stable 3D network is formed that, unlike its linear counterparts, does not readily dissolve in solvents. This network structure, combined with the ionization capacity of some functional groups on the polymer chains (Section 3), allows the material to swell or contract in response to changes in the surrounding pH while maintaining its structural integrity. This characteristic is crucial for controlled drug release in the GIT. This ensures targeted and efficient drug delivery, preventing premature degradation and enhancing bioavailability. Table 2 shows examples of pH-responsive controlled-release systems based on cross-linked carbohydrate polymers.

5.2. Dissolution-controlled systems

Unlike their cross-linked counterparts, uncross-linked carbohydrate polymers are linear or branched structures that rely on their pH-dependent solubility for controlled drug release. These materials can undergo a reversible transition from a solid or viscous state to a soluble one in response to specific pH values, depending on the ionizable groups in the polymer chains (Section 3). For instance, the low pH of the stomach protonates the amine groups on chitosan, causing the polymer to dissolve and facilitating drug release in the stomach. Conversely, the carboxylic acid groups on alginate remain protonated and insoluble in acidic media, but deprotonate and become soluble as the pH increases in the intestine. This mechanism of controlled dissolution provides a straightforward

Table 2. Examples of carbohydrate polymer-based carriers responding to the pH changes in the gastrointestinal tract (swelling)

Carbohydrate polymer	Encapsulated compound	Behavior	References
Anionically modified starch	N/D	Swelling considerably augments with the increase of pH from 1.0 to 5.5 because the carboxyl groups are ionized	49
Starch-poly (sodium acrylate-co-acrylamide)	Ibuprofen	Drug delivery is faster at pH 7.4 than at pH 1.2 due to the ionization of carboxylate groups at basic pH	50
Poly (starch/acrylic acid)	Rutin	Swelling is greater at pH 7.4 than at pH 2.0 due to the carboxylic groups	51
Methyl methacrylate-g-starch/ hydroxypropylated starch	Esomeprazole magnesium	Drug delivery is higher at pH 6.8 than at pH 1.2 due to the presence of carboxylic groups	52
Starch cross-linked with poly (aspartic acid)	5-fluorouracil	Swelling is greater at high pH media than at low pH media due to the presence of carboxylic groups	53
Carboxymethyl sago pulp/carboxymethyl sago starch	Ciprofloxacin hydrochloride and diclofenac sodium	Swelling is greater at high pH media than at low pH media due to the presence of carboxylic groups	54
Starch-g-poly (sodium-2-acrylamido-2-methyl-1-propane sulfonate-co-methacrylic acid)	Amoxicillin trihydrate	Drug release is higher at alkaline pH than at neutral or acidic pH due to the carboxylic groups	55
Chitosan cross-linked starch	Insulin	Drug release is higher at high pH than at low pH due to the presence of carboxylic groups	56
Carboxymethyl starch grafted with poly (methacrylic acid)	5-aminosalicylic acid and salicylic acid	An increase in the content of methacrylic acid results in less swelling in SGF, but greater swelling in SIF	57
Carboxymethyl starch grafted with poly (methacrylic acid)	Sodium diclofenac	An increase in the content of methacrylic acid results in less swelling in SGF, but greater swelling in SIF	58
2-hydroxyethyl methacrylate and acrylic acid grafted on starch	-	Swelling is greater at pH 7.4 than at pH 1.0 due to the presence of carboxylic groups	59
Corn starch/ethylene-co-vinyl alcohol thermoplastic blend	-	The maximum hydration degree is at pH=7.4, and the lowest is observed at an acidic pH due to the presence of carboxylic groups	60
Starch cross-linked with acrylic acid	Paracetamol	Drug release from the polymer is less at pH 1.2 compared to pH 7.4 due to the presence of carboxylic groups	61
High amylose cross-linked with pectin	-	Samples with a higher pectin proportion have greater swelling ability because pectin is more hydrophilic than starch. Besides, the swelling of the polymer increases at high pH values because of the presence of carboxylic groups, which ionize at basic pH	62
Cross-linked starch	Curcumin	Drug delivery is greater in the SGF than in SIF because the solubility of the curcumin is greater at acidic pH. Polymer swelling is not evaluated	63
Cross-linked alginate	N/D	Cross-linked alginate demonstrates pronounced swelling at alkaline pH and contraction in an acidic environment due to the presence of carboxylic groups. The authors propose the use of these compounds as a targeted delivery vehicle	64
Xanthan gum cross-linked with starch	Aspirin and paracetamol	Drug release is significantly higher in pH 7.4 than in pH 1.2 due to the presence of carboxylic groups in xanthan gum	65
Sodium carboxymethyl cellulose cross-linked with fumaric acid	N/D	The polymers show pH-sensitivity due to the presence of carboxylic groups	66
Quaternized cellulose cross-linked with carboxymethyl cellulose	N/D	The polymer exhibits pH-sensitivity due to the presence of $–COO^-$and $–(CH_3)_3N^+$groups	67
Chitosan cross-linked with glutaraldehyde	Chlorhexidine acetate	Drug release is higher at low pH values due to the presence of amino groups, which causes swelling in this pH range	68
Citrate cross-linked chitosan	Riboflavin	Drug release is higher at low pH values due to the presence of amino groups, which causes swelling in this pH range	69

(*Cont'd...*)

Table 2. (*Continued*)

Carbohydrate polymer	Encapsulated compound	Behavior	References
Chitosan cross-linked with hydroxypropyl methylcellulose phthalate	Insulin	Crosslinking avoids chitosan dissociation in the stomach, thus protecting the drug	70
Chitosan cross-linked with polyvinyl pyrrolidone	Cefixime	Drug release is higher at low pH values due to the presence of ionizable groups, which causes swelling in this pH range	71
Bone ash-reinforced cross-linked chitosan-grafted-glycidyl methacrylate and poly (ethylene glycol) diacrylate	Amoxicillin	Drug release is higher at low pH values due to the presence of amino groups, which causes swelling in this pH range	72
Acrylate-grafted-carboxymethyl starch-2-isobutyl-acrylic acid copolymer	Insulin	The copolymer exhibits pH-dependent swelling/deswelling behaviors due to the ionization/deionization transition of the carboxyl groups	73

Abbreviations: N/D: No data; SGF: Simulated gastric fluid; SIF: Simulated intestinal fluid.

Table 3. Examples of carbohydrate polymer-based carriers responding to the pH changes in the gastrointestinal tract (dissolution)

Carbohydrate polymer	Encapsulated compound	Behavior	References
Starch grafted poly (L-glutamic acid)	Insulin	Drug release is higher at basic pH because of the ionization of carboxylic groups on poly (L-glutamic acid), which allows the dissolution of the aggregates	74
High-amylose starch-pectin blend	Diclofenac sodium	Drug release is higher at basic pH because of carboxylic group ionization in pectin, which solubilizes at these pH values. Starch incorporation into the blend delays drug release since it hinders pectin solubilization	75,76
Hyaluronic acid grafted 3-diethylaminopropyl groups	Doxorubicin	The drug is delivered due to nanoparticle destabilization related to the protonation of 3-diethylaminopropyl when the pH decreases	77
Cellulose acetoacetate cross-linked with cystamine dihydrochloride	Rhodamine B	Drug delivery is achieved by a sol–gel transition due to the presence of an enamine moiety in the polymer	78
N-naphthyl-N, O-succinyl chitosan and N-octyl-N, O-succinyl chitosan	Curcumin	Drug delivery increases at high pH values due to polymer dissociation caused by the ionization of the carboxyl groups from the succinic acid moiety	79
High surface area silica-loaded chitosan	Curcumin	Drug delivery increases at low pH values due to polymer dissociation caused by the ionization of the amino groups in the chitosan	80
Chitosan-poly(γ-glutamic acid) complex	Insulin	Drug delivery increases at low pH values due to polymer dissociation caused by the ionization of the amino groups in the chitosan	81
Cellulose acetate phthalate-ethyl cellulose mixture	Ibuprofen	Drug release rate increases in alkaline medium due to the high solubility of cellulose acetate phthalate at basic pH	82
Chitosan-O-carboxymethyl chitosan mixture	Doxorubicin hydrochloride	At high pH values, NH_3^+ions on chitosan and O-carboxymeymethy chitosan are deprotonated, allowing polymer disaggregation	83

Table 4. Examples of carbohydrate polymer-based carriers responding to the pH changes in the gastrointestinal tract (drug-polymer interaction)

Carbohydrate polymer	Encapsulated compound	Behavior	References
Soluble starch	Curcumin	Release in SIF is faster than that in SGF. The different pH values may be responsible for the observed release speed difference, as hydrogen bonding between curcumin and starch is highly influenced by the environmental pH value	85
Methacrylated carboxymethyl cellulose cross-linked with poly (N-isopropylacrylamide)	Hen egg white lysozyme	At pH 7.4, lysozyme is positively charged, and the polymer is negatively charged, which causes a strong attraction between them, resulting in slow release	86

Abbreviations: SGF: Simulated gastric fluid; SIF: Simulated intestinal fluid.

Table 5. Examples of carbohydrate polymer-based carriers responding to the pH changes in the gastrointestinal tract (combined mechanisms)

Carbohydrate polymer	Encapsulated compound	Behavior	References
Alginate-starch blend	Salicylic acid	Drug release is maximal at pH 7.4 and minimum at pH 1.0 due to the presence of carboxylic groups on alginate. Besides, drug release increases as starch content is augmented because it dissolves, leaving pores that accelerate drug release from the polymer	87
Chitosan-starch blend	Antofloxacin	Drug delivery is favored at acidic and basic pH because hydrogen bonds are weakened, caused by ions' interference. At neutral pH, drug release is moderate. Besides, drug delivery is higher at acidic pH than at basic pH because the protonation of amine groups in chitosan makes the polymer swell	88

approach to developing oral drug delivery systems that can protect drugs from harsh environments and achieve targeted release at specific sites in the GIT. Table 3 presents examples of pH-responsive controlled-release systems based on uncross-linked carbohydrate polymers.

5.3. Drug–polymer interactions

In carbohydrate polymer-based drug delivery systems, the direct interaction between the drug and the polymer is a key mechanism for achieving controlled, pH-sensitive release. Instead of relying on polymer dissolution or swelling, these systems leverage hydrogen bonds or ionic interactions between the drug molecules and the polymer chains. The strength of this interaction is directly influenced by the environmental pH. A change in pH can modify the protonation state of either the drug or the polymer, thereby altering the affinity between the two. The interplay between the ionization constants of the drug and the polymer matrix (drug pKa vs. polymer pKa) is a critical determinant of loading efficiency and release performance in pH-responsive systems. For weakly acidic drugs (e.g., ibuprofen, pKa ≈ 4.4), encapsulation within matrices bearing weakly basic or neutral groups can minimize premature ionization in the stomach (pH 1.2–2.0) and promote release in the intestine (pH 6.0–7.4), where deprotonation enhances solubility and diffusion. Conversely, weakly basic drugs (e.g., propranolol, pKa ≈ 9.5) tend to be protonated in acidic media, favoring ionic interactions with negatively charged polysaccharides, such as alginate or carboxymethyl cellulose; drug release is then triggered by polymer deionization at higher pH. Therefore, selecting a polymer whose pKa closely matches the target intestinal pH enables a balance between drug–polymer affinity (for stability) and repulsion (for release), optimizing both loading and responsiveness.[84] Table 4 shows examples of carbohydrate polymers used for pH-sensitive controlled drug release through a drug–polymer interaction mechanism.

5.4. Combined mechanisms

The design of advanced drug delivery systems has increasingly moved toward combining multiple mechanisms to achieve superior control over drug release. This strategy allows a single formulation to leverage the advantages of different approaches, creating a robust, versatile system. Table 5 shows examples of carbohydrate polymer-based carriers that respond to pH changes in the GIT through combined mechanisms.

6. Discussion

Despite significant advances at the laboratory scale, the clinical translation of pH-responsive carbohydrate-based drug delivery systems remains limited due to several regulatory and practical challenges. Most studies demonstrating precise pH-triggered release, biocompatibility, and efficacy are still confined to *in vitro* or small animal models, with only a few progressing to early-phase clinical trials. A major barrier lies in the complexity and variability of biological environments, which can alter the expected release kinetics observed under controlled conditions. Moreover, the regulatory framework for nanocarriers and bioreactive materials requires extensive data on long-term safety, biodegradation pathways, and potential immunogenicity, parameters that are challenging to standardize across different carbohydrate sources and modification methods. Manufacturing scalability and reproducibility further complicate approval, as minor changes in polymer purity or crosslinking chemistry can significantly affect performance. Addressing these issues requires harmonized characterization protocols, improved predictive models linking physicochemical parameters to *in vivo* behavior, and closer collaboration among academia, industry, and regulatory agencies to accelerate the clinical validation of these intelligent drug delivery systems.[89,90]

Beyond classical pH-triggered release, recent research trends emphasize multi-stimuli-responsive strategies that integrate physiological and microbial cues for enhanced site specificity. Mucoadhesive coatings have demonstrated improved retention in the intestinal mucosa, reducing premature drug loss during transit. Enzyme-triggered colon delivery systems incorporating azo-linkers or glycosidic bonds exploit the reductive or hydrolytic

activity of colonic bacteria to achieve selective cleavage and release. Furthermore, hybrid systems combining pH-sensitivity with microbiota responsiveness, such as pectin–Eudragit or chitosan–inulin matrices, represent promising platforms for achieving synchronized responsiveness to both pH and enzymatic environments. These emerging approaches align with the growing interest in personalized and microbiota-informed drug delivery strategies.[91-93]

7. Conclusion

This comprehensive review has highlighted the significant role of carbohydrate polymers as a versatile and effective platform for pH-controlled drug delivery. The inherent biocompatibility, biodegradability, and structural tunability of these materials make them an exceptional choice for the design of sophisticated oral delivery systems. We have explored the various mechanisms of pH-responsive release, from the dissolution of uncross-linked polymers to the structural integrity and controlled diffusion offered by cross-linked matrices. Furthermore, we have examined how direct drug-polymer interactions, such as those mediated by hydrogen bonds, can be leveraged to achieve highly precise, on-demand release.

The successful application of these systems in protecting acid-labile drugs from the harsh stomach environment and ensuring targeted release in the small intestine or colon has been well documented. Future research should focus on developing advanced formulations that combine these mechanisms, creating multi-responsive systems that can adapt to the complex physiological conditions of the GIT. In addition, greater emphasis on enzymatic degradation, scale-up, cost-effectiveness, and regulatory approval will be critical for translating these promising biomaterials from laboratory research into widely available pharmaceutical products. Agencies such as the FDA and EMA currently assess such systems on a case-by-case basis, guided by frameworks including ICH Q8–Q10, ISO 10993, and the FDA Nanotechnology Guidance, all of which emphasize safety, immunogenicity, and long-term biocompatibility. Realistic progress will depend on developing standardized characterization methods, particularly for pH-triggered swelling and dissolution kinetics, alongside GMP-compatible synthesis routes. Integration of *in silico* modeling and machine learning to predict release profiles and biological fate may accelerate translation, but the field must first address regulatory and reproducibility gaps before achieving large-scale clinical validation. Ultimately, continued innovation in this field holds immense potential to develop effective, patient-friendly, and personalized therapeutic solutions.

Acknowledgments

None.

Funding

The author acknowledges the financial support of the Consejo Nacional de Investigaciones Científicas y Técnicas (CONICET) (grant number PIBAA 2022-2023 28720210100304CO) and Agencia Nacional de Promoción Científica y Tecnológica (ANPCyT) (grant number PICT-2021-I-INVI-00116).

Conflict of interest

The author declares no conflict of interest.

Author contributions

This is a single-authored article.

Ethics approval and consent to participate

Not applicable.

Consent for publication

Not applicable.

Availability of data

Not applicable.

References

1. Shukla RK, Tiwari A. Carbohydrate polymers: Applications and recent advances in delivering drugs to the colon. *Carbohydr Polym*. 2012;88(2):399-416.

   doi: 10.1016/j.carbpol.2011.12.043

2. Di X, Liang X, Shen C, Pei Y, Wu B, He Z. Carbohydrates used in polymeric systems for drug delivery: From structures to applications. *Pharmaceutics* (*Basel*). 2022;14(4):739.

   doi: 10.3390/pharmaceutics14040739

3. Bruschi, ML. *Strategies to Modify the Drug Release from Pharmaceutical Systems*. United Kingdom: Woodhead Publishing; 2015.

4. Boldrini DE. Starch-based materials for drug delivery in the gastrointestinal tract-A review. *Carbohydr Polym*. 2023;320:121258.

   doi: 10.1016/j.carbpol.2023.121258

5. Ofridam F, Tarhini M, Lebaz N, Gagnière É, Mangin D, Elaissari A. pH-sensitive polymers: Classification and some fine potential applications. *Polym Adv Technol*. 2021;32(4):1455-1484.

   doi: 10.1002/pat.5186

6. Zhuo S, Zhang F, Yu J, Zhang X, Yang G, Liu X. pH-sensitive

biomaterials for drug delivery. *Molecules*. 2020;25(23):5649.

doi: 10.3390/molecules25235649

7. Balamuralidhara V, Pramodkumar TM, Srujana N, *et al*. pH sensitive drug delivery systems: A review. *Am J Drug Discov Dev*. 2011;1(1):24-48.

doi: 10.3923/ajddad.2011.24.48

8. Zhu YJ, Chen F. pH-responsive drug-delivery systems. *Chem Asian J*. 2015;10(2):284-305.

doi: 10.1002/asia.201402867

9. Vegad U, Patel M, Khunt D, Zupančič O, Chauhan S, Paudel A. pH stimuli-responsive hydrogels from non-cellulosic biopolymers for drug delivery. *Front Bioeng Biotechnol*. 2023;11:1270364.

doi: 10.3389/fbioe.2023.1270364

10. Abbasi YF, Bera H, Cun D, Yang M. Recent advances in pH/enzyme-responsive polysaccharide-small-molecule drug conjugates as nanotherapeutics. *Carbohydr Polym*. 2023;312:120797.

doi: 10.1016/j.carbpol.2023.120797

11. FDA. *Drug Products, Including Biological Products, that Contain Nanomaterials: Guidance for Industry*. United States: U.S. Food and Drug Administration; 2022.

12. EMA. *Reflection Paper on Nanotechnology-based Medicinal Products for Human Use*. Netherlands: European Medicines Agency; 2021.

13. Singh J, Nayak P. pH-responsive polymers for drug delivery: Trends and opportunities. *J Polym Sci*. 2023;61(22): 2828-2850.

doi: 10.1002/pol.20230214

14. Humphrey SP, Williamson RT. A review of saliva: Normal composition, flow, and function. *J Prosthet Dent*. 2001;85(2):162-169.

doi: 10.1067/mpd.2001.113991

15. Kalantzi L, Goumas K, Kalioras V, Abrahamsson B, Dressman JB, Reppas C. Characterization of the human upper gastrointestinal contents under conditions simulating bioavailability/bioequivalence studies. *Pharm Res*. 2006;23(1):165.

doi: 10.1007/s11095-006-8311-2

16. Dressman JB, Berardi RR, Dermentzoglou LC, *et al*. Upper gastrointestinal (GI) pH in young, healthy men and women. *Pharm Res*. 1990;7(7):756-761.

doi: 10.1023/a:1015941724040

17. Koziolek M, Grimm M, Becker D, *et al*. Investigation of pH and temperature profiles in the GI tract of fasted human subjects using the Intellicap® system. *J Pharm Sci*. 2015;104(9):2855-2863.

doi: 10.1002/jps.24474

18. Nugent SG, Kumar D, Rampton DS, Evans DF. Intestinal luminal pH in inflammatory bowel disease: Possible determinants and implications for therapy with aminosalicylates and other drugs. *Gut*. 2001;48(4):571-577.

doi: 10.1136/gut.48.4.571

19. Evans DF, Pye G, Bramley R, Clark AG, Dyson TJ, Hardcastle JD. Measurement of gastrointestinal pH profiles in normal ambulant human subjects. *Gut*. 1988;29(8): 1035-1041.

doi: 10.1136/gut.29.8.1035

20. Hua S. Advances in oral drug delivery for regional targeting in the gastrointestinal tract-influence of physiological, pathophysiological and pharmaceutical factors. *Front Pharmacol*. 2020;11:524.

doi: 10.3389/fphar.2020.00524

21. Klein S. Polysaccharides in oral drug delivery-recent applications and future perspectives. *Expert Opin Drug Deliv*. 2009;6(10):1037-1052.

doi: 10.1517/17425240903173429

22. Madni A, Kanwal R, Tariq M, *et al*. Devising interactive dissolution experiment for pharmacy students (part I): Use of USP type II apparatus for comparison of immediate release and enteric coated tablets in time varying pH conditions. *PSM Biol Res*. 2016;1(2):83-87.

23. Fallingborg J. Intraluminal pH of the human gastrointestinal tract. *Dan Med Bull*. 1999;46(3):183-196.

24. Koziolek M. Gastrointestinal transit and hydrodynamics under fasting and fed conditions. In: Kerc J, editor. *Oral Drug Delivery for Modified Release Formulations*. Berlin: Springer; 2022. p. 25-38.

doi: 10.1007/978-3-030-97771-3_2

25. Nandhra GK, Chaichanavichkij P, Birch M, Scott SM. Gastrointestinal transit times in health as determined using ingestible capsule systems: A systematic review. *J Clin Med*. 2023;12(16):5272.

doi: 10.3390/jcm12165272

26. Damiri F, Fatimi A, Santos ACP, Varma RS, Berrada M. Smart stimuli-responsive polysaccharide nanohydrogels for drug delivery: A review. *J Mater Chem B*. 2023;11(44): 10538-10565.

doi: 10.1039/d3tb01426k

27. Liu L, Yao W, Rao Y, Lu X, Gao J. pH-Responsive carriers for oral drug delivery: Challenges and opportunities of current platforms. *Drug Deliv*. 2017;24(1):569-581.

doi: 10.1080/10717544.2017.1309858

28. Ghitman J, Voicu SI. Controlled drug delivery mediated by cyclodextrin-based supramolecular self-assembled carriers: From design to clinical performances. *Carbohydr Polym Technol Appl*. 2023;5:100266.

doi: 10.1016/j.carpta.2023.100266

29. Udaipuria N, Bhattacharya S. Novel carbohydrate polymer-based systems for precise drug delivery in colon cancer: Improving treatment effectiveness with intelligent biodegradable materials. *Biopolymers*. 2025;116(1):e23632.

doi: 10.1002/bip.23632

30. Çetintaş HC, Tonbul H, Şahin A, Çapan Y. Regulatory guidelines of the US food and drug administration and the european medicines agency for actively targeted nanomedicines. In: *Drug Delivery with Targeted Nanoparticles*. United States: Academic Press; 2021. p. 725-741.

doi: 10.1016/B978-0-12-818274-1.00017-9

31. Bhavyasri K, Vishnumurthy KM, Rambabu D, Sumakanth M. ICH guidelines-"Q" series (quality guidelines)-A review. *GSC Biol Pharm Sci*. 2019;6(3):89-106.

doi: 10.30574/gscbps.2019.6.3.0033

32. Northup SJ. Safety evaluation of medical devices: US food and drug administration and international standards organization guidelines. *Int J Toxicol*. 1999;18(4):275-283.

doi: 10.1080/109158199225721

33. Metselaar JM, Lammers T. Challenges in nanomedicine clinical translation. *Drug Deliv Transl Res*. 2020;10(3): 721-725.

doi: 10.1007/s13346-020-00727-x

34. Peng C. Nanomedicine development and clinical translation. *Front Chem*. 2024;12:1458690.

doi: 10.3389/fchem.2024.1458690

35. Foster S, Duvall CL, Crownover EF, Hoffman AS, Stayton PS. Intracellular delivery of a protein antigen with an endosomal-releasing polymer enhances CD8 T-cell production and prophylactic vaccine efficacy. *Bioconjug Chem*. 2010;21(12):2205-2212.

doi: 10.1021/bc100269x

36. Liu J, Huang Y, Kumar A, *et al*. pH-sensitive nano-systems for drug delivery in cancer therapy. *Biotechnol Adv*. 2014;32(4):693-710.

doi: 10.1016/j.biotechadv.2014.02.008

37. Joseph X, Akhil V, Arathi A, Mohanan PV. Nanobiomaterials in support of drug delivery related issues. *Mater Sci Eng B*. 2022;279:115680.

doi: 10.1016/j.mseb.2022.115680

38. Kocak G, Tuncer C, Bütün V. pH-Responsive polymers. *Polym Chem*. 2017;8(1):144-176.

doi: 10.1039/C6PY01671A

39. Titration P. Ionization equilibrium and potentiometric titration of weak polyelectrolytes. *Phys Chem Polyelectrolyte Solut*. 2015;158:67.

doi: 10.1016/B978-0-12-800188-2.00004-9

40. Saeidi M, Khasreji SN. Spectrophotometric determination of the pKa, isosbestic point and equation of absorbance vs. pH of methyl red indicator. *J Chem*. 2015;2015:1-6.

doi: 10.1155/2015/347621

41. Settimo L, Bellman K, Knegtel RM. Comparison of the accuracy of experimental and predicted pKa values of basic and acidic compounds. *Pharm Res*. 2014;31(4):1082-1095.

doi: 10.1007/s11095-013-1200-4

42. Dos Santos J, da Silva GS, Velho MC, Beck RCR. Eudragit®: A versatile family of polymers for hot melt extrusion and 3D printing processes in pharmaceutics. *Pharmaceutics*. 2021;13(9):1424.

doi: 10.3390/pharmaceutics13091424

43. European Medicines Agency. *Guideline on Excipients in the Dossier for Application for Marketing Authorisation of a Medicinal Product for Human Use (Revision 2)*. Amsterdam: European Medicines Agency; 2006.

44. Food and Drug Administration. *GRN 710 Amendments - Basic Methacrylate Copolymer (Eudragit®) Monograph*. United States: Food and Drug Administration; 2017.

45. Thakral S, Thakral NK, Majumdar DK. Eudragit®: A technology evaluation. *Expert Opin Drug Deliv*. 2013;10(1):131-149.

doi: 10.1517/17425247.2013.737604

46. Zamboulis A, Michailidou G, Koumentakou I, Bikiaris DN. Polysaccharide 3D printing for drug delivery applications. *Pharmaceutics*. 2022;14(1):145.

doi: 10.3390/pharmaceutics14010145

47. Peppas NA, Bures P, Leobandung WS, Ichikawa H. Hydrogels in pharmaceutical formulations. *Eur J Pharm Biopharm*. 2000;50(1):27-46.

doi: 10.1016/S0939-6411(00)00090-4

48. Meng Y, Qiu C, Li X, *et al*. Polysaccharide-based nano-delivery systems for encapsulation, delivery, and pH-responsive release of bioactive ingredients. *Crit Rev Food Sci Nutr*. 2024;64(1):187-201.

doi: 10.1080/10408398.2022.2081510

49. Dragan ES, Apopei DF. Multiresponsive macroporous semi-IPN composite hydrogels based on native or anionically modified potato starch. *Carbohydr Polym*. 2013;92(1):23-32.

doi: 10.1016/j.carbpol.2012.08.064

50. Sadeghi M, Hosseinzadeh H. Synthesis of starch-Poly (sodium acrylate-co-acrylamide) superabsorbent hydrogel with salt and pH-responsiveness properties as a drug delivery system. *J Bioact Compat Polym*. 2008;23(4):381-404.

doi: 10.1177/0883911508093122

51. Ghaffar AA, Radwan RR, Ali HE. Radiation synthesis of poly (starch/acrylic acid) pH sensitive hydrogel for rutin controlled release. *Int J Biol Macromol*. 2016;92:957-964.

doi: 10.1016/j.ijbiomac.2016.08.026

52. Kumar P, Ganure AL, Subudhi BB, Shukla S. Preparation and characterization of pH-sensitive methyl methacrylate-g-starch/hydroxypropylated starch hydrogels: *In vitro* and *in vivo* study on release of esomeprazole magnesium. *Drug Deliv Transl Res*. 2015;5(3):243-256.

doi: 10.1007/s13346-014-0238-7

53. Liu C, Gan X, Chen Y. A novel pH-sensitive hydrogels for potential colon-specific drug delivery: Characterization and *in vitro* release studies. *Starch-Stärke*. 2011;63(8):503-511.

doi: 10.1002/star.201000155

54. Tan HL, Wong YY, Muniyandy S, Hashim K, Pushpamalar J. Carboxymethyl sago pulp/carboxymethyl sago starch hydrogel: Effect of polymer mixing ratio and study of controlled drug release. *J Appl Polym Sci*. 2016;133(28):43697.

doi: 10.1002/app.43697

55. Clara I, Natchimuthu N. Hydrogels based on starch-g-poly (sodium-2-acrylamido-2-methyl-1-propane sulfonate-co-methacrylic acid) as controlled drug delivery systems. *Starch-Stärke*. 2017;69(7-8):1600177.

doi: 10.1002/star.201600177

56. Mahkam M. Modified chitosan cross-linked starch polymers for oral insulin delivery. *J Bioact Compat Polym*. 2010;25(4):406-418.

doi: 10.1177/0883911510373204

57. Saboktakin MR, Maharramov A, Ramazanov MA, Mahkam M. Modification of carboxymethyl starch as nano carriers for oral drug delivery. *Nat Sci*. 2007;5(3):67.

58. Saboktakin MR, Maharramov A, Ramazanov MA. pH-sensitive starch hydrogels via free radical graft copolymerization, synthesis and properties. *Carbohydr Polym*. 2009;77(3):634-638.

doi: 10.1016/j.carbpol.2009.02.016

59. Gils PS, Ray D, Mohanta GP, Manavalan R, Sahoo PK. Designing of new acrylic based macroporous superabsorbent polymer hydrogel and its suitability for drug delivery. *Int J Pharm Pharm Sci*. 2009;1:43-54.

60. Elvira C, Mano JF, San Roman J, Reis RL. Starch-based biodegradable hydrogels with potential biomedical applications as drug delivery systems. *Biomaterials*. 2002;23(9):1955-1966.

doi: 10.1016/S0142-9612(01)00331-5

61. Shaikh MMM, Gramopadhye NS, Wardole AA, Lonikar SV. Starch-acrylic acid hydrogel: Synthesis, characterization and drug release study. *World J Pharm Pharm Sci*. 2015;4:942-954.

62. Soares GA, Carbinatto FM, Cury BS, Evangelista RC. Effect of drying technique on some physical properties of cross-linked high amylose/pectin mixtures. *Drug Dev Ind Pharm*. 2013;39(2):284-289.

doi: 10.3109/03639045.2012.673895

63. Pereira AG, Fajardo AR, Nocchi S, Nakamura CV, Rubira AF, Muniz EC. Starch-based microspheres for sustained-release of curcumin: Preparation and cytotoxic effect on tumor cells. *Carbohydr Polym*. 2013;98(1):711-720.

doi: 10.1016/j.carbpol.2013.06.079

64. Chan AW, Whitney RA, Neufeld RJ. Semisynthesis of a controlled stimuli-responsive alginate hydrogel. *Biomacromolecules*. 2009;10(3):609-616.

doi: 10.1021/bm801047v

65. Sethi S, Saruchi S, Kaith BS, Kaur M, Sharma N, Kumar V. Cross-linked xanthan gum-starch hydrogels as promising materials for controlled drug delivery. *Cellulose*. 2020;27(8):4565-4589.

doi: 10.1007/s10570-020-03079-y

66. Akar E, Altınışık A, Seki Y. Preparation of pH-and ionic-strength responsive biodegradable fumaric acid crosslinked carboxymethyl cellulose. *Carbohydr Polym*. 2012;90(4):1634-1641.

doi: 10.1016/j.carbpol.2012.07.034

67. Chang C, He M, Zhou J, Zhang L. Swelling behaviors of pH-and salt-responsive cellulose-based hydrogels. *Macromolecules*. 2011;44(6):1642-1648.

doi: 10.1021/ma1027137

68. Yao KD, Peng T, Feng HB, He YY. Swelling kinetics and release characteristic of crosslinked chitosan: Polyether polymer network (semi-IPN) hydrogels. *J Polym Sci Part A Polym Chem*. 1994;32(7):1213-1223.

doi: 10.1002/pola.1994.080320703

69. Shu XZ, Zhu KJ, Song W. Novel pH-sensitive citrate cross-linked chitosan film for drug controlled release. *Int J Pharm*. 2001;212(1):19-28.

doi: 10.1016/S0378-5173(00)00574-6

70. Makhlof A, Tozuka Y, Takeuchi H. Design and evaluation of novel pH-sensitive chitosan nanoparticles for oral insulin delivery. *Eur J Pharm Sci*. 2011;42(5):445-451.

doi: 10.1016/j.ejps.2011.01.012

71. Ata S, Rasool A, Islam A, *et al*. Loading of Cefixime to pH sensitive chitosan based hydrogel and investigation of controlled release kinetics. *Int J Biol Macromol*. 2020;155:1236-1244.

doi: 10.1016/j.ijbiomac.2020.04.053

72. Aycan D, Alemdar N. Development of pH-responsive chitosan-based hydrogel modified with bone ash for

controlled release of amoxicillin. *Carbohydr Polym*. 2018;184:401-407.

doi: 10.1016/j.carbpol.2017.12.052

73. Liu L, Zhang Y, Yu S, *et al*. pH-and amylase-responsive carboxymethyl starch/poly (2-isobutyl-acrylic acid) hybrid microgels as effective enteric carriers for oral insulin delivery. *Biomacromolecules*. 2018;19(6):2123-2136.

doi: 10.1021/acs.biomac.8b00288

74. Zhang Z, Shan H, Chen L, He C, Zhuang X, Chen X. Synthesis of pH-responsive starch nanoparticles grafted poly (l-glutamic acid) for insulin controlled release. *Eur Polym J*. 2013;49(8):2082-2091.

doi: 10.1016/j.eurpolymj.2013.05.008

75. Desai KGH. Preparation and characteristics of high-amylose corn starch/pectin blend microparticles: A technical note. *AAPS PharmSciTech*. 2005;6(2):30.

doi: 10.1208/pt060230

76. Desai KG. Properties of tableted high-amylose corn starch-pectin blend microparticles intended for controlled delivery of diclofenac sodium. *J Biomater Appl*. 2007;21(3):217-233.

doi: 10.1177/0885328206064503

77. Kim SW, Oh KT, Youn YS, Lee ES. Hyaluronated nanoparticles with pH-and enzyme-responsive drug release properties. *Colloids Surf B Biointerfaces*. 2014;116:359-364.

doi: 10.1016/j.colsurfb.2014.01.026

78. Liu H, Rong L, Wang B, *et al*. Facile fabrication of redox/pH dual stimuli responsive cellulose hydrogel. *Carbohydr Polym*. 2017;176:299-306.

doi: 10.1016/j.carbpol.2017.08.106

79. Woraphatphadung T, Sajomsang W, Rojanarata T, Ngawhirunpat T, Tonglairoum P, Opanasopit P. Development of chitosan-based pH-sensitive polymeric micelles containing curcumin for colon-targeted drug delivery. *AAPS PharmSciTech*. 2018;19(3):991-1000.

doi: 10.1208/s12249-017-0941-0

80. Gaware SA, Rokade KA, Kale SN. Silica-chitosan nanocomposite mediated pH-sensitive drug delivery. *J Drug Deliv Sci Technol*. 2019;49:345-351.

doi: 10.1016/j.jddst.2018.11.029

81. Sung HW, Sonaje K, Liao ZX, Hsu LW, Chuang EY. pH-responsive nanoparticles shelled with chitosan for oral delivery of insulin: From mechanism to therapeutic applications. *Acc Chem Res*. 2012;45(4):619-629.

doi: 10.1021/ar200231h

82. Chandran S, Asghar LF, Mantha N. Design and evaluation of ethyl cellulose based matrix tablets of ibuprofen with pH modulated release kinetics. *Indian J Pharm Sci*. 2008;70(5):596.

doi: 10.4103/0250-474X.45970

83. Feng C, Wang Z, Jiang C, *et al*. Chitosan/o-carboxymethyl chitosan nanoparticles for efficient and safe oral anticancer drug delivery*: In vitro* and *in vivo* evaluation. *Int J Pharm*. 2013;457(1):158-167.

doi: 10.1016/j.ijpharm.2013.08.058

84. Hillery A, Park K. *Drug Delivery: Fundamentals and Applications*. United States: CRC Press; 2016.

85. Li J, Shin GH, Lee IW, Chen X, Park HJ. Soluble starch formulated nanocomposite increases water solubility and stability of curcumin. *Food Hydrocoll*. 2016;56:41-49.

doi: 10.1016/j.foodhyd.2015.12.001

86. Dutta S, Samanta P, Dhara D. Temperature, pH and redox responsive cellulose based hydrogels for protein delivery. *Int J Biol Macromol*. 2016;87:92-100.

doi: 10.1016/j.ijbiomac.2016.02.049

87. Wang Q, Hu X, Du Y, Kennedy JF. Alginate/starch blend fibers and their properties for drug controlled release. *Carbohydr Polym*. 2010;82(3):842-847.

doi: 10.1016/j.carbpol.2010.06.014

88. Huo W, Xie G, Zhang W, *et al*. Preparation of a novel chitosan-microcapsules/starch blend film and the study of its drug-release mechanism. *Int J Biol Macromol*. 2016;87:114-122.

doi: 10.1016/j.ijbiomac.2016.02.056

89. Verkhovskii RA, Ivanov AN, Lengert EV, *et al*. Current principles, challenges, and new metrics in pH-responsive drug delivery systems for systemic cancer therapy. *Pharmaceutics*. 2023;15(5):1566.

doi: 10.3390/pharmaceutics15051566

90. Wang Z, Wang X, Xu W, *et al*. Translational challenges and prospective solutions in the implementation of biomimetic delivery systems. *Pharmaceutics*. 2023;15(11):2623.

doi: 10.3390/pharmaceutics15112623

91. Ghodratı AD, Çomoğlu T. Mucoadhesive polymers in colon targeted drug delivery systems: A comprehensive review. *J Fac Pharm Ankara Univ*. 2023;48(2):696-713.

doi: 10.33483/jfpau.1206584

92. Jain A, Gupta Y, Jain SK. Azo chemistry and its potential for colonic delivery. *Crit Rev Ther Drug Carr Syst*. 2006;23(5):373-401.

doi: 10.1615/critrevtherdrugcarriersyst.v23.i5.30

93. Kumari A, Singh B. Emerging trends in designing polysaccharide based mucoadhesive network hydrogels as versatile platforms for innovative delivery of therapeutic agents: A review. *Int J Biol Macromol*. 2025;293(Pt 2):140229.

doi: 10.1016/j.ijbiomac.2024.140229

ACCSCIENCE PUBLISHING

Innovative Medicines & Omics

ORIGINAL RESEARCH ARTICLE

Antibacterial potential, phytochemical constituents, and toxicity assessment of *Azadirachta indica* leaf extracts in combination with antibiotics

Gagan Tiwana[1], Ian Edwin Cock[2,3], and Matthew James Cheesman[1]*

[1]School of Pharmacy and Medical Sciences, Gold Coast Campus, Griffith University, Parklands Drive, Southport, Queensland, Australia

[2]School of Environment and Science, Nathan Campus, Griffith University, Nathan, Queensland, Australia

[3]Environmental Futures Research Institute, Nathan Campus, Griffith University, Nathan, Queensland, Australia

Abstract

The rise of antimicrobial resistance (AMR) has highlighted the need for exploration of alternative therapeutic agents, including medicinal plants. This study investigates the antibacterial potential, phytochemical composition, and toxicity of *Azadirachta indica* leaf extracts, along with their interactions with conventional antibiotics. Extracts prepared in water (AQ), methanol (MeOH), and ethyl acetate (EtOAc) were evaluated for growth-inhibitory effects against a range of bacterial species, including drug-resistant isolates, through both disc diffusion and microdilution methods. Zone of inhibition (ZOI) measurements ranged from 7 to 10 mm, while minimum inhibitory concentration values varied between 2938 and 5875 μg/mL for AQ extracts, and between 1175 and 4700 μg/mL for MeOH extracts. Notably, EtOAc extracts did not inhibit bacterial growth in either assay. Fractional inhibitory concentration (FIC) analysis revealed additive interactions of extracts with β-lactam antibiotics (penicillin G, oxacillin, amoxicillin) and protein synthesis inhibitors (tetracycline, chloramphenicol), particularly against *Bacillus cereus*, *Staphylococcus aureus*, and *Shigella* spp., suggesting a potential role as antibiotic adjuvants. However, antagonistic interactions were also observed in combinations containing gentamicin and polymyxin B. Liquid chromatography–mass spectrometry (LC-MS) analysis confirmed the presence of phytochemicals, including flavonoids, tannins, and phenolics, which are known for their antimicrobial properties. Evaluation of extract safety using brine shrimp (*Artemia franciscana*) assays revealed no toxic responses. To ensure their safety for therapeutic applications, future toxicity evaluations should be conducted on mammalian cell lines to confirm these findings. Future research should focus on isolating bioactive compounds from the extracts, elucidating their mechanisms of action, and optimizing extract-antibiotic formulations to combat resistant bacterial infections effectively.

Keywords: Phytochemicals; Medicinal plants; Antibiotic combinations; Natural antibacterial agents; LC-MS profiling

***Corresponding author:**
Matthew James Cheesman
(m.cheesman@griffith.edu.au)

Citation: Tiwana G, Cock IE, Cheesman MJ. Antibacterial potential, phytochemical constituents, and toxicity assessment of *Azadirachta indica* leaf extracts in combination with antibiotics. *Innov Med Omics*. 2026;3(1):15-31.
doi: 10.36922/IMO025310036

Received: July 30, 2025

Revised: September 22, 2025

Accepted: October 10, 2025

Published online: November 28, 2025

1. Introduction

Antimicrobial resistance (AMR) develops as microbes such as bacteria, parasites, fungi, and viruses acquire resistance to drugs, which compromises standard therapies and allows infections to continue unchecked.[1] This issue represents a major challenge to global health by undermining the treatment of routine infections and contributing to extended sickness, long-term complications, and mortality. The impact of AMR on healthcare systems is profound. In the United States alone, more than 2.8 million antimicrobial-resistant infections occur each year, leading to over 35,000 deaths.[2] Globally, drug-resistant infections were responsible for approximately 5 million deaths in 2019, with nearly 1.3 million directly attributable to AMR. Projections suggest that if effective measures are not implemented, AMR could result in 10 million deaths annually by 2050, surpassing the mortality rates of cancer.[2] AMR also imposes a substantial economic burden. The World Bank estimates that by 2050, unchecked AMR could reduce global gross domestic product by 3.8% annually and push 28 million people into poverty.[2] In the healthcare sector, treating AMR threats contributes more than $4.6 billion to healthcare costs annually in the United States.[3] These economic strains are exacerbated by increased hospital stays, the need for more intensive care, and the use of expensive drugs.

In response to the escalating AMR crisis, there is a growing interest in exploring alternative therapeutic options, including the use of medicinal plants. Historically, plants have been a rich source of antimicrobial agents. Indeed, flavonoids, alkaloids, and essential oils extracted from medicinal plants have demonstrated significant antimicrobial properties.[4] Recent studies have also highlighted the potential of plant-derived compounds to combat multidrug-resistant pathogens.[4,5] For example, sophoraflavanone G isolated from *Sophora flavescens* Aiton. has potent antibacterial activity against clinical isolates of methicillin-resistant *Staphylococcus aureus* (MRSA), with minimum inhibitory concentrations (MICs) of 0.5–8 μg/mL.[6] In addition, synergistic interactions of sophoraflavanone G were observed with ampicillin and oxacillin against MRSA.

The integration of medicinal plants into antimicrobial strategies offers a promising avenue to address the challenges posed by AMR.[7,8] Their diverse chemical structures and mechanisms of action provide a valuable resource for developing new antimicrobial agents that can either serve as alternatives to, or enhance the efficacy of, existing antibiotics.[9] However, it is crucial to conduct further research to fully understand their potential, ensure their safety, and develop effective formulations for clinical use.

The current research examines the inhibitory effects of *Azadirachta indica* A. Juss. leaf extracts on different bacterial species. Previous studies have demonstrated the antibacterial activity of *A. indica* leaf extracts against *S. aureus*, *Escherichia coli*, *Klebsiella pneumoniae* using standard disc diffusion and agar well diffusion methods.[10-12] While these assays provide preliminary insights into the inhibitory effects of *A. indica*, they are qualitative and limited in their ability to determine the precise MIC required to inhibit bacterial growth. The absence of microdilution assays, which are the gold standard for quantifying MIC values,[13] raises concerns regarding the accuracy and reproducibility of these findings. Without MIC determination, it is difficult to assess the true potency of *A. indica* extracts, especially against resistant strains.

Furthermore, many of these studies have not investigated the potential synergistic or antagonistic interactions between *A. indica* plant extracts and antibiotics. The combinatory effects of plant extracts with conventional antibiotics may offer valuable insights into alternative therapeutic approaches to combat AMR. However, the lack of such studies leaves a significant gap in understanding the full potential of these combinations. Addressing these gaps by incorporating rigorous MIC determination and combinational studies would provide more reliable and comprehensive data on the efficacy of plant extracts.

This research aims to bridge existing knowledge gaps by investigating the antibacterial properties of *A. indica* leaf extracts against multiple bacterial strains, including *Bacillus cereus*, *Shigella flexneri*, *Shigella sonnei*, *S. aureus*, MRSA, *E. coli*, *K. pneumoniae*, and extended-spectrum β-lactamase (ESBL)-producing isolates of *E. coli* and *K. pneumoniae*. Liquid chromatography–mass spectrometry (LC–MS) was employed to characterize compounds potentially contributing to the antibacterial effects. We further assessed extract–antibiotic combinations by calculating the fractional inhibitory concentration (FIC) index, which allowed evaluation of synergistic antibacterial effects. Furthermore, an initial toxicity examination was carried out using *Artemia franciscana* nauplii lethality assays (ALA) to evaluate the safety profile of the plant extracts. By integrating these methodologies, this study aims to provide comprehensive and reliable data on the potential of *A. indica* leaf extracts as an alternative to, or complementary strategy against bacterial resistance to, clinical antibiotics.

2. Materials and methods

2.1. Plant supplies

Powdered leaf material of *A. indica* (batch no: NLP1020) was purchased from Sattvic Goods and Services (Melbourne, Australia) and supplied by Aarshaveda. The

plant product was identified on the supplier's website using its Ayurvedic names, *i.e.*, Neem and Indian Lilac. According to the supplier, the material was verified for purity and authenticity, and originated from India, where mature leaves had been dried under ambient conditions before being finely milled. A voucher specimen (NBG-AzI0221GU) has been deposited in the School of Pharmacy and Medical Sciences, Griffith University (Southport, Australia).

2.2. Extract preparation

The extraction of *A. indica* leaf powder followed a previously described method.[14] Briefly, 1 g of powdered leaves was soaked in 50 mL of sterile deionized water (AzI-AQ), methanol (AzI-MeOH), or ethyl acetate (AzI-EtOAc) and kept at room temperature with gentle agitation on a roller for 24 h. Analytical-grade solvents were sourced from Thermo Fisher Scientific Inc. (Melbourne, Australia). After extraction, the mixtures were vacuum-filtered. The aqueous extracts were subsequently lyophilized in a freeze dryer (Martin Christ, Germany) for 72 h, whereas the organic solvent extracts were evaporated in a water bath under a fume hood at 42°C. The dried material was then weighed, redissolved in 10 mL of 1% DMSO (Merck Life Science Pty. Ltd., Bayswater, Australia), filtered through 0.2 μm membranes (Sarstedt Australia Pty. Ltd., Mawson Lakes, Australia), and preserved at −20°C until further testing.

2.3. Antibiotics and bacterial strains

Antibiotics used in this study, either in powdered or disc form, included penicillin G, ciprofloxacin, polymyxin B, oxacillin, amoxicillin, erythromycin, tetracycline, chloramphenicol, gentamicin, vancomycin, Augmentin®, and cefotixin (Merck Life Science Pty. Ltd., Bayswater, Australia). Stock solutions of powdered antibiotics were prepared at 1 mg/mL for microdilution assays and stored at −20°C. Amoxicillin discs were prepared by applying 10 μL of a 10 μg/mL stock solution onto sterile filter paper discs.

Reference bacterial strains included *S. sonnei* (American Type Culture Collection [ATCC] 25931), *Salmonella enterica* serovar *typhimurium* (ATCC 14028), *S. flexneri* (ATCC 12022), *B. cereus* (ATCC 14579), *K. pneumoniae* (ATCC 13883), ESBL-producing *K. pneumoniae* (ATCC 700603), *E. coli* (ATCC 25922), *S. aureus* (ATCC 25923), and MRSA (ATCC 43300), sourced from the ATCC through In Vitro Technologies (Noble Park North, Australia). In addition, an ESBL-producing *E. coli* clinical isolate was provided by Gold Coast University Hospital (Southport, Australia). Cultures were maintained on Mueller–Hinton (MH) agar and broth, with MRSA grown at 35°C and all other strains at 37°C for 18–24 h.[14]

2.4. Antibacterial susceptibility test

The antibacterial activity of the plant extracts was examined using a modified Kirby–Bauer disc diffusion approach.[14] Overnight bacterial cultures were prepared in MH broth and standardized to a 0.5 McFarland turbidity. For the assays, 100 μL of each suspension was spread evenly across MH agar plates (37°C incubation, or 35°C in the case of MRSA). Sterile 6.0 mm Whatman filter paper discs were loaded with 10 μL of extract dissolved in 1% DMSO, while discs containing reference antibiotics were included as comparators. Each assay was carried out in triplicate, and all plates were subsequently incubated under the same temperature conditions for 18–24 h.

2.5. Calculation of MIC

MICs of the extracts and reference drugs were assessed through a 96-well plate microdilution assay.[14] In each well, 100 μL of MH broth was dispensed, and the first well of each row received 100 μL of extract or antibiotic solution. Serial twofold dilutions were then prepared across the row. Each well was subsequently inoculated with 100 μL of a 1:100 dilution of a 0.5 McFarland bacterial suspension, except for sterile controls. Plates were incubated at 37°C for 20–24 h. Following incubation, 40 μL of p-iodonitrotetrazolium violet (INT) (0.4 mg/mL, Sigma Aldrich, Australia) was added, and plates were further incubated at room temperature for 2–4 h. MIC values were identified as the lowest concentration of the extract or antibiotic that completely suppressed bacterial growth, confirmed by the absence of a red or pink color change. All assays were conducted in duplicate. The antibacterial activity of extracts was interpreted according to the classification proposed by Eloff,[15] where MIC values are categorized as outstanding (<20 μg/mL), excellent (21–40 μg/mL), very good (41–80 μg/mL), good (81–160 μg/mL), average (161–320 μg/mL), and weak (>320 μg/mL).

2.6. Fractional inhibitory concentration analysis

Extracts and antibiotics showing antibacterial effects (MIC ≤6000 μg/mL for extracts; ≤2.5 μg/mL for antibiotics) were selected for subsequent combination testing. Extract–antibiotic mixtures were prepared in equal volumes (1:1 ratio), and their effects against the bacterial panel were assessed using the sum of fractional inhibitory concentration (ΣFIC) approach.

The ΣFIC values for each combination were calculated using the following formulas:

$$FIC(A) = \frac{\text{MIC of A in combination}}{\text{MIC of A alone}}$$

$$FIC(B) = \frac{\text{MIC of B in combination}}{\text{MIC of B alone}}$$

$$\Sigma FIC = FIC(A) + FIC(B)$$

Outcomes were interpreted as follows: synergistic when $\Sigma FIC \leq 0.5$, additive when $0.5 < \Sigma FIC \leq 1.0$, indifferent when $1.0 < \Sigma FIC \leq 4.0$, and antagonistic when $\Sigma FIC > 4.0$.[16]

2.7. Toxicity assays

The safety of the extracts was evaluated through the ALA.[14] Briefly, 400 µL of each extract (2 mg/mL in artificial seawater) was combined with 400 µL of artificial seawater containing newly hatched *A. franciscana* nauplii (≤1 day old) in 48-well plates. Negative controls consisted of seawater alone (32 g/L, Red Sea), while sodium azide (1 mg/mL) served as the positive control. All assays were carried out in parallel and incubated at 25 ± 1°C for 24 h. Survival of the nauplii was then recorded, and lethal concentration 50 (LC_{50}) values, representing the concentration required to kill 50% of the test organisms, were determined using probit analysis. The LC_{50} values represent averages obtained from three separate experiments.

2.8. LC-MS-based metabolomic profiling

Untargeted metabolic profiling of the extracts was conducted using a Vanquish UHPLC system (Thermo Fisher Scientific) coupled to an Orbitrap Exploris 120 mass spectrometer. Separation was achieved on an Accucore™ RP-MS column with a flow rate of 0.6 mL/min, employing a 24-min gradient elution.[14] The mobile phases consisted of ultrapure water with 0.1% formic acid (A) and acetonitrile with 0.1% formic acid (B). Mass spectrometric analysis was performed in negative ionization mode using electrospray ionization, with predefined parameters for spray voltage, temperature, and gas flow. Data were processed in Compound Discoverer™ 3.3, employing the natural product unknown ID workflow. Detected metabolites were filtered against blanks and annotated through databases such as MzCloud, ChemSpider, and MassList. Identified metabolites were exported into Excel spreadsheets, and their relative levels were reported as percentages of the overall detected signal.

2.9. Statistical analysis

For disc diffusion assays, inhibition zone diameters (zone of inhibition [ZOI]) were measured in millimeters, with 6 mm taken as the baseline for non-active extracts. Data are expressed as mean ± standard error of the mean and visualized using bar graphs based on at least three independent replicates. Statistical comparisons were carried out using one-way ANOVA, where $p<0.01$ (* significant) and $p<0.001$ (** highly significant) indicated statistical significance. MIC data from broth microdilution tests were analyzed in triplicate, and outcomes for each extract and antibiotic were reported separately. All MIC and FIC values were calculated following two independent experiments on separate days to ensure the reproducibility of the findings.

3. Results

3.1. Antimicrobial susceptibility analysis

The antimicrobial activity of aqueous (AzI-AQ), methanol (AzI-MeOH), and ethyl acetate (AzI-EtOAc) extracts was evaluated against ten bacterial strains using disc diffusion (ZOI) and broth microdilution (MIC) assays. The results varied significantly among the bacterial strains, with the MeOH extract demonstrating the most promising antibacterial potential (Figures 1 and 2, Table 1). In contrast, AQ and EtOAc extracts were largely inactive, exhibiting high MIC values and minimal ZOI.

B. cereus exhibited moderate antibacterial susceptibility, particularly to the MeOH extract, which produced a ZOI of 9.0 mm and the lowest MIC value (1175 µg/mL). The AQ extract produced a ZOI of 7.0 mm, but its high MIC value (5875 µg/mL) suggested weak inhibition. The EtOAc extract was entirely inactive, as indicated by a ZOI of 6.0 mm and an MIC exceeding 10,000 µg/mL.

S. flexneri was substantially more susceptible compared to *S. sonnei*. *S. flexneri* was moderately susceptible to the MeOH extract (ZOI = 10.0 mm, MIC = 4700 µg/mL), whilst the AQ extract exhibited only weak inhibitory activity (ZOI = 7.0 mm, MIC = 5875 µg/mL). The EtOAc extract was completely inactive. In contrast, *S. sonnei* was far less susceptible, showing no significant inhibition across all extracts, as evidenced by ZOI values of 6.0 mm (equivalent to the filter paper control). However, the AQ extract had an MIC of 2938 µg/mL, and MeOH exhibited an MIC of 4700 µg/mL, suggesting some minor inhibition at high concentrations. The difference in response between these two strains of the same species suggests strain-dependent variation in susceptibility to plant extracts. *Salmonella typhimurium* followed a trend similar to *B. cereus* and *S. flexneri*, with moderate activity in the MeOH extract (ZOI = 8.7 mm, MIC = 4700 µg/mL), but weak activity for the AQ extract (ZOI = 7.0 mm, MIC = 5875 µg/mL). The EtOAc extract was inactive against both bacteria.

The MeOH extract demonstrated activity against *S. aureus*, exhibiting a ZOI of 9.0 mm and an MIC of 2350 µg/mL. In contrast, neither the AQ nor EtOAc

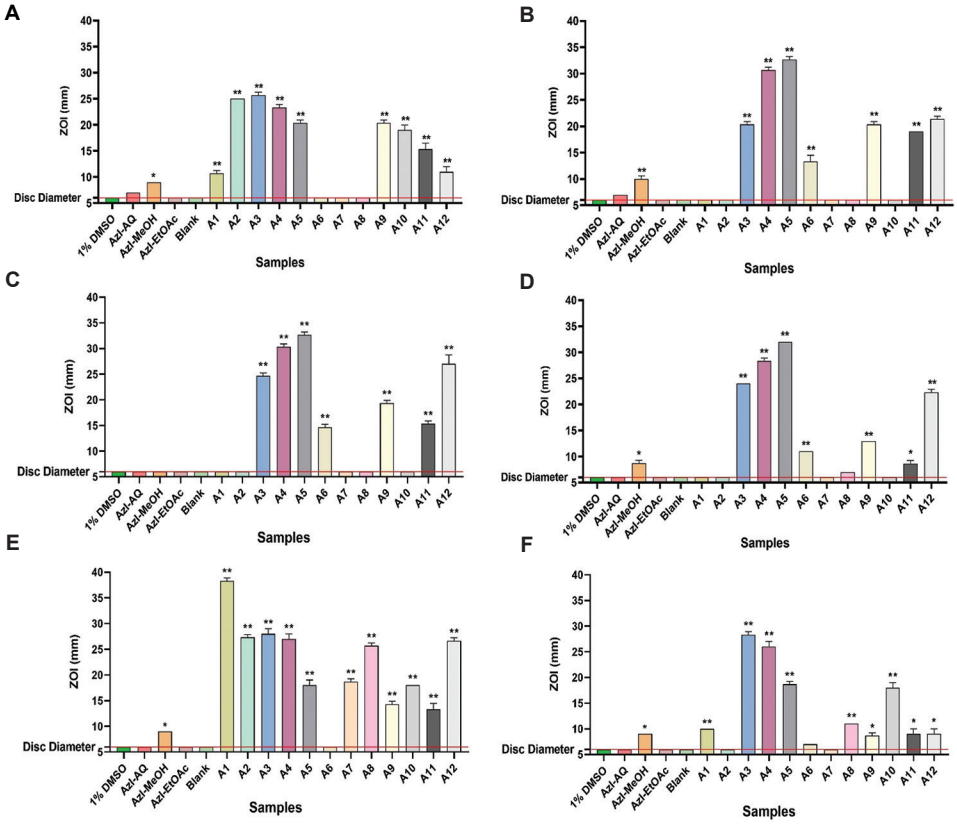

Figure 1. Antibacterial effects of *Azadirachta indica* leaf extracts were assessed using the disc diffusion method against bacterial species: (A) *Bacillus cereus*, (B) *Shigella flexneri*, (C) *S. sonnei*, (D) *Salmonella typhimurium*, (E) *Staphylococcus aureus*, and (F) methicillin-resistant *Staphylococcus aureus* (MRSA). Extracts tested included aqueous (AzI-AQ), methanolic (AzI-MeOH), and ethyl acetate (AzI-EtOAc). Negative controls consisted of 1% DMSO and sterile water (Blank). A panel of reference antibiotics was included for comparison: A1 (penicillin G), A2 (erythromycin), A3 (tetracycline), A4 (chloramphenicol), A5 (ciprofloxacin), A6 (polymyxin B), A7 (oxacillin), A8 (amoxicillin), A9 (gentamicin), A10 (vancomycin), A11 (Augmentin®), and A12 (cefoxitin). The y-axis line at 6 mm denotes the disc diameter employed in the study. Results are expressed as mean inhibition zones (±standard error of the mean) based on three independent experiments. *p<0.01, **p<0.001.

extracts exhibited any activity. Interestingly, MRSA showed a similar susceptibility pattern, with MeOH (ZOI = 9.0 mm, MIC = 2350 µg/mL) being active whilst AQ and EtOAc extracts were ineffective. The MeOH extract was not significantly affected by the resistance mechanism of MRSA, indicating that its active compounds may act through a different pathway.

E. coli was also moderately susceptible to the MeOH extract, with a ZOI of 9.3 mm and an MIC of 4700 µg/mL. The AQ and EtOAc extracts were inactive in both assays. The MeOH extract exhibited consistent activity against ESBL *E. coli*, with a ZOI of 9.3 mm and an MIC of 4700 µg/mL. This suggests that the resistance mechanism in this strain does not interfere with the extract's mode of action.

None of the extracts showed activity against *K. pneumoniae* in the disc diffusion assay, with all producing ZOI values of only 6.0 mm in the disc diffusion assay for all extracts. However, the MeOH extract produced an MIC of 4700 µg/mL, suggesting weak antibacterial activity. AQ and EtOAc extracts were completely inactive against this bacterium. ESBL-producing *K. pneumoniae* was completely resistant to all extracts, with no measurable antibacterial effects in either assay. Thus, the ESBL-producing *K. pneumoniae* strain was the most resistant bacterium screened in this study.

3.2. Combinational analysis: Fractional inhibitory concentration determination

The ∑FIC analysis revealed varying degrees of interaction between *A. indica* extracts and reference antibiotics against the tested bacterial strains (Table 2). Additive interactions were observed in 20 instances, indicating cases where the combination moderately enhanced antibacterial activity. Indifferent interactions were the most common class of interaction, with 32 occurrences, suggesting that the extract-antibiotic combinations did not significantly

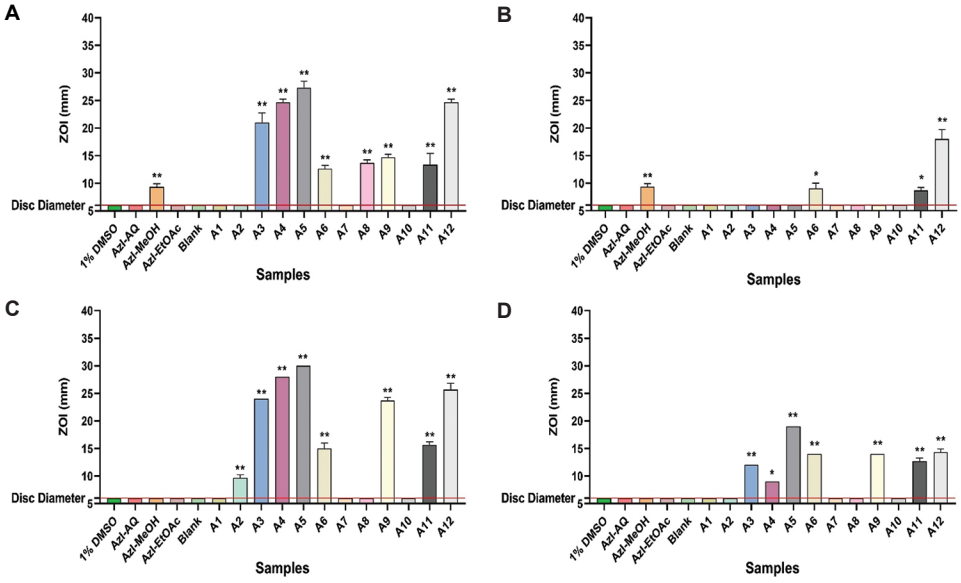

Figure 2. Antibacterial effects of *Azadirachta indica* leaf extracts were assessed using the disc diffusion method against bacterial species: (A) *Escherichia coli*, (B) ESBL-producing *Escherichia coli*, (C) *Klebsiella pneumoniae*, (D) ESBL-producing *Klebsiella pneumoniae*. Extracts tested included aqueous (AzI-AQ), methanolic (AzI-MeOH), and ethyl acetate (AzI-EtOAc). Negative controls consisted of 1% DMSO and sterile water (Blank). A panel of reference antibiotics was included for comparison: A1 (penicillin G), A2 (erythromycin), A3 (tetracycline), A4 (chloramphenicol), A5 (ciprofloxacin), A6 (polymyxin B), A7 (oxacillin), A8 (amoxicillin), A9 (gentamicin), A10 (vancomycin), A11 (Augmentin®), and A12 (cefoxitin). The y-axis line at 6 mm denotes the disc diameter employed in the study. Results are expressed as mean inhibition zones (±standard error of the mean) based on three independent experiments. *p<0.01, **p<0.001.

Table 1. Minimum inhibitory concentrations (MIC) of *Azadirachta indica* leaf extracts (AzI-AQ, AzI-MeOH, AzI-EtOAc) and control antibiotics evaluated against a panel of ten bacterial species

Extract type or antibiotic	Bacterial species and MIC (μg/mL)									
	Bacillus cereus	*Shigella flexneri*	*Shigella sonnei*	*Shigella typhimurium*	*Shigella aureus*	MRSA	*Escherichia coli*	ESBL-producing *E. coli*	*Klebsiella pneumoniae*	ESBL-producing *Klebsiella pneumoniae*
AzI-AQ	5875	5875	2938	5875	-	-	-	-	-	-
AzI-MeOH	1175[a]	4700	4700	4700	2350	2350	4700	4700	4700	-
AzI-EtOAc	-	-	-	-	-	-	-	-	-	-
A1	-	-	-	0.625	1.25	-	-	-	-	-
A2	-	-	-	0.08	0.31	-	-	-	-	-
A3	0.625	0.31	0.625	0.08	0.16	0.04	0.31	-	0.625	-
A4	-	2.5	1.25	1.25	-	-	2.5	-	2.5	-
A5	0.02	0.02	0.02	0.08	0.16	0.625	0.02	-	0.02	0.16
A6	0.31	0.31	0.31	-	-	-	0.02	0.02	0.02	0.04
A7	-	-	-	1.25	0.16	-	-	-	-	-
A8	-	-	-	0.625	0.625	-	-	-	-	-
A9	0.625	2.5	0.625	0.16	-	-	0.625	-	0.625	-
A10	-	-	-	0.625	1.25	1.25	-	-	-	-

Notes: MIC values of the extracts are categorized by activity: >10,000 μg/mL are considered inactive (–); low activity ranges from 2000 to 6000 μg/mL; moderate activity ranges from 1000 to 2000 μg/mL, denoted with [a]. Active antibiotics are shown in bold, whilst those with MIC >2.5 μg/mL are marked as inactive (–). Reference antibiotics: A1 (penicillin G), A2 (erythromycin), A3 (tetracycline), A4 (chloramphenicol), A5 (ciprofloxacin), A6 (polymyxin B), A7 (oxacillin), A8 (amoxicillin), A9 (gentamicin), A10 (vancomycin).

impact each other's effectiveness. Antagonistic interactions were noted in 17 cases, demonstrating instances where the combination reduced antibacterial efficacy. These results not only highlight the potential of *A. indica* extracts

Table 2. Fractional inhibitory concentration (ΣFIC) indices from interactions between *Azadirachta indica* leaf extracts and reference antibiotics

Bacteria	Extracts	A1	A2	A3	A4	A5	A6	A7	A8	A9	A10
Bacillus cereus	AzI-Aq	0.62[a]	2.06	2.06	1.50	1.03	-	1.00a	2.50	8.30b	1.25
	AzI-MeOH	0.51[a]	2.25	2.25	1.50	2.25	-	0.51[a]	0.51[a]	8.81[b]	2.00
Shigella flexneri	AzI-Aq	-	-	0.63[a]	0.75[a]	1.03	31.50[b]	-	-	1.25	-
	AzI-MeOH	-	-	0.63[a]	0.75[a]	2.06	31.50[b]	-	-	>4[b]	-
Shigella sonnei	AzI-Aq	-	-	1.25	0.75[a]	1.06	31.75[b]	-	-	0.75[a]	-
	AzI-MeOH	-	-	4.50[b]	1.00[a]	2.06	31.50[b]	-	-	1.00[a]	-
Shigella typhimurium	AzI-Aq	-	-	1.25	1.00[a]	2.06	4.53[b]	-	-	>4[b]	-
	AzI-MeOH	-	-	0.63[a]	1.00[a]	1.06	4.53[b]	-	-	>4[b]	-
Shigella aureus	AzI-MeOH	1.00[a]	1.25	1.13	-	2.19	-	2.25	0.75[a]	-	1.00[a]
MRSA	AzI-MeOH	-	-	1.03	-	1.50	-	-	-	-	2.00
E. coli	AzI-MeOH	-	-	1.06	1.00[a]	1.06	>4[b]	-	-	1.06	-
ESBL-producing *E. coli*	AzI-MeOH	-	-	-	-	-	63.00[b]	-	-	-	-
Klebsiella pneumoniae	AzI-MeOH	-	-	1.25	>4[b]	2.13	63.00[b]	-	-	>4[b]	-

Notes: TheΣFIC values of *A. indica* extracts—aqueous (AzI-AQ), methanolic (AzI-MeOH), and ethyl acetate (AzI-EtOAc) were assessed in combination with standard antibiotics against *Bacillus cereus*, *Shigella flexneri*, *Shigella sonnei*, *Shigella typhimurium*, *Shigella aureus*, MRSA, *E. coli*, ESBL-producing *E. coli*, and *Klebsiella pneumoniae*. Additive effects (ΣFIC>0.5–1.0) are indicated with [a]; indifferent effects (>1.0–4.0) are shown with the exact values; and antagonistic effects (>4.0) are indicated with [b]. A dash (–) indicates inactivity of either the extract or antibiotic. Reference antibiotics: A1 (penicillin G), A2 (erythromycin), A3 (tetracycline), A4 (chloramphenicol), A5 (ciprofloxacin), A6 (polymyxin B), A7 (oxacillin), A8 (amoxicillin), A9 (gentamicin), A10 (vancomycin).
Abbreviation: *E. coli: Escherichia coli.*

in combination therapy but also emphasize the need for careful selection, as antagonistic interactions may compromise treatment effectiveness. Further investigation is necessary to determine the mechanisms behind these interactions and optimize extract-antibiotic pairings for enhanced therapeutic outcomes.

3.3. LC-MS-based metabolomic profiling and compound identification

LC-MS was employed for metabolomic profiling of the extracts, and compounds were identified by comparison across several databases. The profiling aimed to capture a broad range of metabolites, with particular focus on flavonoids, phenolic acids, tannins, and terpenoids. The majority of detected compounds showed moderate to low polarity, aligning with their elution in the 30–90% acetonitrile gradient region of the chromatogram (Figure S1).[17] Polar compounds such as organic acids and amines appeared at the beginning of the chromatogram, whereas less polar metabolites eluted later at higher acetonitrile levels because of their stronger interaction with the non-polar stationary phase. To maintain reliability, only compounds confirmed by at least one database were retained in the final list (Table S1). The study emphasized phenolic acids, tannins, flavonoids, and terpenoids (Table 3) due to their documented biological importance.[18]

3.4. Toxicity examination

The plant extracts were evaluated for toxicity through the *Artemia franciscana* nauplii lethality bioassay.[14] Toxicity was assigned to extracts that produced LC_{50} values at or below 1000 μg/mL after a 24-h treatment period.[19] Results showed no significant difference between extracts and the negative control (artificial seawater) (p>0.05), as none of the extracts caused ≥50% mortality at 1000 μg/mL. Therefore, the tested extracts were considered non-toxic.

4. Discussion

This investigation assessed *A. indica* leaf extracts against clinically important bacterial pathogens, including drug-resistant strains. Both aqueous (AQ) and methanolic (MeOH) extracts demonstrated inhibitory activity, suppressing the growth of four and nine out of ten tested organisms, respectively, highlighting their potential as candidates for antibacterial drug development. Methanol-derived extracts exhibited the highest levels of inhibition in disc diffusion and broth microdilution assays, in contrast to the weaker activity observed with

Table 3. LC-MS–based tentative identification and percentage relative abundance of phytochemicals detected in *Azadirachta indica* extracts

Retention time (minutes)	Molecular weight	Empirical formula	Putative compounds	Relative abundance (% of total area)		
				AQ	MeOH	EtOAc
1.622	192.06319	$C_7H_{12}O_6$	D-(-)-Quinic acid	0.12	0.17	-
1.648	356.0376	$C_{14}H_{12}O_{11}$	(+)-Chebulic acid	0.24	-	-
1.671	134.02139	$C_4H_6O_5$	D-(+)-Malic acid	-	5.76	-
1.881	322.03203	$C_{14}H_{10}O_9$	Digallic acid	0.06	-	-
1.893	332.07405	$C_{13}H_{16}O_{10}$	6-Galloylglucose	0.11	0.08	-
1.973	126.03156	$C_6H_6O_3$	Pyrogallol	-	0.52	-
2.215	244.05813	$C_{10}H_{12}O_7$	1-O-Galloylglycerol	-	0.11	-
2.928	484.08511	$C_{20}H_{20}O_{14}$	Hamamelitannin	-	S	-
3.238	324.1782	$C_{14}H_{28}O_8$	Caryophyllan	0.04	-	-
3.504	306.07383	$C_{15}H_{14}O_7$	(+) -Gallocatechin	-	0.02	-
3.385	212.06823	$C_{10}H_{12}O_5$	Propyl gallate	-	-	0.87
4.292	484.08512	$C_{20}H_{20}O_{14}$	1,6-Bis-O-(3,4,5-trihydroxybenzoyl) hexopyranose	-	0.14	-
4.679	388.13699	$C_{17}H_{24}O_{10}$	Geniposide	0.02	0.04	-
5.428	178.02645	$C_9H_6O_4$	Aesculetin	-	0.03	-
6.89	192.02685	$C_6H_8O_7$	Citric acid	0.24	0.15	-
7.114	196.07336	$C_{10}H_{12}O_4$	Cantharidin	0.08	0.08	-
8.728	288.08412	$C_{12}H_{16}O_8$	Phlorin	0.02	-	-
9.117	294.09484	$C_{11}H_{18}O_9$	Tuliposide B	S	-	-
9.559	596.17414	$C_{27}H_{32}O_{15}$	Hovetrichoside D	0.03	-	-
9.677	478.07486	$C_{21}H_{18}O_{13}$	8-Hydroxyluteolin 8-glucuronide	-	0.03	-
9.758	342.13117	$C_{16}H_{22}O_8$	Coniferin	-	S	-
9.996	610.15321	$C_{27}H_{30}O_{16}$	Rutin	S	10.23	1.27
10.216	304.05805	$C_{15}H_{12}O_7$	Nigrescin	S	0.10	-
9.758	342.13117	$C_{16}H_{22}O_8$	Coniferin	-	S	-
10.252	636.0961	$C_{27}H_{24}O_{18}$	1,2,6-Trigalloyl-β-D-glucopyranose	-	0.58	-
10.468	490.205	$C_{22}H_{34}O_{12}$	Cymorcin diglucoside	0.02	-	-
10.494	450.11711	$C_{21}H_{22}O_{11}$	Hovetrichoside C	0.02	-	-
10.58	610.15312	$C_{27}H_{30}O_{16}$	Quercetin 3-O-rhamnoside-7-O-glucoside	0.02	-	-
10.66	434.04844	$C_{19}H_{14}O_{12}$	Ellagic acid arabinoside	S	-	-
10.679	222.0526	$C_{11}H_{10}O_5$	Isofraxidin	S	-	-
10.706	480.09005	$C_{21}H_{20}O_{13}$	Myricetin 3-O-β-D-galactopyranoside	-	0.95	-
10.869	192.04216	$C_{10}H_8O_4$	7-Hydroxy-6-methoxy-2H-chromen-2-one	1.32	0.55	9.26
10.885	302.00606	$C_{14}H_6O_8$	Ellagic acid	1.93	4.17	-
10.893	318.00087	$C_{14}H_6O_9$	flavellagic acid	0.02	-	-
10.931	254.07899	$C_{12}H_{14}O_6$	Balticol C	0.02	-	-
10.955	568.21535	$C_{27}H_{36}O_{13}$	Citrusin B	0.04	-	-
10.965	192.04212	$C_{10}H_8O_4$	Scopoletin	-	1.06	-
10.971	190.13559	$C_{13}H_{18}O$	Heptanophenone	0.07	-	1.67
10.987	286.04744	$C_{15}H_{10}O_6$	Maritimetin	0.02	-	-
11.026	418.16258	$C_{22}H_{26}O_8$	Lirioresinol A	S	-	-

(Cont'd...)

Table 3. ***(Continued)***

Retention time (minutes)	Molecular weight	Empirical formula	Putative compounds	Relative abundance (% of total area)		
				AQ	MeOH	EtOAc
11.026	176.04729	$C_{10}H_8O_3$	4-Methylumbelliferone hydrate	0.28	-	-
11.066	262.04771	$C_{13}H_{10}O_6$	Maclurin	S	S	-
11.103	524.22562	$C_{26}H_{36}O_{11}$	Mascaroside	0.09	-	-
11.135	304.05816	$C_{15}H_{12}O_7$	(2R,3R) -Taxifolin	0.03	-	-
11.233	464.09493	$C_{21}H_{20}O_{12}$	Hyperoside	-	1.41	-
11.287	196.10975	$C_{11}H_{16}O_3$	Angupyrone E	0.15	-	-
11.287	464.09536	$C_{21}H_{20}O_{12}$	Myricitrin	0.61	6.71	-
11.348	312.12097	$C_{15}H_{20}O_7$	Nivalenol	-	S	-
11.42	126.03156	$C_6H_6O_3$	Phloroglucinol	0.16	0.16	-
11.445	522.2101	$C_{26}H_{34}O_{11}$	Lariciresinol 4-O-glucoside	0.05	0.13	-
11.485	304.058	$C_{15}H_{12}O_7$	Taxifolin	0.03	0.08	-
11.487	302.04207	$C_{15}H_{10}O_7$	Bracteatin	S	-	-
11.487	450.11609	$C_{21}H_{22}O_{11}$	Astilbin	0.06	0.25	0.40
11.493	594.15831	$C_{27}H_{30}O_{15}$	Nictoflorin	-	0.36	-
11.502	598.18966	$C_{27}H_{34}O_{15}$	Phloretin 3',5'-Di-C-glucoside	-	0.16	-
11.549	506.10615	$C_{23}H_{22}O_{13}$	Quercetin 3- (6"-acetylgalactoside)	0.03	-	-
11.669	378.16759	$C_{20}H_{26}O_7$	Carinol	S	-	-
11.684	594.158	$C_{27}H_{30}O_{15}$	5,7-Dihydroxy-2-(4-hydroxyphenyl)-4-oxo-4H-chromen-3-yl 6-O-(6-deoxyhexopyranosyl) hexopyranoside	-	3.85	3.61
11.685	362.13776	$C_{19}H_{22}O_7$	Machaerol B	S	-	-
11.759	448.10062	$C_{21}H_{20}O_{11}$	Trifolin	0.13	0.50	1.92
11.83	302.04253	$C_{15}H_{10}O_7$	Quercetin	1.08	6.59	1.43
11.845	436.13653	$C_{21}H_{24}O_{10}$	Phloridzin	-	0.02	-
11.899	374.15775	$C_{17}H_{26}O_9$	Deoxyloganin	0.02	-	-
11.999	264.09963	$C_{14}H_{16}O_5$	1'-Acetoxyeugenol acetate	0.04	-	-
12.002	316.05803	$C_{16}H_{12}O_7$	Isorhamnetin	-	0.13	-
12.018	680.37682	$C_{36}H_{56}O_{12}$	Tenuifolin	-	S	-
12.076	404.11076	$C_{20}H_{20}O_9$	Chalconaringenin 2'-xyloside	S	-	-
12.079	464.09535	$C_{21}H_{20}O_{12}$	Quercetin-3β-D-glucoside	-	0.06	0.36
12.183	286.04753	$C_{15}H_{10}O_6$	Fisetin	-	0.05	0.69
12.192	534.1007	$C_{24}H_{22}O_{14}$	Kaempferol 3-O-(6-malonyl-glucoside)	-	0.10	-
12.194	338.09994	$C_{16}H_{18}O_8$	4-Methylumbelliferyl-α-D-glucopyranoside	0.04	0.09	-
12.214	462.17169	$C_{20}H_{30}O_{12}$	Bioside	0.04	-	-
12.258	288.06315	$C_{15}H_{12}O_6$	Maesopsin	-	0.07	-
12.331	188.10475	$C_9H_{16}O_4$	Azelaic acid	0.24	0.25	3.23
12.356	170.02143	$C_7H_6O_5$	Gallic acid	3.32	0.15	-
12.359	286.04733	$C_{15}H_{10}O_6$	Kaempferol	0.04	0.16	0.37
12.371	582.2314	$C_{28}H_{38}O_{13}$	(7'R)-(+)-Lyoniresinol 9'-glucoside	0.04	-	-
12.433	348.142	$C_{15}H_{24}O_9$	Ajugol	0.02	0.03	-
12.477	432.1056	$C_{21}H_{20}O_{10}$	Afzelin	-	0.27	-
12.49	346.10525	$C_{18}H_{18}O_7$	Hamilcone	S	-	-

(Cont'd...)

Table 3. ***(Continued)***

Retention time (minutes)	Molecular weight	Empirical formula	Putative compounds	Relative abundance (% of total area)		
				AQ	MeOH	EtOAc
13.039	274.08413	$C_{15}H_{14}O_5$	Phloretin	0.07	-	-
13.697	314.18749	$C_{20}H_{26}O_3$	Kahweol	-	-	0.50
13.777	428.18319	$C_{24}H_{28}O_7$	Heteroflavanone B	S	-	-
13.851	226.12029	$C_{12}H_{18}O_4$	Allixin	0.06	-	-
13.888	472.20995	$C_{26}H_{32}O_8$	Kushenol H	0.02	-	-
13.949	208.11007	$C_{12}H_{16}O_3$	β-Asarone	0.02	0.02	-
14.102	722.31464	$C_{36}H_{50}O_{15}$	Physagulin G	0.11	-	-
14.137	272.0684	$C_{15}H_{12}O_5$	Naringenin	0.03	0.02	-
14.499	470.19435	$C_{26}H_{30}O_8$	Zapoterin	-	0.07	-
14.552	406.12623	$C_{20}H_{22}O_9$	Anadanthoside	S	-	-
14.559	558.28306	$C_{31}H_{42}O_9$	Glycinoeclepin B	0.02	-	-
15.587	530.21479	$C_{28}H_{34}O_{10}$	7-Acetoxy-6-hydroxylimonin	-	0.39	-
16.063	324.20863	$C_{22}H_{28}O_2$	Cannabinol monomethyl ether	0.04	-	-
16.337	328.22487	$C_{18}H_{32}O_5$	Corchorifatty acid F	0.09	0.48	3.05
16.382	312.20833	$C_{21}H_{28}O_2$	Tetrahydrogestrinone	-	-	1.27
16.687	216.18777	$C_{16}H_{24}$	Cyperotundone	S	-	-
16.72	408.23001	$C_{26}H_{32}O_4$	Methyllinderatin	S	-	-
16.786	504.34497	$C_{30}H_{48}O_6$	Arjungenin	0.53	0.08	-
16.977	822.40365	$C_{42}H_{62}O_{16}$	Glycyrrhizin	0.04	-	-
17.081	468.2149	$C_{27}H_{32}O_7$	Exiguaflavanone E	-	0.02	-
17.127	646.37157	$C_{36}H_{54}O_{10}$	Gypsogenin 3-O-β-D-glucuronide	-	S	-
17.201	574.3505	$C_{33}H_{50}O_8$	Favolon B	S	-	-
17.366	676.23644	$C_{33}H_{40}O_{15}$	Icariin	0.03	-	-
17.552	256.07338	$C_{15}H_{12}O_4$	Isoliquiritigenin	0.02	-	-
17.56	254.11522	$C_{13}H_{18}O_5$	Aplojaveediin C	0.02	-	-
17.574	452.18324	$C_{26}H_{28}O_7$	Derrichalcone	S	-	-
17.673	650.32998	$C_{34}H_{50}O_{12}$	Thapsigargin	-	0.11	-
17.728	294.1828	$C_{17}H_{26}O_4$	(±)-Gingerol	-	0.05	-
18.457	466.19849	$C_{27}H_{30}O_7$	Nimbolide	-	0.07	-
19.166	354.14656	$C_{21}H_{22}O_5$	Xanthohumol	-	-	3.13
22.132	412.37029	$C_{29}H_{48}O$	Stigmasterol	-	S	-

Notes: Relative percentage abundance (%) indicates the proportion of each compound detected in the extract, based on its peak area in chromatographic analysis. It reflects how much of each compound is present relative to the total composition. Compounds detected in very small amounts ≤0.01% are considered minor and marked with 'S'. Phytochemicals that do not present in either of the extracts are denoted by dash (-).
Abbreviation: LC-MS: Liquid chromatography–mass spectrometry.

ethyl acetate (EtOAc) extracts. These differences are likely explained by variations in phytochemical composition, since methanol and water extract a greater range of mid-polar to polar compounds, while EtOAc yields fewer non-polar constituents.[20] Variability in antibacterial activity may also be influenced by differences in cell penetration and solubility. The comparatively lower activity observed for EtOAc extracts may stem from the limited diffusion of their compounds through agar media, reducing their effectiveness.[21] In addition, differences in broth solubility can affect MIC values.

The antibacterial activity of *A. indica* extracts varied based on the solvent used for extraction, with MeOH and AQ extracts displaying different levels of inhibition

across bacterial strains. The AQ extracts showed MIC values ranging from 2938 to 5875 μg/mL against four gastrointestinal pathogens: *B. cereus*, *S. flexneri*, *S. sonnei*, and *S. typhimurium*. This outcome points to limited inhibition, which may be attributed to water-soluble constituents such as flavonoids and tannins. However, the relatively high MIC values indicate that these extracts may not be highly potent as standalone antimicrobial agents. The MICs obtained in our study (1175–5875 μg/mL) fall into the weak activity range as classification mentioned in section 2.5. The MeOH fraction demonstrated stronger activity across a broader spectrum of bacteria, with MICs spanning 1175–4700 μg/mL for nine strains. The lowest MIC of 1175 μg/mL was observed against *B. cereus*, indicating a moderate inhibitory effect. In contrast, *S. flexneri*, *S. sonnei*, and *S. typhimurium* had higher MIC values of 4700 μg/mL, suggesting low activity against these Gram-negative enteric pathogens.

The MeOH extract also exhibited MIC values of 2350 μg/mL against *S. aureus* and MRSA, demonstrating equal effectiveness against both strains, which could indicate potential activity against antibiotic resistance mechanisms. However, MIC values of 4700 μg/mL against *E. coli*, ESBL-producing *E. coli*, and *K. pneumoniae* suggest weaker inhibition against these Gram-negative bacteria. Interestingly, the extract was not active against ESBL-producing *K. pneumoniae*, highlighting possible resistance mechanisms that limit its efficacy. However, differences in bacterial susceptibility may be influenced by factors such as cell wall composition, endogenous enzymes, and efflux pump activity.[22,23] The relatively strong activity against *B. cereus* suggests that the extract contains specific compounds effective against spore-forming Gram-positive bacteria. Conversely, the higher MIC values against *Shigella* and *Salmonella* species imply that these pathogens may have structural or biochemical resistance mechanisms that reduce the extract's effectiveness.[24,25] Overall, the *A. indica* methanolic extracts' antibacterial activity is encouraging, whilst their efficacy varies across bacterial strains. However, the relatively high MIC values indicate that their standalone use may be limited.

A previous study reported low antibacterial activity of *A. indica* leaf and seed extracts using aqueous and 80% ethanol solvents. Leaf extracts showed MICs of 128–256 mg/mL against *S. aureus*, while seed extracts were more active with MICs of 8–64 mg/mL.[26] Notably, these MIC values are very high and generally would not be considered to be active by most standards. In contrast, the methanol extract tested in our study had an MIC of 2350 μg/mL against *S. aureus* and MRSA, which is nearly 100 times more potent than the 80% ethanol leaf extract examined in the earlier study (based on MIC values), and approximately 3 times as potent as the corresponding seed extract tested in that study. While the differences in extraction solvents (80% ethanol in the earlier study, versus 100% methanol in our study) are likely to contribute to these differences, the scale of the differences indicates that other factors may also contribute, including the plant source as well as its storage and handling. The authors in the earlier study state that they used the same plant material that they used in an earlier study. Depending on the time that the plant material had been stored and the storage conditions, there may have been substantial losses of volatile compounds. In addition, specific antibacterial compounds may have become inactivated (*e.g.*, through oxidation) during the prolonged storage period. Furthermore, methodological differences in the microdilution assays used in the two studies may also account for these differences. Our study used iodonitrotetrazolium salt (INT) as a colorimetric indicator, which allows rapid and sensitive determination of the MIC values. In contrast, Arsene *et al.*'s study[26] relied on visual examination of the treated cultures to evaluate the point at which growth was not visually apparent. This method lacks sensitivity and is prone to experimenter error. These differences may likely contribute to the differences in MIC between the two studies.

In addition, only the 80% ethanol seed extract was tested in combination with antibiotics in the earlier study,[26] showing additive effects with kanamycin and synergistic interactions with ampicillin and nitrofurantoin against *S. aureus*. Notably, it also exhibited synergy with ampicillin, kanamycin, and nitrofurantoin against *E. coli*.[26] Notably, the FIC assay used in that study followed similar protocols (including the visual growth detection method) and would be subject to the same inaccuracies as already discussed for the MIC results obtained in that study. A separate study demonstrated limited antibacterial efficacy of neem seed oil against *E. coli* and *K. pneumoniae*, with an MIC ranging from 3750 to 7500 mg/mL.[27] However, the combination of the extract with standard antibiotics was not evaluated in that study. Another investigation reported that aqueous and methanolic leaf extracts exhibited antibacterial effects, respectively, with MICs of 500 and 60 μg/mL against *S. aureus* and 500 and 125 μg/mL against MRSA.[28] That study used Soxhlet extraction (rather than maceration used in our study), and therefore, the phytochemical composition may vary substantially between the extracts tested in the two studies. This may account for the differences in MIC values between the studies. However, that study demonstrated no antibacterial activity against Gram-negative strains, including *K. pneumoniae*, *E. coli*, ESBL-producing *E. coli*, and *Salmonella* species, and failed to assess the combinatorial interactions of extracts

with antibiotics. Furthermore, that study did not report extraction yield or the volumes of extracts added in broth assays,[28] making dose normalization impossible. Dilution procedures were vaguely described (highest to lowest concentration) without specifying the dilution factor, starting concentration, or final solvent levels. In some cases, 10% DMSO was used at stock concentrations as high as 80 mg/mL for diffusion assays,[28] but it was unclear whether the same preparations were applied to broth microdilution, raising concerns about solvent-related artifacts. Furthermore, ATCC codes or strain provenance were not provided, which reduces reproducibility and introduces variability in susceptibility profiles. The absence of appropriate reference antibiotics for benchmarking was another major limitation; that study used cefiderocol as the only comparator in broth assays,[28] a Gram-negative-specific agent unsuitable for Gram-positive pathogens such as *S. aureus*.

In comparison, our work adhered to standardized microdilution protocols: We reported extraction yield, controlled DMSO at ≤1%, employed a defined dilution scheme (4-fold pre-step followed by two-fold dilutions), and tested well-characterized ATCC strains alongside a panel of reference antibiotics covering both Gram-positive and Gram-negative pathogens. This methodological rigor likely explains the lower MICs observed in our study compared with inflated values reported in previous literature. We also would like to acknowledge that lower MIC values, while indicative of antibacterial activities of the complex extract mixtures, should be studied cautiously with regard to their pharmacological relevance when compared to extracts that possess far greater potency.

Antimicrobial activity of plant extracts against bacterial pathogens is attributed to multiple mechanisms of action, depending on the bioactive compounds present. One of the primary mechanisms is cell wall and membrane disruption, where phenolics, flavonoids, and tannins destabilize bacterial cell walls, increasing permeability and leading to lysis.[4,8] Inhibition of protein synthesis is another key mechanism, where alkaloids and flavonoids interfere with ribosomal function, preventing bacterial translation and growth.[18,29] Furthermore, certain phytochemicals act as efflux pump inhibitors, reducing bacterial resistance by preventing the expulsion of antimicrobial agents.[18] In addition, polyphenols and flavonoids induce oxidative stress by generating reactive oxygen species, leading to cellular damage and bacterial death. These diverse mechanisms not only contribute to the antibacterial potential of plant extracts but also offer potential synergy with conventional antibiotics, enhancing their efficacy against resistant bacterial strains.

Combination FIC assays further highlighted distinct patterns. We observed additive interactions between both AQ and MeOH extracts and β-lactam antibiotics (penicillin G, oxacillin, amoxicillin) against *B. cereus* and *S. aureus*, suggesting enhanced cell wall-targeting effects. Additive interactions were also seen with tetracycline and chloramphenicol against *S. flexneri*, *S. sonnei*, and *S. typhimurium*, as well as with chloramphenicol against *E. coli*. These results support the hypothesis that neem phytochemicals may interfere with bacterial protein synthesis pathways in a complementary manner to ribosome-targeting antibiotics. By contrast, both AQ and MeOH extracts displayed strong antagonism with polymyxin B against multiple Gram-negative strains, implying that extract constituents may interfere with the antibiotic's membrane-disrupting activity. The observed antagonism between the AQ and MeOH extracts and polymyxin B against multiple Gram-negative bacteria may be attributed to interactions between bioactive phytochemicals and the antibiotic. Compounds within the extracts may interact with polymyxin B, limiting its uptake and diminishing its ability to disrupt bacterial membranes.[30] In addition, the pH-dependent activity of polymyxin B may have been influenced by the introduction of plant extracts into the broth medium. Changes in the local pH could alter the charge properties of polymyxin B, leading to a diminished binding affinity to bacterial membranes and a subsequent reduction in its antimicrobial potency.[31] This suggests that specific phytochemical properties, such as pH-modulating effects, may contribute to the antagonistic interactions observed. Similarly, antagonistic interactions were noted, particularly with gentamicin, where both extracts reduced its efficacy against *B. cereus*, *S. flexneri*, *S. typhimurium*, and *K. pneumoniae*. In addition, the MeOH extract antagonized tetracycline against *S. sonnei* and *K. pneumoniae*, indicating possible interference with its mechanism of action. While these postulations remain speculative, they provide some insight into the safety of using such combinations in therapy, as antagonistic combinations abolish the effectiveness of antibacterial treatments, putting patients at risk of exacerbated infections.

A previous study of neem extracts reported synergy only in selective contexts, such as additive or synergistic effects of 80% ethanol seed extracts with kanamycin, nitrofurantoin, or ampicillin against *S. aureus* and *E. coli.*[26] Indeed, that study represents methodological clarity in those reports, including a detailed combination design (checkerboard) and defined solvent controls and confidence in their conclusions. In contrast, our study applied standardized FIC analysis, allowing a more rigorous and quantitative assessment of interactions. However, we did not test the combination of extracts with kanamycin, nitrofurantoin, or ampicillin.

Extracts' MICs should not be directly compared with purified antibiotics, as they represent complex mixtures in which active constituents are present at relatively low abundance. The high MIC values observed, therefore, emphasize the importance of bioassay-guided fractionation and compound isolation, which may yield individual phytochemicals with substantially lower MICs that approach pharmacologically relevant benchmarks. Overall, our findings reinforce that while crude neem extracts are not highly potent as standalone agents, they can enhance the efficacy of selected antibiotics through additive effects, particularly against Gram-positive bacteria. At the same time, the observed antagonism with polymyxin B emphasizes the importance of evaluating potential negative interactions before clinical consideration. By addressing methodological gaps in the literature, our study provides a more reliable assessment of neem's antibacterial potential and its role in combination therapy.

The absence of synergistic interactions between extracts and antibiotics suggests that while the extracts exhibited some antibacterial potential, they did not significantly enhance antibiotic efficacy beyond an additive effect. This could be due to the extracts lacking strong potentiating compounds or the failure of the potentiating compounds to target bacterial resistance mechanisms effectively. In addition, potential compound-antibiotic interactions may have resulted in competitive binding, preventing synergy. It is also important to note that the concentrations of some of the extracts may have been suboptimal and thus unable to elicit synergistic interactions. While no synergy was observed, the additive effects indicate some potential for combination use. Future studies should place emphasis on isolating specific bioactive compounds and assessing their ability to improve antibiotic activity against resistant bacteria.

LC-MS studies highlighted several phytochemicals in the plant extracts, particularly flavonoids, phenolic acids, tannins, terpenoids, as well as several other compounds. The flavonoids included astilbin (Figure 3A), (+)-gallocatechin (Figure 3B), kaempferol (Figure 3C), myricitrin (Figure 3D), naringenin (Figure 3E), hyperoside (Figure 3F), nictoflorin (Figure 3G), quercetin (Figure 3H), quercetin 3-O-rhamnoside-7-O-glucoside (Figure 3I), rutin (Figure 3J), and pyrogallol (Figure 3K). Tannins detected in the extracts comprise gallic acid (Figure 3L), digallic acid (Figure 3M), 6-galloylglucose (Figure 3N), 1-O-galloylglycerol (Figure 3O), (+)-chebulic acid (Figure 3P), 1,6-bis-O-(3,4,5-trihydroxybenzoyl) hexopyranose (Figure 3Q), 1,2,6-trigalloyl-β-D-glucopyranose (Figure 3R), ellagic acid arabinoside (Figure 3S), and ellagic acid (Figure 3T). Earlier investigations have also reported additional phytochemicals in *A. indica* leaf extracts, such as genistein 7-O-glucoside, (−)-epicatechin, nimonol, zafaral, meliacinanhydride, nimocinol, isomeldenin, rutin, β-sitosterol, ellagic acid, ferulic acid, lupeol, quercetin, stigmasterol, terpinen-4-ol, sugiol, 4-cymene, nimbiol, α-terpinene, and vitamin E.[32-35]

Quercetin has previously demonstrated antibacterial activity against resistant strains of *E. coli*, and *K. pneumoniae*, with MICs ranging from 16 to 256 μg/mL depending on the strain.[36] It disrupts bacterial membranes and inhibits the expression of efflux pumps and carbapenemase genes. In the same study, the combination of quercetin and meropenem showed synergistic effects against carbapenem-resistant *E. coli* and *K. pneumoniae*, reducing meropenem MICs from 1024 μg/mL to 8–512 μg/mL.

Against resistant *E. coli* strains, naringenin showed MIC values between 1 and 8 mg/mL, whereas rutin exhibited stronger activity with MICs of 125–1000 mg/mL.[37,38] Both compounds, when combined with amikacin, showed a synergistic antibacterial effect against multidrug-resistant *E. coli*. The combination disrupted the bacterial cell wall and inner membrane, as evidenced by increased leakage of alkaline phosphatase, K^+ and proteins.[37,38] This suggests enhanced membrane permeability as a key mechanism.

Gallic acid has additive antibacterial effects when combined with β-lactams (ampicillin, amoxicillin, penicillin G) against *S. aureus* and MRSA, by reducing the MICs of these antibiotics from 62.5 to 8–16 μg/mL.[39] Gallic acid had synergistic effects in combination with gentamicin and norfloxacin against *S. aureus*. When combined with norfloxacin, it reduced the MIC from 156 to 49 μg/mL, and with gentamicin, the MIC dropped from 49 to 3 μg/mL.[40] A separate investigation examined gallic acid for both antibacterial and antibiofilm effects against *S. flexneri*, reporting an MIC of 2000 μg/mL and minimum bactericidal concentration (MBC) of 8000 μg/mL. The authors of that study also reported that gallic acid inhibited bacterial growth by disrupting cell membranes and altering morphology.[41] It also significantly reduced biofilm formation by penetrating the extracellular polymeric matrix and downregulating *mdoH* gene and OpgH protein expression, leading to decreased polysaccharide content. However, no studies in combination with antibiotics were conducted in that work.

Pyrogallol enhanced the activity of gentamicin and norfloxacin against *S. aureus*, inducing synergy by lowering the MIC of gentamicin from 49.21 to 2.44 μg/mL and norfloxacin from 156 to 78 μg/mL.[39] Pyrogallol demonstrates strong antibacterial activity against MRSA, with both MIC and MBC at 16 μg/mL. Its mechanism involves disrupting the bacterial cell

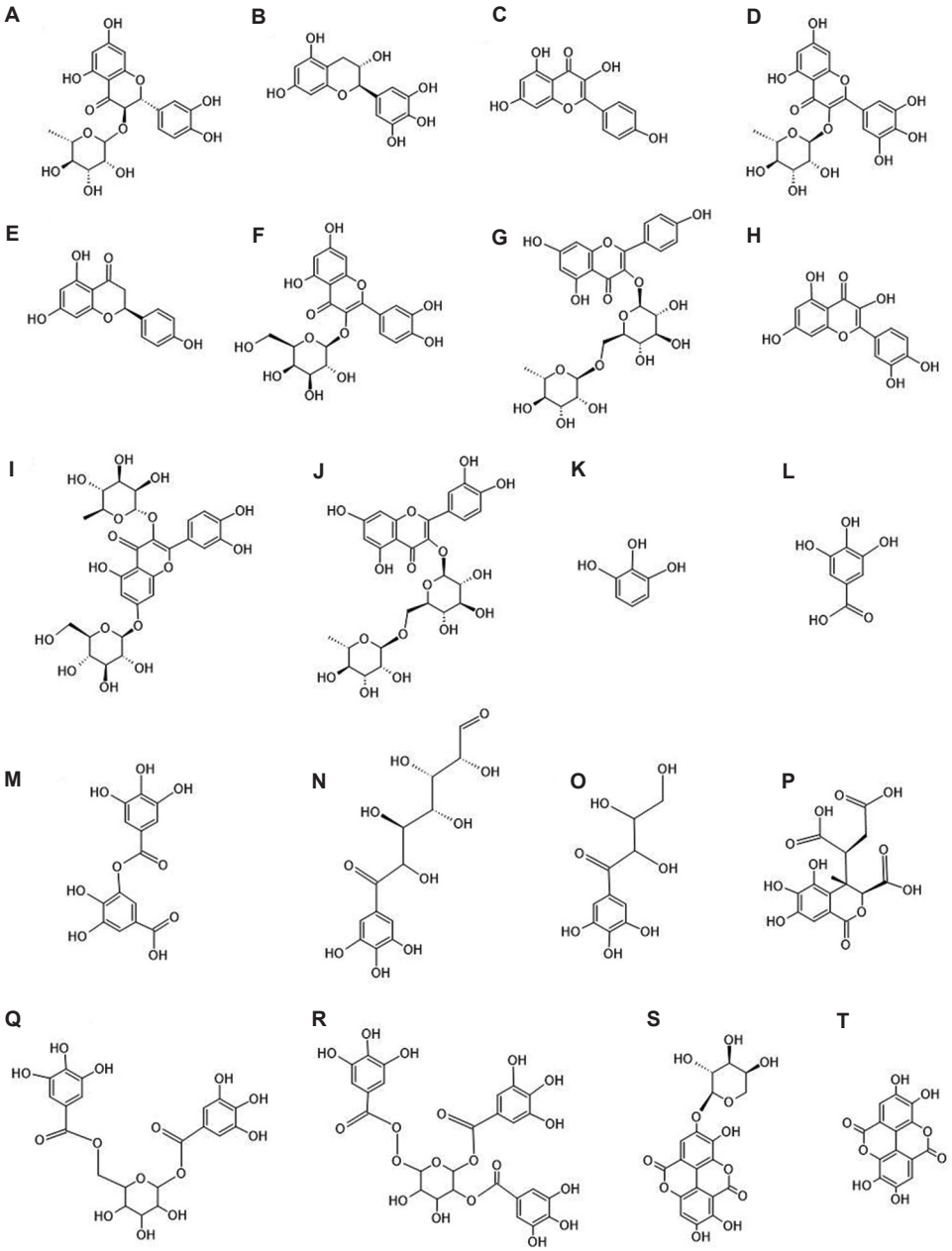

Figure 3. Structures of key phytochemicals detected in *Azadirachta indica* leaf extracts. (A) Astilbin, (B) (+)-gallocatechin, (C) kaempferol, (D) myricitrin, (E) naringenin, (F) hyperoside, (G) nictoflorin, (H) quercetin, (I) quercetin 3-O-rhamnoside-7-O-glucoside, (J) rutin, (K) pyrogallol, (L) gallic acid, (M) digallic acid, (N) 6-galloylglucose, (O) 1-O-galloylglycerol, (P) (+)-chebulic acid, (Q) 1,6-bis-O-(3,4,5-trihydroxybenzoyl) hexopyranose (R) 1,2,6-trigalloyl-β-D-glucopyranose, (S) ellagic acid arabinoside, and (T) ellagic acid. Structures were prepared using ChemSketch (Freeware) 2023.2.4.

membrane by modifying components like fatty acids and peptidoglycans.[42]

Among the compounds detected by LC-MS, quercetin, naringenin, rutin, gallic acid, and pyrogallol are of particular interest due to their well-documented antibacterial activity in the literature. These phytochemicals have been reported to inhibit *S. aureus*, MRSA, *E. coli*, resistant *E. coli*, *K. pneumoniae*, and *Shigella* strains, which overlap with the pathogens tested in this study. While our current data reflect their relative abundance in the extracts, we suggest that these compounds may contribute to the antibacterial activity observed. Future studies are underway to evaluate these molecules as antibacterial agents, both individually and in combination with conventional antibiotics, against the same panel of bacterial strains.

Overall, this study demonstrates the antibacterial potential of methanolic and aqueous *A. indica* leaf extracts, which showed notable activity against various bacterial strains. Additive interactions with penicillin G, oxacillin, tetracycline, and chloramphenicol suggest potential for use as antibiotic adjuvants. Whilst no synergistic interactions were observed, the ability of the extracts to inhibit several bacterial strains and selectively enhance antibiotic activity is encouraging. The absence of toxicity in *Artemia franciscana* assays reinforces the potential of *A. indica* as a safe and viable option for future antimicrobial applications. Future work should focus on fractionation, bioactive compound isolation, mechanism elucidation, and expanded toxicity assessments using mammalian cell lines to better define its therapeutic potential.

5. Conclusion

This study demonstrates the antibacterial potential of *A. indica* leaf extracts against various pathogens, including resistant strains. FIC analysis showed additive effects with some antibiotics, particularly β-lactams and protein synthesis inhibitors, suggesting enhanced efficacy. The antagonism noted in the combination of polymyxin B and gentamicin highlights the need for caution with the use of combination therapies. Phytochemical analysis revealed flavonoids, tannins, and phenolics as key antimicrobial constituents, with extract efficacy influenced by solvent polarity. All extracts were non-toxic in *Artemia franciscana* assays, supporting their safety, although this invertebrate model is only a preliminary assessment of toxicity. Further studies will focus on isolating active compounds, evaluating cytotoxicity on mammalian cells, and understanding mechanisms behind both synergistic and antagonistic interactions.

Acknowledgments

Gagan Tiwana was supported by a PhD stipend from Griffith University, Gold Coast, Australia.

Funding

None.

Conflict of interest

The authors declare that they have no competing interests.

Author contributions

Conceptualization: Ian Cock, Matthew Cheesman
Data curation: Gagan Tiwana
Formal analysis: Gagan Tiwana
Investigation: All authors
Methodology: Gagan Tiwana
Project administration: Matthew Cheesman
Supervision: Ian Cock, Matthew Cheesman
Writing–original draft: Gagan Tiwana
Writing–review & editing: All authors

Ethics approval and consent to participate

Not applicable.

Consent for publication

Not applicable.

Availability of data

Data supporting the findings and conclusions are available on reasonable request from the corresponding author.

References

1. Arip M, Selvaraja MR, Tan LF, *et al*. Review on plant-based management in combating antimicrobial resistance - mechanistic perspective. *Front Pharmacol.* 2022;13:879495.

   doi: 10.3389/fphar.2022.879495

2. World Bank Group. *Antimicrobial Resistance (AMR)*. World Bank Group; 2025, Available from: https://www.worldbank.org/en/topic/health/brief/antimicrobial-resistance-amr [Last accessed on 2025 Jul 27].

3. Centers for Disease Control and Prevention (CDC). *CDC Partners Estimate Healthcare Cost of Antimicrobial-resistant Infection*. Centers for Disease Control and Prevention; 2025. Available from: https://www.cdc.gov/antimicrobial-resistance/stories/partner-estimates.html [Last accessed on 2025 Aug 14].

4. Khameneh B, Eskin NAM, Iranshahy M, Bazzaz BSF. Phytochemicals: A promising weapon in the arsenal against antibiotic-resistant bacteria. *Antibiotics (Basel).* 2021;10(9):1044.

   doi: 10.3390/antibiotics10091044

5. Vaou N, Stavropoulou E, Voidarou C, Tsigalou C, Bezirtzoglou E. Towards advances in medicinal plant antimicrobial activity: A review study on challenges and future perspectives. *Microorganisms.* 2021;9(10):2041.

   doi: 10.3390/microorganisms9102041

6. Cha JD, Moon SE, Kim JY, Jung EK, Lee YS. Antibacterial activity of sophoraflavanone G isolated from the roots of *Sophora flavescens* against methicillin-resistant *Staphylococcus aureus*. *Phytother Res*. 2009;23:1326-1331.

   doi: 10.1002/ptr.2540

7. Tiwana G, Cock IE, Cheesman MJ. Combinations of *Terminalia bellirica* (Gaertn.) Roxb. and *Terminalia chebula* Retz. extracts with selected antibiotics against antibiotic-resistant bacteria: Bioactivity and phytochemistry. *Antibiotics (Basel).* 2024;13(10):994.

doi: 10.3390/antibiotics13100994

8. Tiwana G, Cock IE, Cheesman MJ. A review of Ayurvedic principles and the use of Ayurvedic plants to control diarrhoea and gastrointestinal infections. *Pharmacogn Commun.* 2023;13(4):152-162.

   doi: 10.5530/pc.2023.4.25

9. Cheesman M, Ilanko A, Blonk B, Cock IE. Developing new antimicrobial therapies: Are synergistic combinations of plant extracts/compounds with conventional antibiotics the solution? *Pharmacogn Rev.* 2017;11(22):57-72.

   doi: 10.4103/phrev.phrev_21_17

10. Francine U, Jeannette U, Pierre R. Assessment of antibacterial activity of neem plant (*Azadirachta indica*) on *Staphylococcus aureus* and *Escherichia coli*. *J Med Plant Stud.* 2015;3(4):85-91.

11. Koona S, Budida S. Antibacterial potential of the extracts of the leaves of *Azadirachta indica* Linn. *Not Sci Biol.* 2011;3(1):65-69.

    doi: 10.15835/nsb315470

12. Altayb HN, Yassin NF, Hosawi S, Kazmi I. *In-vitro* and *in-silico* antibacterial activity of *Azadirachta indica* (neem), methanolic extract, and identification of Beta.d-mannofuranoside as a promising antibacterial agent. *BMC Plant Biol.* 2022;22:262.

    doi: 10.1186/s12870-022-03650-5

13. Balouiri M, Sadiki M, Ibnsouda SK. Methods for *in vitro* evaluating antimicrobial activity: A review. *J Pharm Anal.* 2016;6(2):71-79.

    doi: 10.1016/j.jpha.2015.11.005

14. Tiwana G, Cock IE, Cheesman MJ. Phytochemical analysis and antimicrobial activity of *Terminalia bellirica* (Gaertn.) Roxb. and *Terminalia chebula* Retz. fruit extracts against gastrointestinal pathogens: Enhancing antibiotic efficacy. *Microorganisms.* 2024;12:2664.

    doi: 10.3390/microorganisms12122664

15. Eloff JN. A proposal towards a rational classification of the antimicrobial activity of acetone tree leaf extracts in a search for new antimicrobials. *Planta Med*. 2021;87:836-840.

    doi: 10.1055/a-1482-1410

16. Doern CD. When does 2 plus 2 equal 5? A review of antimicrobial synergy testing. *J Clin Microbiol*. 2014;52(12):4124-4128.

    doi: 10.1128/jcm.01121-14

17. Cajka T, Hricko J, Rudl Kulhava L, Paucova M, Novakova M, Kuda O. Optimization of mobile phase modifiers for fast LC-MS-based untargeted metabolomics and lipidomics. *Int J Mol Sci.* 2023;24(3):1987.

    doi: 10.3390/ijms24031987

18. Angelini P. Plant-derived antimicrobials and their crucial role in combating antimicrobial resistance. *Antibiotics (Basel).* 2024;13:746.

    doi: 10.3390/antibiotics13080746

19. Tiwana G, Cock IE, White A, Cheesman MJ. Use of specific combinations of the Triphala plant component extracts to potentiate the inhibition of gastrointestinal bacterial growth. *J Ethnopharmacol.* 2020;260:112937.

    doi: 10.1016/j.jep.2020.112937

20. Altemimi A, Lakhssassi N, Baharlouei A, Watson DG, Lightfoot DA. Phytochemicals: Extraction, isolation, and identification of bioactive compounds from plant extracts. *Plants (Basel).* 2017;6(4):42.

    doi: 10.3390/plants6040042

21. Bonev B, Hooper J, Parisot J. Principles of assessing bacterial susceptibility to antibiotics using the agar diffusion method. *J Antimicrob Chemother.* 2008;61(6):1295-1301.

    doi: 10.1093/jac/dkn090

22. Paterson DL, Bonomo RA. Extended-spectrum beta-lactamases: A clinical update. *Clin Microbiol Rev*. 2005;18(4):657-686.

    doi: 10.1128/cmr.18.4.657-686.2005

23. Auda IG, Ali Salman IM, Odah JG. Efflux pumps of gram-negative bacteria in brief. *Gene Rep.* 2020;20:100666.

    doi: 10.1016/j.genrep.2020.100666

24. Puzari M, Sharma M, Chetia P. Emergence of antibiotic resistant *Shigella* species: A matter of concern. *J Infect Public Health.* 2018;11(4):451-454.

    doi: 10.1016/j.jiph.2017.09.025

25. Alenazy R. Antibiotic resistance in *Salmonella*: Targeting multidrug resistance by understanding efflux pumps, regulators and the inhibitors. *J King Saud Univ Sci.* 2020;34:102275.

    doi: 10.1016/j.jksus.2022.102275

26. Arsene MM, Viktorovna PI, Davares AK, *et al.* Antimicrobial and antibiotic-resistance reversal activity of some medicinal plants from Cameroon against selected resistant and non-resistant uropathogenic bacteria. *Front Biosci (Elite Ed).* 2022;14(4):4-25.

    doi: 10.31083/j.fbe1404025

27. Singh AA, Naaz ZT, Rakaseta E, *et al.* Antimicrobial activity of selected plant extracts against common food borne pathogenic bacteria. *Food Humanity.* 2023;1:64-70.

    doi: 10.1016/j.foohum.2023.04.002

28. Ousman BM, Mennane Z, Boussaoudi I, *et al.* First investigation of phytochemical screening, HPLC-MS characterization, and antibacterial activity of *Azadirachta indica* A. Juss (Mim or Neem) leaf extracts, grown in the

Republic of Chad. *Nat Prod Commun.* 2025;20(2):1-16.

doi: 10.1177/1934578X251322360

29. Gibbons S. Phytochemicals for bacterial resistance--strengths, weaknesses and opportunities. *Planta Med.* 2008;74(6):594-602.

doi: 10.1055/s-2008-1074518

30. Zavascki AP, Goldani LZ, Li J, Nation RL. Polymyxin B for the treatment of multidrug-resistant pathogens: A critical review. *J Antimicrob Chemother.* 2007;60(6):1206-1215.

doi: 10.1093/jac/dkm357

31. Cai X, Javor S, Gan BH, Köhler T, Reymond JL. The antibacterial activity of peptide dendrimers and polymyxin B increases sharply above pH 7.4. *Chem Commun.* 2021;57(46):5654-5657.

doi: 10.1039/d1cc01838h

32. Siddiqui BS, Rasheed M. Three new triterpenoids from *Azadirachta indica*. *Helv Chim Acta.* 2001;84(7):1962-1928.

doi: 10.1002/1522-2675(20010711)84:7<1962:AID-HLCA1962>3.0.CO;2-V

33. Pandey G, Verma K, Singh M. Evaluation of phytochemical, antibacterial and free radical scavenging properties of *Azadirachta indica* (neem) leaves. *Int J Pharm Pharm Sci.* 2014;6(2):444-447.

34. Gupta R, Nand P, Drabu S. Insignificant anti-acne activity of *Azadirachta indica* leaves and bark. *J Pharm Negat Results.* 2012;3(1):29-33.

doi: 10.4103/0976-9234.99650

35. Saleem S, Muhammad G, Hussain MA, Bukhari SNA. A comprehensive review of phytochemical profile, bioactives for pharmaceuticals, and pharmacological attributes of *Azadirachta indica*. *Phytother Res.* 2018;32(7):1241-1272.

doi: 10.1002/ptr.6076

36. Pal A, Tripathi A. Demonstration of bactericidal and synergistic activity of quercetin with meropenem among pathogenic carbapenem resistant *Escherichia coli* and *Klebsiella pneumoniae*. *Microb Pathog.* 2020;143:104120.

doi: 10.1016/j.micpath.2020.104120

37. Yi L, Cao M, Chen X, *et al. In vitro* antimicrobial synergistic activity and the mechanism of the combination of naringenin and amikacin against antibiotic-resistant *Escherichia coli*. *Microorganisms.* 2024;12(9):1871.

doi: 10.3390/microorganisms12091871

38. Yi L, Bai Y, Chen X, *et al.* Synergistic effects and mechanisms of action of rutin with conventional antibiotics against *Escherichia coli*. *Int J Mol Sci.* 2024;25:13684.

doi: 10.3390/ijms252413684

39. Jiamboonsri P, Eurtivong C, Wanwong S. Assessing the potential of gallic acid and methyl gallate to enhance the efficacy of β-lactam antibiotics against methicillin-resistant *Staphylococcus aureus* by targeting β-lactamase: *In silico* and *in vitro* studies. *Antibiotics (Basel).* 2023;12(11):1622.

doi: 10.3390/antibiotics12111622

40. Lima VN, Oliveira-Tintino CDM, Santos ES, *et al.* Antimicrobial and enhancement of the antibiotic activity by phenolic compounds: Gallic acid, caffeic acid and pyrogallol. *Microb Pathog.* 2016;99:56-61.

doi: 10.1016/j.micpath.2016.08.004

41. Kang J, Liu L, Liu M, Wu X, Li J. Antibacterial activity of gallic acid against *Shigella flexneri* and its effect on biofilm formation by repressing mdoH gene expression. *Food Control.* 2018;94:147-154.

doi: 10.1016/j.foodcont.2018.07.011

42. Chew YL, Arasi C, Goh JK. Pyrogallol induces antimicrobial effect and cell membrane disruption on methicillin-resistant *Staphylococcus aureus* (MRSA). *Curr Bioact Compd.* 2021;18:38-46.

doi: 10.2174/1573407217666210526121512

ACCSCIENCE PUBLISHING

Innovative Medicines & Omics

ORIGINAL RESEARCH ARTICLE

Effect of Darjeeling black tea aromatics on central nervous system function: An *in silico* study of glutamate receptor–ligand interactions

Moumita Saha[1], Anup Sardar[2], Sirshendu Chatterjee[1]*, and Anirban Ghosh[2]*

[1]Department of Biotechnology, Techno India University, Kolkata, West Bengal, India

[2]Department of Zoology, Cell Development and Immunobiology Laboratory, School of Sciences, Netaji Subhas Open University, Kalyani, West Bengal, India

Abstract

Darjeeling tea (*Camellia sinensis* var. *sinensis*) is recognized for its unique aroma and taste, associated with mood and cognitive enhancement. However, the underlying neurochemical mechanisms remain unclear. The present study investigates the potential interaction of Darjeeling tea's volatile aroma compounds with glutamate receptors (GluRs), the predominant excitatory receptors in the central nervous system (CNS). We hypothesized that these compounds target GluRs to elicit their effects. An *in silico* approach was employed to analyze the physicochemical properties, bioactivity scores, and toxicity profiles of the aroma compounds. Subsequently, molecular docking simulations were performed using the retrieved 3D structures of relevant GluRs to predict the binding affinity of selected compounds exhibiting high bioactivity, drug-likeness, and bioavailability, and identify key amino acid residues within the receptor binding pockets. Our findings revealed α-ionone and safranal as prominent ligands exhibiting strong binding interactions. Among metabotropic GluRs, mGluR1 (1EWK), GluR5 (3FUZ), and GluR6 (3G3F) showed the highest affinity. Ionotropic receptor subtypes α-amino-3-hydroxy-5-methyl-4-isoxazolepropionic acid receptor (2WJW) and N-methyl-D-aspartate receptor (7EOR) also displayed significant binding scores, where greater structural dynamics were found in metabotropic GluRs on ligand binding compared to ionotropic subtypes. Given that inhalation via the nasal passage is a primary exposure route and the presence of GluR-expressing cells along this pathway, the high bioavailability of α-ionone and safranal suggests their potential to interact with neuroglial cells and subsequently influence CNS neurons and microglia/macrophages. In conclusion, the identified binding of Darjeeling tea's aromatic ligands and GluRs offers a promising framework for elucidating the mechanisms underlying the tea's effects on mood, psychological states, and immune-physiological responses.

Keywords: Aroma; Darjeeling tea; Glutamate receptors; Molecular docking; Neuro-immune modulation

***Corresponding authors:**
Sirshendu Chatterjee (sirshendu.c@technoindiaeducation.com)
Anirban Ghosh (aghosh06@gmail.com)

Citation: Saha M, Sardar A, Chatterjee S, Ghosh A. Effect of Darjeeling black tea aromatics on central nervous system function: An *in silico* study of glutamate receptor–ligand interactions. *Innov Med Omics*. 2026;3(1):32-47. doi: 10.36922/IMO025350042

Received: August 26, 2025

Revised: October 14, 2025

Accepted: November 12, 2025

Published online: February 5, 2026

1. Introduction

Black tea, particularly harvested and processed from the slopes of the Darjeeling Himalayan region, is famous for its rich flavor and is widely consumed worldwide

and is valued for its distinctive flavor. The Darjeeling tea (*Camellia sinensis var. sinensis*), famous for its rich aromatic properties, has been associated with mood-related effects and other bioactivities, including roles in metabolic regulation, atherosclerosis, inflammation, and cancer.[1,2] Chemical analysis of the black tea processed using a specific extraction procedure shows a rich presence of polyphenol and catechin compounds. Theaflavins and thearubigins, in particular, contribute to its distinctive coloration upon brewing.[3,4] Recent studies have reported anti-cancer activity of theaflavins and other compounds from black tea.[4-6] In addition, tea polysaccharides are gaining attention for their potential in managing metabolic diseases. They are also noted for their prebiotic effects, skin-care benefits, and predicted anti-tumor activity.[7,8]

However, the aroma compounds responsible for the characteristic flavor of Darjeeling black tea and their potential contributions to psychophysiological stress and mood responses have yet to be properly evaluated. In a comparison between Darjeeling and Assam tea, Yoto *et al.*[9] showed that black tea aroma can attenuate stress-related changes in brain function by attenuating autonomic stress responses after inhalation, as reflected by reduced salivary chromogranin-A released from adrenal chromaffin cells and adrenergic neurons, thereby improving mood as observed in tension–anxiety score in Profile of Mood States. Odor stimuli derived from black tea are the aromatic volatile compounds that reach the olfactory tract and bulb, where olfactory nerve receptors bind the molecules and trigger corresponding signals to the brain.[10] This indicates a receptor–ligand interaction between the aroma compounds and receptors on the neuronal projections. As the Darjeeling tea aroma has a mood-enhancing effect, we hypothesize that such compounds may bind to glutamate receptors (GluRs), as glutamate is the most abundant excitatory neurotransmitter found in the nervous system.[11] GluRs are widely expressed in neurons and glial cells and are broadly classified into metabotropic and ionotropic families. Metabotropic GluRs (mGluR1–8) are further subdivided into three groups, whereas ionotropic GluRs include α-amino-3-hydroxy-5-methyl-4-isoxazolepropionic acid receptor (AMPA) (GluR1–4) and N-methyl-D-aspartate receptor (NMDA).[11,12] In addition, the olfactory nerve fibers around the olfactory bulb are accompanied by the immunoregulatory cells of the brain, that is, microglia, which are highly responsive and active protectors of the central nervous system (CNS) against any microenvironmental modifications in the tissue. GluRs are also highly expressed on these myeloid lineage cells.[13] Therefore, it is likely that tea aroma compounds bind to GluRs on both neurons and microglia or macrophages. If volatile aroma compounds from Darjeeling black tea bind to these receptors, they can trigger both neurophysiological and neuro-immune cascades, thereby relieving stress and improving mood.

In our investigation, we selected specific volatile aroma compounds associated with the characteristic Darjeeling black tea aroma, not necessarily containing a benzene ring, and validated their molecular properties as ligand candidates. Both metabotropic and ionotropic GluRs identified in neuronal cells, microglia, and macrophages were selected for their stable structural forms and subjected to *in silico* receptor–ligand binding and docking. This approach estimates the likelihood of receptor–ligand interactions of tea aroma compounds to GluRs, thereby providing valuable insights into potential mood-enhancement pathways and aroma-driven modulation of immune functions.

2. Materials and methods

2.1. Selection and preparation of ligands

Available aroma compounds in Darjeeling black tea were screened and selected based on a literature search of online databases, including Web of Science, Scopus, ScienceDirect, PubMed, and others, with an emphasis on studies that analyzed black tea chemical composition and aromatic formation.[3,14,15] We selected 10 specific fragrant compounds characterizing the Darjeeling tea aroma of the first and second flush harvests, regardless of whether they contain aromatic rings (Table 1). Molecules were retrieved from online chemical database: PubChem (www.pubchem.ncbi.nlm.nih.gov/) and later converted to their three-dimensional (3D) Protein Data Bank (PDB) format using Open Babel software (Version 2023). A PDBQT format file was created after adding hydrogens and defining rotatable bonds (torsions) to a PDB format file,[16] and the 3D models of the molecules are shown in Figure 1.

2.2. Validation of ligands

The lack of pharmacokinetic studies is one of the main obstacles in the commercial implementation of plant-based products as therapeutic agents. Thus, we used computational methods to evaluate the physicochemical, pharmacokinetic, and drug-likeness properties. Physiologically significant properties of a ligand, designated by absorption, distribution, metabolism, and excretion (ADME), were assessed using the SwissADME website (https://www.swissadme.ch/).[17] Ligand toxicity was predicted to assess potential systemic toxicity using molecular data of compounds with similar physical,

Table 1. Specific fragrant compounds characterizing the Darjeeling tea aroma of the first and second flush harvests

No.	Fragrant compounds	Characteristic fragrance (when exposed to air and matured/aged)	Two-dimensional chemical structure
1	(E, E)-2,4-decadienal	Citrus, on maturation fatty, fried odor	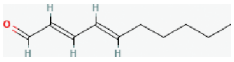
2	(E, E)-2,4-hexadienal	Citrus, on maturation fatty, fried odor	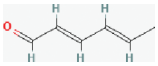
3	Benzyl alcohol	Fruity to almond-like burnt odor	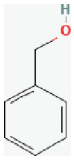
4	2-Acetyl-3-methylpyrazine	Roasted nutty and/or grain-roasted odor	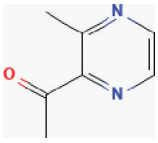
5	2-Acetyl-2-thiazoline	Nutty, popcorn-like roasted odor	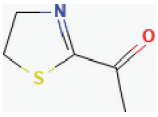
6	2-Acetyl-1-pyrroline	Cooked rice, popcorn-like odor	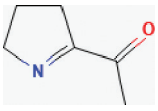
7	α-Ionone	Hay-like, iris, violet, warm-woody, faint balsamic-floral odor	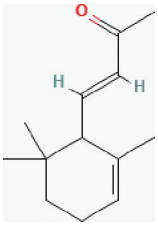
8	Safranal	Spicy saffron-like note with herbaceous, tobacco facets and floral undertones	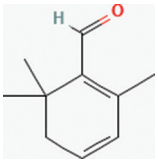
9	2-Acetyl 3,5-dimethylpyrazine	Nutty, roasted hazelnut odor	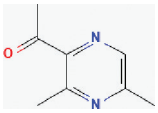
10	5-Ethyl 2,3-dimethylpyrazine	Nutty to deep roasted cocoa-like odor	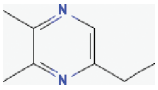

structural, and chemical properties from the online server PreADMET (https://preadmet.bmdrc.kr/). In the PreADMET server, the structural data files retrieved from the PubChem were converted to mol2 format using Open Babel software and then submitted to the online server for toxicity prediction, including mutagenicity (Ames mutagenicity test), carcinogenicity, and human Ether-à-go-go-related gene (hERG) inhibition.

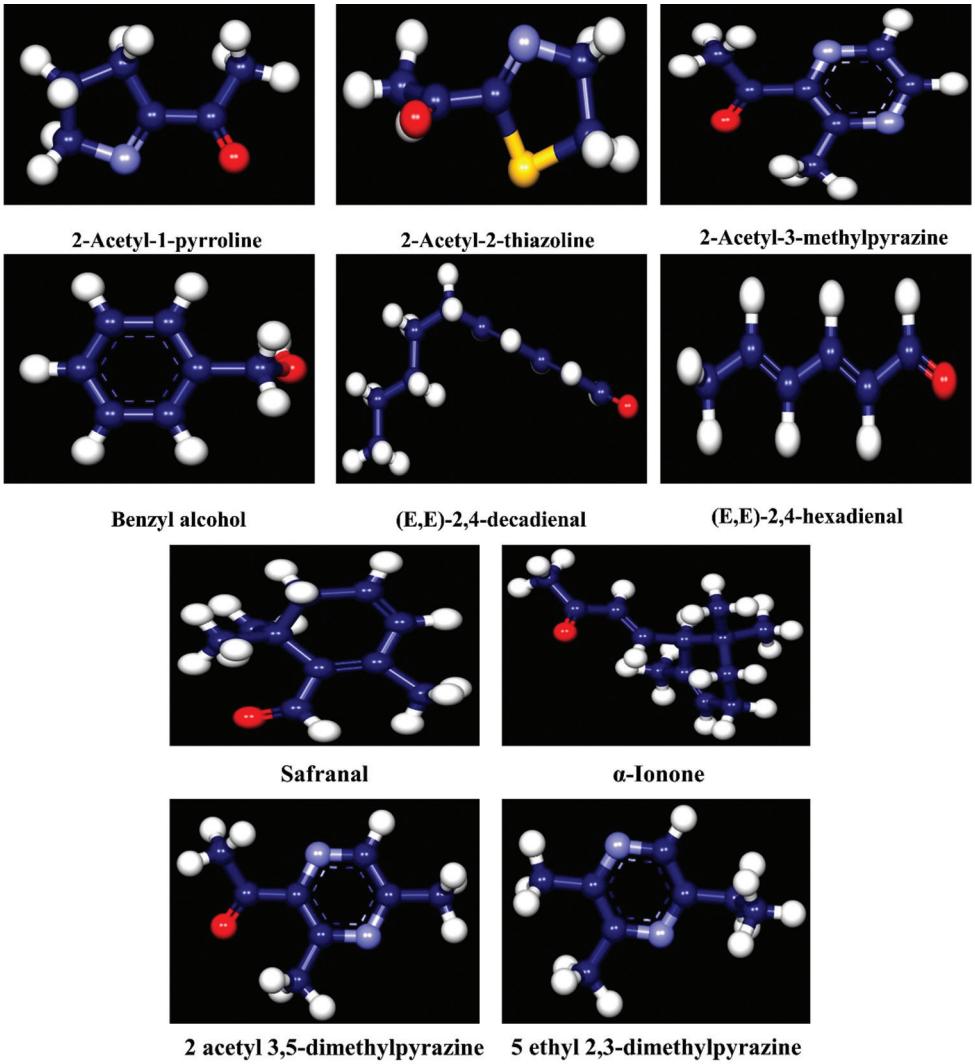

Figure 1. Three-dimensional structures of selected aromatic bioactive compounds

2.3. Receptor protein selection and validation

Based on the literature and database analysis, GluRs identified in both neuronal and non-neuronal cells in the CNS, particularly in microglia and CNS-associated macrophages, were selected. Both metabotropic and ionotropic GluRs are commonly expressed on neuronal and myelomonocytic cells in the nervous system (Table 2; Figure 2A and B). The 3D structures were retrieved from the PDB (http://www.rcsb.org/). Then, using BIOVIA Discovery Studio 2020 software (Version 20.1, Dassault Systèmes, USA) (https://discover.3ds.com/discovery-studio-visualizer-download/), the co-crystallized ligands, water molecules, and other non-protein components were removed to prepare receptors for docking. Then, the newly generated protein PDB structure underwent a series of quality analyses, including ERRAT and Procheck, using SAVES 6.0 (https://saves.mbi.ucla.edu/) as per standard protocol.[18]

2.4. Molecular docking interaction in AutoDock Vina

AutoDock Vina software (Version 1.2.0, Scripps Research, CA, USA) (http://vina.scripps.edu/) was used for molecular docking and virtual screening to predict protein–ligand binding poses and estimate binding affinities.[19] Docking was performed within a predefined grid box covering the binding site, and poses were ranked by the Vina scoring function. Kollman charges and other modifications were applied to the purified protein before proceeding to the final docking phase and converting it to a properly readable PDBQT file format. The ligand is similarly converted into a PDBQT file. A grid box was created around the protein's active residues, with various grid sizes and centers, but a

consistent grid spacing of 0.375 Å. Using the AutoDock Vina, binding affinity was predicted with an exhaustiveness value of 8. The final visualization of the docked structure was performed using BIOVIA Discovery Studio 2020.

2.5. Assessment of binding pockets, structural hotspots, and dynamics of receptor proteins

A systematic quantitative characterization of protein surface topography is available in the Computer Atlas Surface Topography of Protein (CASTp).[20] Active amino acid residues, structural hotspots, and different binding pockets of varied sizes on the receptor protein molecules were predicted using the CASTp 3.0 service. The iMod Server Prediction (http://imods.chaconlab.org/) application was used to assess the transition paths in internal coordinates naturally produced in collective functional motions within biomolecules,[21] providing advanced visualization and an improved affinity-model-based representation of domain dynamics.

Table 2. Selected ionotropic and metabotropic receptors with their respective PDB IDs

Type	PDB ID	Description
Metabotropic	1EWK	Glutamate receptor subtype 1
	3FUZ	Glutamate receptor, GluR5
	3G3F	Glutamate receptor, GluR6
	3KS9	Glutamate receptor mGluR1
	6BSZ	Glutamate receptor mGlu8
Ionotropic	5L1F	AMPA subtype glutamate receptor GluA2 in complex with Perampanel
	2WJW	Glutamate receptor AMPA subtype GluA2
	5L1G	Glutamate receptor AMPA subtype GluA2 in complex with GYKI-Br
	6IRH	Glutamate receptor, GluN1/GluN2A NMDA subtype
	7EOR	Glutamate receptor, GluN1/GluN2A NMDA subtype

Abbreviations: AMPA: α-amino-3-hydroxy-5-methyl-4-isoxazolepropionic acid receptor; NMDA: N-methyl-D-aspartate receptor; PBD: Protein Data Bank.

3. Results

3.1. SwissADME prediction of ligands

On submission of ligand structure in SMILES format, the SwissADME result was generated on the basis of ADME/toxicity analysis and Lipinski filter analysis (Table 3 and Figure 3). Various parameters, including physicochemical properties, lipophilicity, pharmacokinetics, and drug likeness, were included. Table 3 shows that all the compounds had molecular weights below the acceptable range (≤500 Da) and also met Lipinski's Rule of Five criteria (number of hydrogen bond acceptors ≤ 10 and number of hydrogen bond donors ≤5). This indicated that all the compounds could be easily absorbed, diffused, and transported.[22] The number of rotatable bonds is a measure of molecular flexibility and is widely used as a filter during the drug discovery process. In this criterion, all compounds fell within the acceptable range (≤ 15), indicative of their potential permeability and oral bioavailability. Table 4 shows that all compounds had a calculated logarithm of the partition coefficient below 5, indicating favorable lipophilicity and potential for membrane permeability. According to Table 5, most compounds exhibited high potential for absorption across the gastrointestinal tract and the blood–brain barrier (BBB). However, 2-acetyl-2-thiazoline and 2-acetyl-1-pyrroline showed low BBB permeation (Figure 3). Penetration across the BBB is essential for compounds targeting the CNS, and 8 out of 10 selected compounds were capable. Metabolism prediction data for compounds against five cytochrome P450 isoforms is a main priority during the drug discovery process. All compounds in our study had negative LogKp

Table 3. Physicochemical properties of the selected aroma compounds of Darjeeling black tea

Compound name	Formula	Molecular weight	Number of rotatable bonds	Number of H acceptors	Number of H donors
(E, E)-2,4-decadienal	$C_{10}H_{16}O$	153.23 g/mol	6	1	0
(E, E)-2,4-hexadienal	C_6H_8O	96.13 g/mol	2	1	0
Benzyl alcohol	C_7H_8O	108.14 g/mol	1	1	1
2-Acetyl-3-methylpyrazine	$C_7H_8N_2O$	136.15 g/mol	1	3	0
2-Acetyl-2-thiazoline	C_5H_7NOS	129.18 g/mol	1	2	0
2-Acetyl-1-pyrroline	C_6H_9NO	111.14 g/mol	1	2	0
α-Ionone	$C_{13}H_{20}O$	192.30 g/mol	2	1	0
Safranal	$C_{10}H_{14}O$	150.22 g/mol	1	1	0
2-Acetyl-3,5-dimethylpyrazine	$C_8H_{10}N_2O$	150.18 g/mol	1	3	0
5-Ethyl-2,3-dimethylpyrazine	$C_8H_{12}N_2$	136.19 g/mol	1	2	0

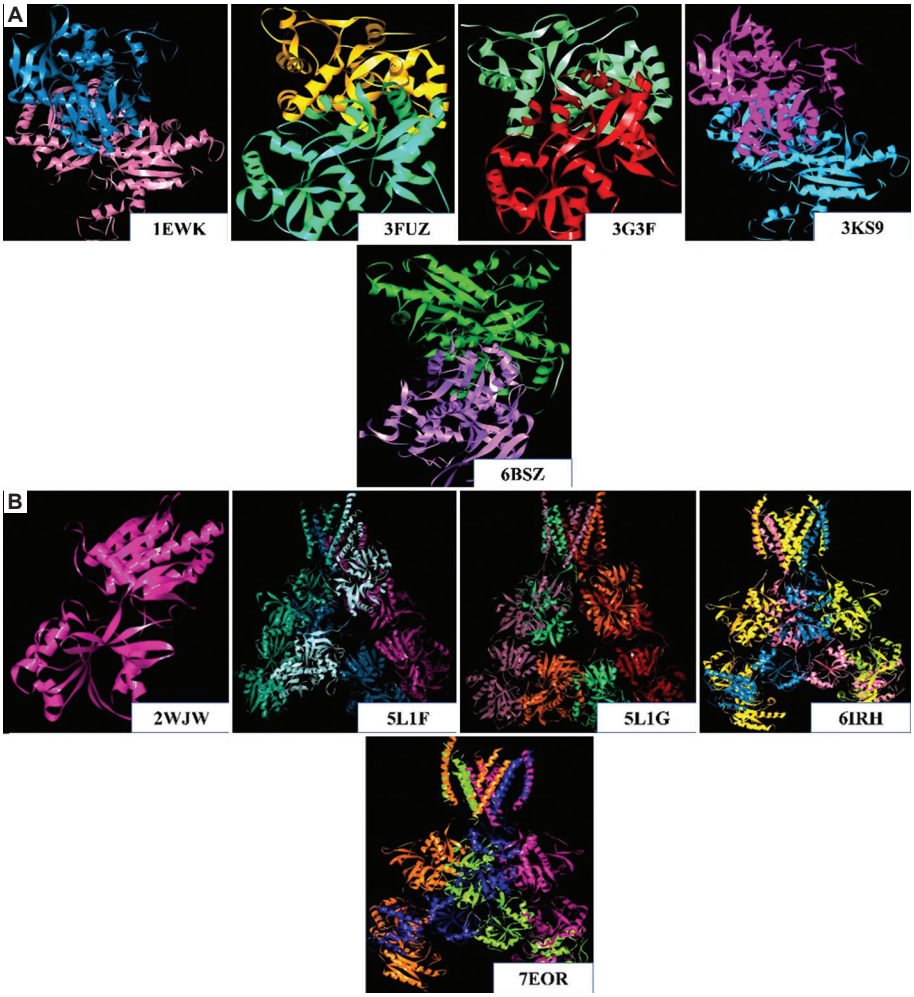

Figure 2. Three-dimensional structures of the (A) metabotropic and (B) ionotropic receptor proteins

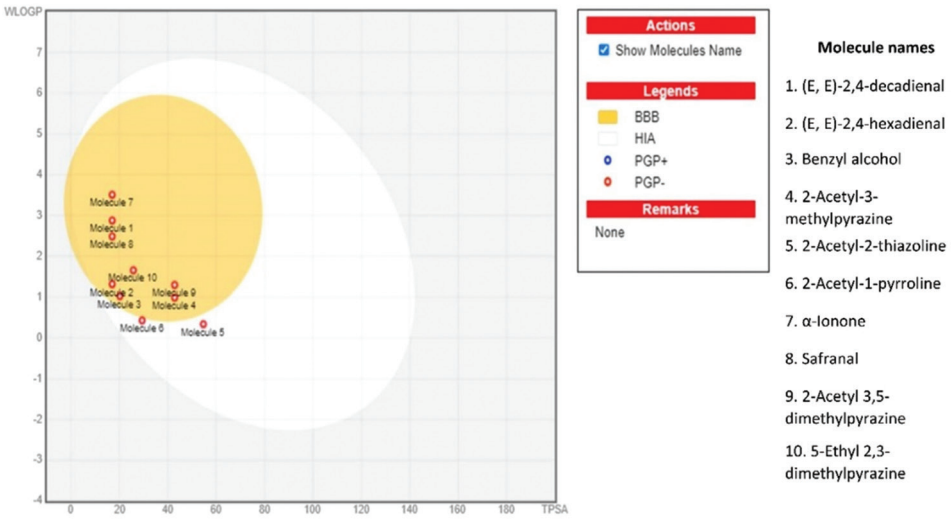

Figure 3. Boiled egg structure showing the permeability and other potential of the selected tea aroma compounds
Abbreviations: BBB: Blood–brain barrier; HIA: Human intestinal absorption; PGP: P-glycoprotein.

Table 4. Lipophilicity of the selected aroma compounds of Darjeeling black tea

Compound name	Log Pa/w (iLOGP)	Log Pa/w (XLOGP3)	Log Pa/w (WLOGP)	Log Pa/w (MLOGP)	Log Pa/w (SILICOS-IT)	Consensus log Pa/w
(E, E)-2,4-decadienal	2.67	3.25	2.88	2.49	2.96	2.85
(E, E)-2,4-hexadienal	1.63	1.19	1.32	1.18	1.23	1.31
Benzyl alcohol	1.66	1.10	1.03	1.54	1.74	1.41
2-Acetyl-3-methylpyrazine	1.50	0.20	0.99	−0.75	1.61	0.71
2-Acetyl-2-thiazoline	1.51	0.22	0.34	−0.42	2.21	0.77
2-Acetyl-1-pyrroline	1.07	−0.43	0.43	−0.04	2.17	0.64
α-Ionone	2.81	3.85	3.51	2.94	3.41	3.31
Safranal	2.13	2.14	2.49	2.10	2.62	2.30
2-Acetyl-3,5-dimethylpyrazine	1.29	0.60	1.30	−0.42	2.06	0.97
5-Ethyl-2,3-dimethylpyrazine	2.02	1.38	1.66	0.55	2.53	1.63

Table 5. Physiological properties of the selected aroma compounds of Darjeeling black tea

Compound name	GI absorption	BBB permeant	P-gp substrate	CYP1A2 inhibitor	CYP2C19 inhibitor	CYP2C9 inhibitor	CYP2D6 inhibitor	CYP3A4 inhibitor	Log Kp (skin permeation)
(E, E)-2,4-decadienal	High	Yes	No	No	No	No	No	No	−4.92 cm/s
(E, E)-2,4-hexadienal	High	Yes	No	No	No	No	No	No	−6.02 cm/s
Benzyl alcohol	High	Yes	No	Yes	No	No	No	No	−6.18 cm/s
2-Acetyl-3-methylpyrazine	High	Yes	No	No	No	No	No	No	−6.99 cm/s
2-Acetyl-2-thiazoline	High	No	No	No	No	No	No	No	−6.93 cm/s
2-Acetyl-1-pyrroline	High	Yes	No	No	No	No	No	No	−7.28 cm/s
α-Ionone	High	Yes	No	No	No	Yes	No	No	−4.74 cm/s
Safranal	High	Yes	No	No	No	No	No	No	−5.70 cm/s
2-Acetyl-3,5-dimethylpyrazine	High	Yes	No	No	No	No	No	No	−6.79 cm/s
5-Ethyl-2,3-dimethylpyrazine	High	Yes	No	No	No	No	No	No	−6.15 cm/s

Abbreviations: BBB: Blood–brain barrier; CYP: Cytochrome P450; GI: Gastrointestinal; Kp: Skin permeation coefficient; P-gp: P-glycoprotein.

values, indicating low predicted skin permeation. The drug-likeness results (Table 6) showed that all compounds met the criteria, with no parameter violations. Table 6 also shows the bioavailability scores that define the extent and rate at which compounds administered can enter systemic circulation and ultimately reach the targeted sites upon oral administration. Nine compounds showed a similar score of 0.55, except benzyl alcohol, scoring 0.85. This value indicates that the compounds adhered to Lipinski's Rule of Five and had a predicted oral bioavailability of 55% or higher.

3.2. Toxicity prediction of the ligands

During drug development, small-molecule toxicity testing is an essential step. Table 7 displays toxicological predictions from the PreADMET service, including mutagenicity, carcinogenicity, and hERG inhibition, where a negative prediction indicates carcinogenic

Table 6. Drug likeness of the selected aroma compounds of Darjeeling black tea

Compound name	Lipinski's rule satisfactory	Number of violations	Bioavailability score
(E, E)-2,4-decadienal	Yes	0	0.55
(E, E)-2,4-hexadienal	Yes	0	0.55
Benzyl alcohol	Yes	0	0.85
2-Acetyl-3-methylpyrazine	Yes	0	0.55
2-Acetyl-2-thiazoline	Yes	0	0.55
2-Acetyl-1-pyrroline	Yes	0	0.55
α-Ionone	Yes	0	0.55
Safranal	Yes	0	0.55
2-Acetyl-3,5-dimethylpyrazine	Yes	0	0.55
5-Ethyl-2,3-dimethylpyrazine	Yes	0	0.55

Table 7. Results of mutagenicity, carcinogenicity, and hERG inhibition of the selected aroma compounds of black tea

Compound name	Ames test	Carcinogenicity (mouse)	Carcinogenicity (rat)	hERG inhibition
(E, E)-2,4-decadienal	Mutagen	Negative	Positive	Medium risk
(E, E)-2,4-hexadienal	Mutagen	Positive	Positive	Medium risk
Benzyl alcohol	Mutagen	Negative	Negative	Medium risk
2-Acetyl-3-methylpyrazine	Mutagen	Negative	Negative	Low risk
2-Acetyl-2-thiazoline	Mutagen	Negative	Negative	Medium risk
2-Acetyl-1-pyrroline	Mutagen	Negative	Negative	Medium risk
α-Ionone	Mutagen	Positive	Negative	Low risk
Safranal	Mutagen	Negative	Negative	Low risk
2-Acetyl-3,5-dimethylpyrazine	Mutagen	Negative	Negative	Low risk
5-Ethyl-2,3-dimethylpyrazine	Mutagen	Negative	Negative	Low risk

Abbreviation: hERG: human Ether-à-go-go-related gene.

activity and a positive means the compound possesses no carcinogenic activity. The Ames test, based on bacterial mutagenicity, showed that all selected black tea aromatic molecules had mutagenic properties as ligand candidates. The hERG inhibition test, conducted to assess the effect of the molecules on the cardiac potassium channel,[23] showed moderate to low risk, with selected pyrazine, ionone, and safranal compounds having much lower risk to cardiac function. Probable carcinogenicity assessment in the PreADMET service indicated that most selected candidates were non-carcinogenic in mice and rats, except for the decadienal compound in rats, α-ionone in mice, and the hexadienal compound in both species (Table 7).

3.3. Validation of protein structures

The overall quality of all 3D protein PDB structures was assessed using the online tools (Figure S1). By confirming the protein PDB model against several quality criteria, the ideal protein structures were approved. The "overall quality factor" that ERRAT displayed indicated that proteins with higher scores are of greater quality. Most proteins had quality scores between 86% and 98%, except for 6IRH (43%), indicating that most are all well-modeled. The Ramachandran plots of most protein models showed that over 80% of residues were found in the most preferred regions, followed by the extra allowed, generously allowed, and banned regions, in accordance with the Procheck results. Together, these strong validations ensured the precision of molecular docking investigations by demonstrating that the interactions between ligands and proteins were faithfully reproduced.

3.4. Molecular docking interaction using AutoDock Vina

Docking analyses were conducted using AutoDock Vina. The overall binding affinities of all tea bioactive compounds for the five metabotropic receptors were depicted pictorially (Figure 4). When the stability of the docking interactions was calculated, several specific receptor–ligand interactions emerged as the most potent and stable, with binding affinities around −6 kcal/mol or lower. α-ionone and safranal were the most prominent ligands, and mGluR1 (IEWK), GluR5 (3FUZ), and GluR6 (3G3F) were the most common metabotropic receptors, providing stable interactions. Table 8 shows the best interactions and their binding affinities. Based on the graphical view generated through BIOVIA Discovery Studio 2020, two-dimensional and 3D modes of binding interactions of top docked compounds are presented in Figure 5A-E, where the affinity score ranged between −5.7 and −7.1 kcal/mol.

For ionotropic GluRs, specific subtypes of AMPA (2WJW) and NMDA (7EOR) exhibited stronger binding affinities for α-ionone and safranal (Figure 6). Two-dimensional and 3D models of binding prediction using BIOVIA Discovery Studio 2020 showed binding pockets and molecular interactions with the ionotropic receptors (Figure 7A-E), with affinity scores ranging from −4.7 to −6.4 kcal/mol.

3.5. Assessment of binding pockets, active amino acid residues, and dynamics

Table 9 shows the results from the CASTp 3.0 online server for structural hotspots or active amino acid residues of the protein PDB structure. The best-fit receptor–ligand complexes with the highest binding affinity were used to identify the active amino acid residues during ligand binding. Numerous amino acid types distributed across different regions create the receptors' structural pockets and are implicated in molecular interactions with ligands. The interaction showed that the most potential binding may occur between GluR6 metabotropic receptor (3G3F)

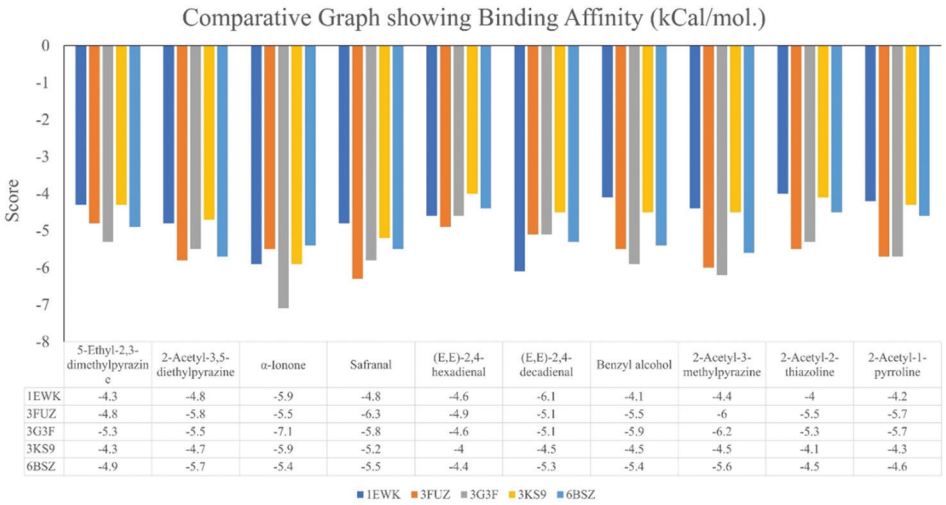

	5-Ethyl-2,3-dimethylpyrazine	2-Acetyl-3,5-diethylpyrazine	α-Ionone	Safranal	(E,E)-2,4-hexadienal	(E,E)-2,4-decadienal	Benzyl alcohol	2-Acetyl-3-methylpyrazine	2-Acetyl-2-thiazoline	2-Acetyl-1-pyrroline
1EWK	-4.3	-4.8	-5.9	-4.8	-4.6	-6.1	-4.1	-4.4	-4	-4.2
3FUZ	-4.8	-5.8	-5.5	-6.3	-4.9	-5.1	-5.5	-6	-5.5	-5.7
3G3F	-5.3	-5.5	-7.1	-5.8	-4.6	-5.1	-5.9	-6.2	-5.3	-5.7
3KS9	-4.3	-4.7	-5.9	-5.2	-4	-4.5	-4.5	-4.5	-4.1	-4.3
6BSZ	-4.9	-5.7	-5.4	-5.5	-4.4	-5.3	-5.4	-5.6	-4.5	-4.6

Figure 4. Graphical representation of binding affinity along with the score (kcal/mol) toward the target metabotropic receptors of glutamate by the respective compounds or ligands

Table 8. Results of maximum binding affinity scores in AutoDoc Vina between glutamate receptors and the best selected aroma compounds of black tea

Ranking	Receptor (common name)	Receptor (PDB ID)	Ligand	Affinity score (kcal/mol)
1	GluR6 metabotropic receptor	3G3F	α-Ionone	−7.1
2	GluN1/GluN2A NMDA ionotropic receptor subtype	7EOR	α-Ionone	−6.4
3	GluR5 metabotropic receptor	3FUZ	Safranal	−6.3
4	GluR-AMPA ionotropic receptor subtype	2WJW	Safranal	−6.2
5	GluR1 metabotropic receptor	1EWK	(E, E)-2,4-decadienal	−6.1
6	Glutamate Receptor mGlu8	6BSZ	2-Acetyl-3,5-dimethylpyrazine	−5.7
7	Glutamate Receptor AMPA Subtype	5L1G	α-Ionone	−4.7
8	GluR1 metabotropic receptor	3KS9	α-Ionone	−5.9
9	GluN1/GluN2A NMDA ionotropic receptor subtype	6IRH	α-Ionone	−5.9
10	AMPA Subtype Glutamate Receptor GluA2	5L1F	α-Ionone	−4.8

Abbreviations: AMPA: α-amino-3-hydroxy-5-methyl-4-isoxazolepropionic acid receptor; NMDA: N-methyl-D-aspartate receptor; PDB: Protein Data Bank.

and α-ionone, with an affinity scoring of −7.1 kcal/mol, where the ligand interacted with the Thr108 and Lys248 of B chain of the receptor through the hydrogen bond and alkyl bond, respectively, providing a stable interaction output (Figures 5, S1C, and S2VIII). Next significant docking and interaction occurred between the ionotropic GluN1/Glu2A NMDA receptor (7EOR) with α-ionone, having affinity scoring of −6.4 kcal/mol, where the α-ionone terminal oxygen of C=O interacted with B chain Ser700, a pi-alkyl bond formed between the benzene ring of ligand and Trp795 of C chain, and pi-sigma bond forms with same residue (Figure 7). Further analysis of the structure and dynamics showed a lower level of interaction favorability than in the previous one (Figures S1J and S2E). The next higher probability of structural interaction was observed with safranal and the GluR5 metabotropic receptor (3FUZ), with a binding affinity score of −6.3 kcal/mol. In this interaction, safranal interacted with the adjacent Ser674 and Thr675 of the B chain of the receptor through hydrogen bonding, and the ligand benzene ring interacted with the receptor B chain Tyr474 through pi-alkyl and pi-sigma bonding in the binding pocket (Figure 5). Further protein structure analysis showed favorable structural stability and molecular dynamics of receptor–ligand interactions (Figures S1B and S2VII). Safranal also showed potential binding to the Glu–AMPK ionotropic receptor (2WJW), where it interacted in the binding pocket through hydrogen and alkyl bonds with the receptor A chain Arg129, Arg156, and Tyr295 (Figure 7), but this interaction was dynamic and unstable (Figure S2A). Other interactions showed similar or lesser docking potential and structural stability.

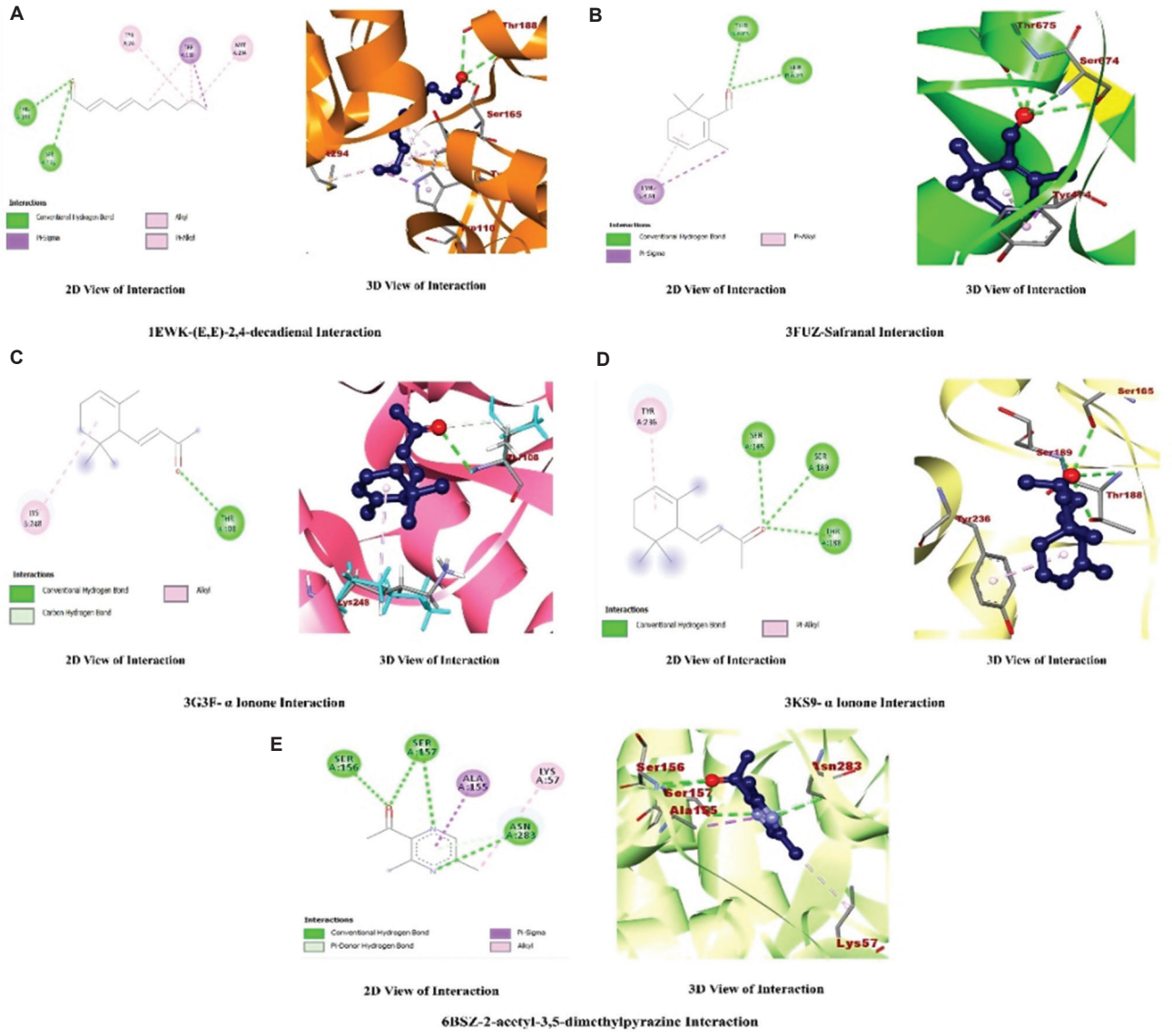

Figure 5. Complete representation and close insight into 2D and 3D interactions between best-scored metabotropic glutamate receptors and ligands. (A) 1EWK–(E,E)-2,4-decadienal interaction. (B) 3FUZ–safranal interaction. (C) 3G3F–α-ionone interaction. (D) 3KS9–α-ionone interaction. (E) 6BSZ–2-acetyl-3,5-dimethylpyrazine interaction.
Abbreviations: 2D: Two-dimensional; 3D: Three-dimensional.

Among the amino acid residues, polar uncharged serine and threonine, along with positively charged arginine and lysine, were most frequently observed within the binding pockets that interacted with α-ionone and safranal, indicating favorable receptor–ligand interactions. Other amino acids in the binding pockets were hydrophobic residues, such as tyrosine, tryptophan, valine, leucine, isoleucine, alanine, and methionine, which were available to interact with aromatic ligands. The iMOD server analysis showed specific eigenvalues of the receptor–ligand complex systems (eigenvectors) as per the principal component analysis, where three out of five metabotropic receptors, namely, GluR type 1 (1EWK), GluR5 (3FUZ), GluR6 (3G3F), and only one out of five ionotropic receptors, namely, AMPA receptor (5LIG), showed high eigenvalue that signified a large variance or dynamics in the system. In general, upon ligand binding, metabotropic receptors are structurally dynamic; whereas ionotropic receptors are structurally stiffer, except for the AMPA receptor 5L1G (Figure S2). Overall, we observed that the most suitable binding occurred between α-ionone and 3G3F, as well

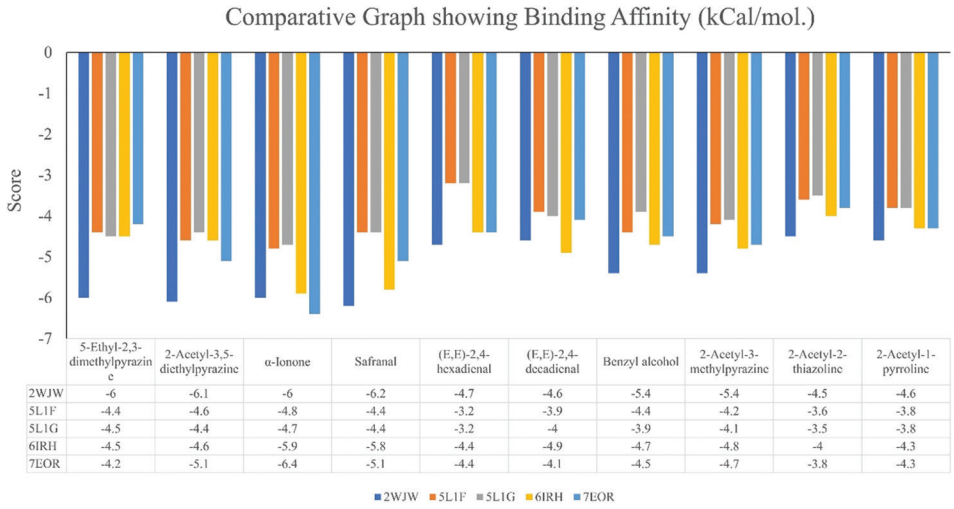

	5-Ethyl-2,3-dimethylpyrazine	2-Acetyl-3,5-diethylpyrazine	α-Ionone	Safranal	(E,E)-2,4-hexadienal	(E,E)-2,4-decadienal	Benzyl alcohol	2-Acetyl-3-methylpyrazine	2-Acetyl-2-thiazoline	2-Acetyl-1-pyrroline
2WJW	-6	-6.1	-6	-6.2	-4.7	-4.6	-5.4	-5.4	-4.5	-4.6
5L1F	-4.4	-4.6	-4.8	-4.4	-3.2	-3.9	-4.4	-4.2	-3.6	-3.8
5L1G	-4.5	-4.4	-4.7	-4.4	-3.2	-4	-3.9	-4.1	-3.5	-3.8
6IRH	-4.5	-4.6	-5.9	-5.8	-4.4	-4.9	-4.7	-4.8	-4	-4.3
7EOR	-4.2	-5.1	-6.4	-5.1	-4.4	-4.1	-4.5	-4.7	-3.8	-4.3

Figure 6. Graphical representation of binding affinity along with the score (kcal/mol) towards the target ionotropic receptors of glutamate by the respective compounds/ligands

Table 9. Active amino acid residues of the receptors using Computer Atlas Surface Topography of Protein 3.0 with best-fitted ligand aroma compounds derived from Darjeeling black tea

No.	Receptor (PDB ID)	Ligand	Active amino acid residues for binding
1	3G3F	α-Ionone	THR 108, LYS 248
2	7EOR	α-Ionone	SER 700, TRP 795
3	3FUZ	Safranal	TYR 474, SER 674, THR 675
4	2WJW	Safranal	ARG 129, ARG 156, TYR 295
5	1EWK	(E, E)-2,4-decadienal	TYR 74, TRP 110, SER 165, THR 188, MET 294
6	6BSZ	2-Acetyl-3,5-dimethylpyrazine	LYS 57, ALA 155, SER 156, SER 157, SER 283
7	5L1G	α-Ionone	ILE 664, ARG 675, LYS 761, LYS 765
8	3KS9	α-Ionone	SER 165, THR 188, SER 189, TYR 236
9	6IRH	α-Ionone	ASN 432, LYS 457, LEU 794, TRP 795
10	5L1F	α-Ionone	ARG 453, VAL 484, SER 654

Abbreviation: PDB: Protein Data Bank.

as between safranal and 3FUZ, which may have greater biological significance.

4. Discussion

Tea consumption is one of the most common cultural practices worldwide and has putative public health benefits. Depending on preparation, particularly for green and black tea, it releases wide variations of bioactive compounds and flavors in infusions, such as catechins, flavonoids, polyphenols, L-theanine, and numerous aroma compounds, as well as their derivatives.[3,14] Previous studies have shown that L-theanine, unique to green and black tea and some mushrooms, induces relaxation and improves attention in humans.[1,24] Additionally, routine intake of tea has been reported to have a significant effect on mood and improve the restoration of cortisol at the basal level after stress, resulting in quicker stress recovery, as evidenced in various population-based studies.[9,25,26]

There are a variety of aroma compounds that characterize different tea types for the world population. Among which, one of the best authentic aromatic tea varieties is Darjeeling tea, produced and processed in the cool, humid southern hill slopes of the Himalayas, at altitudes of 1,000 m–3,000 m, from Nepal to Bhutan, centered on the Darjeeling district of West Bengal, India. The tea leaves are harvested in spring and summer, selected, weathered, rolled, fermented-oxidized, and processed to produce signature Darjeeling black tea. In hot, aqueous infusion, it releases the flavor and taste for which it is widely recognized.[14,15,27] In the current study, some of the prominent compounds associated with Darjeeling tea flavor were selected (Table 1) with their fragrance characteristics. When different physical and chemical parameters of the compounds, including BBB permeability and drug likeness, were tested, they were found to be highly absorbable through gastric endothelial tissue, and most were BBB permeable except 2-acetyl-2-thiazoline. However, all tested aroma compounds met Lipinski's criteria, demonstrating drug-likeness with persistent bioavailability scores of 0.55 and above, with a maximum score of 0.85 for benzyl alcohol (Tables 3-6). Most of these compounds were low

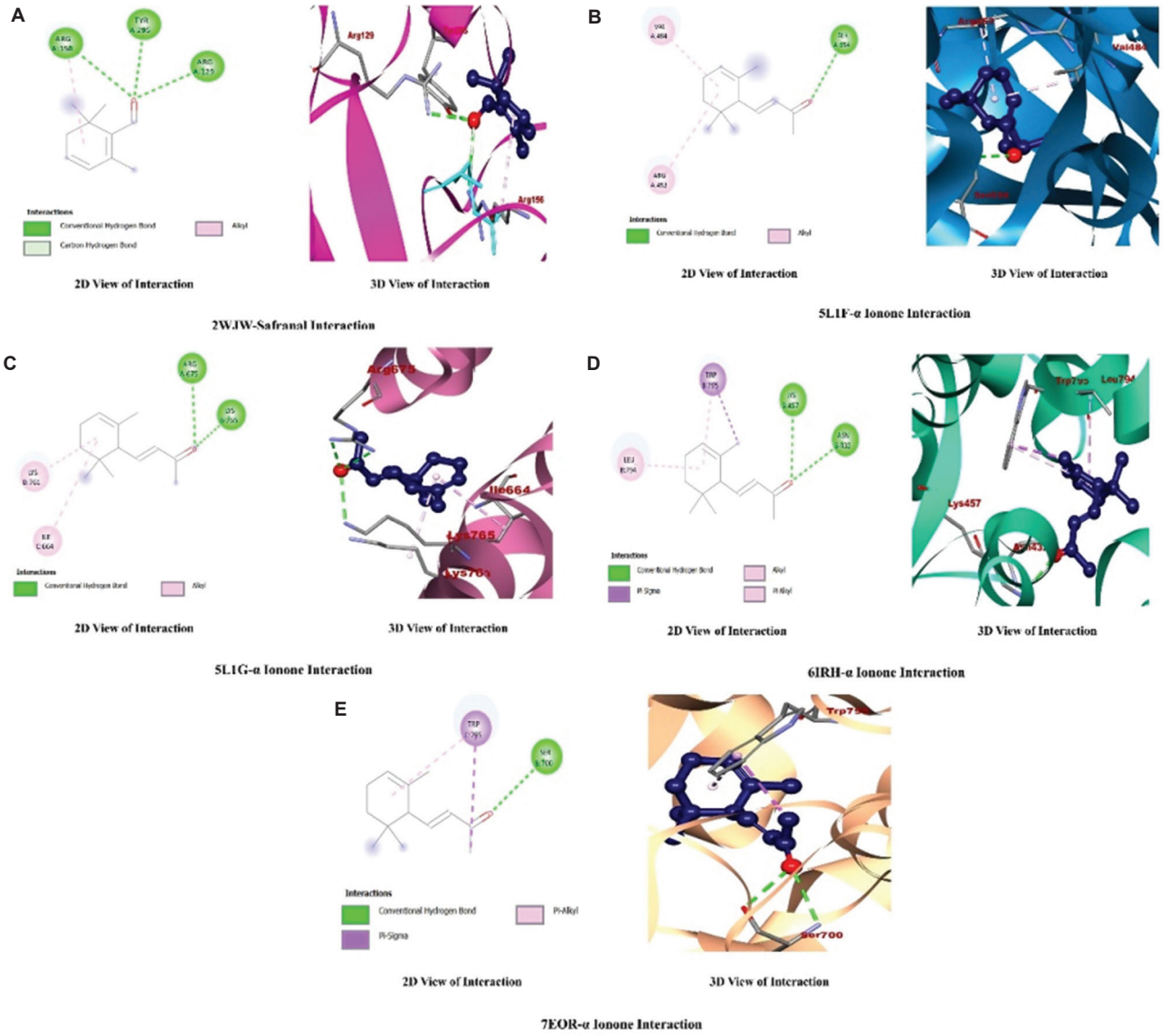

Figure 7. Complete representation and close insight into 2D and 3D interactions between the best-scoring ionotropic glutamate receptors and ligands. (A) 2WJW–safranal interaction. (B) 5L1F–α-ionone interaction. (C) 5L1G–α-ionone interaction. (D) 6IRH–α-ionone interaction. (E) 7EOR–α-ionone interaction.
Abbreviations: 2D: Two-dimensional; 3D: Three-dimensional.

to medium-risk mutagens, with most of them showing no carcinogenicity, thereby qualifying as effective ligands. Prominent metabotropic and ionotropic GluRs (Table 2) were subjected to the structural validation of the PDB models on which the ligand docking experiments were performed (Figure S1). The experiments showed binding affinities ranging from −7.1 to −4.8 kcal/mol for the top 10 receptor–ligand pairs, within the flexible-ligand docking range, indicating biological efficiency of this interaction.[28] Hence, interactions of metabotropic receptors—GluR1 (1EWK), GluR5 (3FUZ), and GluR6 (3G3F)—with (E, E)-2,4-decadienal, safranal, or α-ionone, respectively, and ionotropic receptors—GluN1/GluN2A NMDA subtype (7EOR) and GluR-AMPA subtype (2WJW)—with α-ionone or safranal, respectively, were found to be the most promising and probable. Among the ligands, safranal and α-ionone were monoterpenoids with a characteristic aroma of the black tea variant well-known to tea lovers.[15,27] Analysis through the iMOD server on the structural coordinates of the receptors showed that metabotropic receptors had higher eigenvalues and spread, indicating higher dynamics. Whereas ionotropic receptors involved in

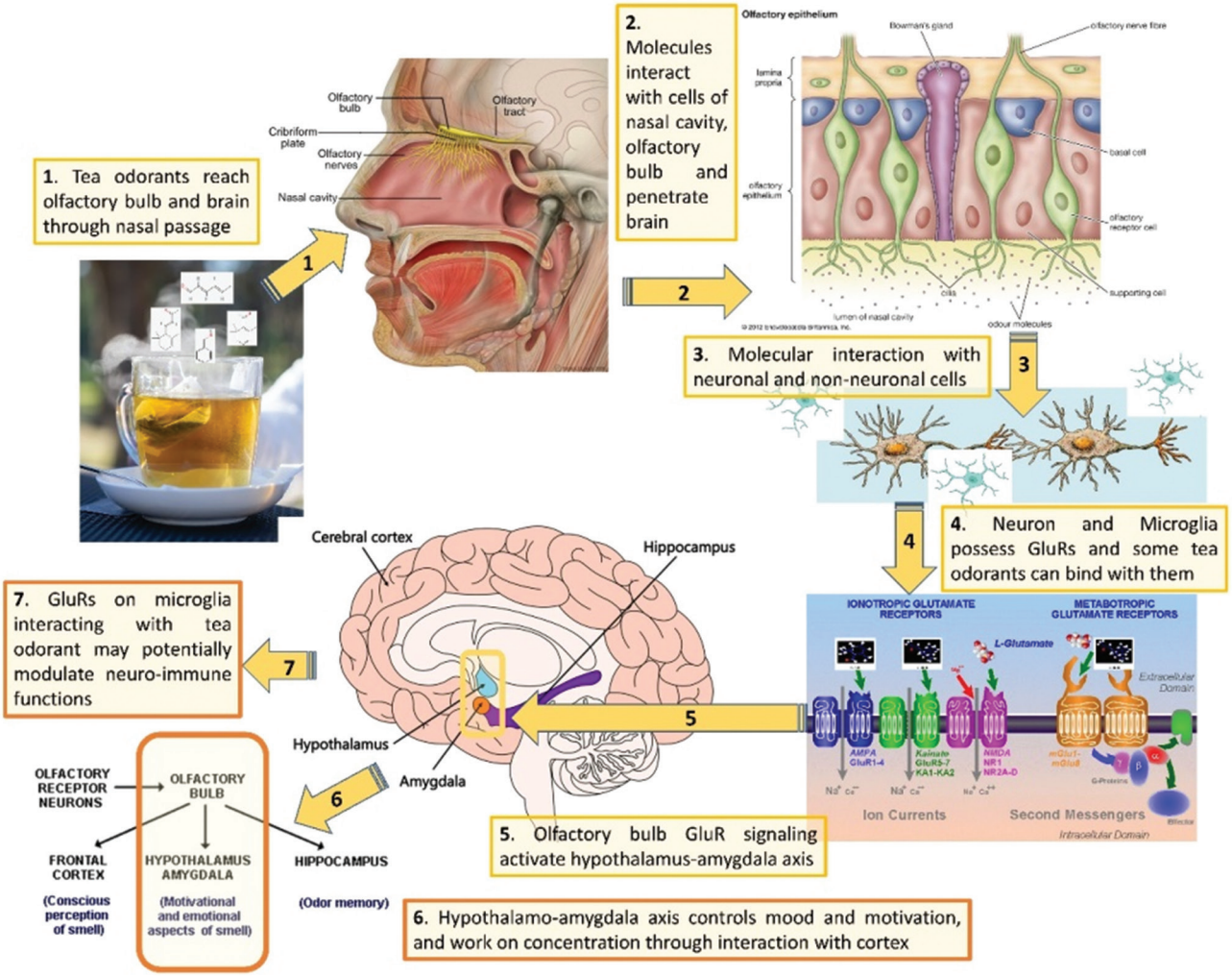

Figure 8. Concept diagram of the prospective mechanism of action of Darjeeling tea aromatics on mood, attention, and neuro-immune physiology

binding showed lower eigenvalues and spread, indicating structural stiffness (Figure S2).[21,28] However, the most dynamic components were the metabotropic GluR5 and GluR6, and the ionotropic AMPA receptor also exhibits notable dynamicity. The top four ligand receptor bindings showed that the interactions between ligands (α-ionone and safranal) and receptors were occurring in between only 2–3 amino acid residues, either polar or hydrophobic in nature (Figures 5 and 7).

As found, the ligands were mostly capable of crossing the endothelial lining, absorbing through the gastrointestinal tract and BBB with sufficient bioavailability scores, and can be delivered via both oral and olfactory routes to reach their target receptors. Therefore, the black tea volatile compounds selected in this study had ample opportunity to interact with, dock onto, and exert subsequent effects on the neuroglial cells associated with this passage. In addition, their high absorption score through the gastrointestinal tract, moderate to high bioavailability, and penetration capability through the BBB (except 2-acetyl-2-thiazoline) (Figure 3) ensure their systemic reach to the CNS matrix and capability to interact with the neuroglial population from regions of cerebral cortex to the hippocampus and the hypothalamus, thus supporting possibility that these compounds could influence neurophysiology, behavior, and neuroimmune signaling.

In a recent study, glutamate ionotropic AMPA and NMDA receptors, including GluA1, GluA2, GluN1, and GluN2A, were identified in the hypothalamus and showed their critical role in glutaminergic synaptic transmission.[29] Such signaling is significantly related to learning and memory, as well as neuroendocrine functions, and is associated with circadian, feeding, and behavioral disorders.[30,31] In addition to the widespread presence of GluRs throughout the CNS, including the olfactory circuit, olfactory tissue exhibits a robust innate

immune defense. Immune cells migrate across the lamina propria into olfactory neurons, express ionized calcium-binding adapter molecule 1 and C-X3-C motif chemokine receptor 1, and release inflammatory mediators, such as inducible nitric oxide synthase, interleukin 6, and tumor necrosis factor alpha (TNF-α).[32] These cells, particularly microglia, express a wide range of neurotransmitter receptors and membrane proteins, including cluster of differentiation (CD)200, CD22, and CD47, which facilitate interactions with neurons. Microglia can modulate neuronal function by releasing glutamate, ATP, ADP, reactive oxygen species, nitric oxide, prostaglandin E2, brain-derived neurotropic factor, miRNAs, and various cytokines/chemokines.[33] Previous studies have shown that activation of Group III metabotropic GluRs (mGluR4/6/8) promotes a neuroprotective microglial phenotype, whereas activation of Group II receptors (mGluR2/3) is associated with a neurotoxic phenotype characterized by the release of TNFs and Fas receptor signaling, as well as R, Ca^{+2}-wave-driven neuronal injury. NMDA expression in these cells follows nuclear factor κB signaling and the release of nitric oxide, interleukin 1β, and TNF-α, thereby mediating increased excitability of hippocampal cornu ammonis area 3 neurons.[33-35] Evidence shows that microglia are present throughout the nasal epithelium and olfactory nerves, extending along the subventricular zone–olfactory bulb axis. These cells play a protective role against pathogenic insults and the development of olfactory dysfunctions, and can receive glutamate signals to modulate neuronal activity.[36,37] As AMPA and NMDA receptors and metabotropic GluRs are expressed on both neurons and microglia, their reciprocal interactions and functional responses under glutamate release or storming are crucial for a wide range of neurophysiological conditions. In all these situations, safranal, α-ionone, and other aroma compounds derived from tea may play a pivotal role from multiple perspectives.

5. Conclusion

Our study explored the potential of several prominent Darjeeling tea aroma compounds to modulate neuroglial function, thereby influencing neurophysiology and behavior via GluRs (Figure 8). These compounds, prominently α-ionone, safranal, (E, E)-2,4-decadienal, are found to be sufficiently bioavailable to the olfactory bulb and CNS, and capable of interacting with group I metabotropic receptors (mGluR1 and mGluR5), as well as Group III metabotropic receptors (mGluR6 and mGluR8). As a Group, I receptors are the moderators capable of increasing NMDA receptor activity; they can synergistically uplift the function of neuronal circuitry. In contrast, Group III metabotropic receptors are characterized by downregulation of secondary messenger-dependent signaling and by neurotoxic effects.[11,12] The same aroma compounds, such as safranal and α-ionone, can also bind to GluR-AMPA and GluN1/GluN2A NMDA ionotropic receptor subtypes, which are widespread on neuroglial cells throughout the naso-buccal cavity, cortex, and hypothalamus. These interactions may have broad functional implications, including activation of the hypothalamo–amygdala axis, as discussed previously. Simultaneously, they can bind to GluRs expressed on microglia and brain macrophages, thereby activating the neuro-immuno axis as previously discussed. This study highlights the novel potential of Darjeeling tea aroma compounds and suggests a new avenue for investigating their effects on neuroglial function.

Acknowledgments

The authors extend their sincere thanks to the authorities of the Netaji Subhas Open University and Techno India University, West Bengal, India, for providing the required infrastructural and institutional support.

Funding

None.

Conflict of interest

The authors declare that they have no competing interests.

Author contributions

Conceptualization: Anirban Ghosh
Data curation: Moumita Saha, Anup Sardar
Formal analysis: Anirban Ghosh, Sirshendu Chatterjee
Investigation: All authors
Methodology: Moumita Saha
Supervision: Anirban Ghosh
Writing-original draft: Moumita Saha
Writing-review & editing: Anirban Ghosh, Sirshendu Chatterjee

Ethics approval and consent to participate

Not applicable.

Consent for publication

Not applicable.

Availability of data

All data were obtained from the website/databank and derived from software or open platforms as described in the text.

References

1. Skotnicka M, Chorostowska-Wynimko J, Jankun J, Skrzypczak-Jankun E. The black tea bioactivity: An

overview. *Cent Eur J Immunol*. 2011;36(4):284-292.

2. Fatima M, Rizvi SI. Health beneficial effects of black tea. *Biomedicine*. 2011;31:3-8.
3. Li S, Lo CY, Pan MH, Lai CS, Ho CT. Black tea: Chemical analysis and stability. *Food Funct*. 2013;4(1):10-18.

   doi: 10.1039/c2fo30093a
4. Pan MH, Lai CS, Wang H, *et al.* Black tea in chemo-prevention of cancer and other human diseases. *Food Sci Hum Wellness*. 2013;2(1):12-21.

   doi: 10.1016/j.fshw.2013.03.004
5. Cao J, Han J, Xiao H, Qiao J, Han M. Effect of tea polyphenol compounds on anticancer drugs in terms of anti-tumor activity, toxicology and pharmacokinetics. *Nutrients*. 2016;8(12):762.

   doi: 10.3390/nu8120762
6. Gao Y, Rankin GO, Tu Y, Chen C. Inhibitory effects of the four main theaflavin derivatives found in black tea on ovarian cancer cells. *Anticancer Res*. 2016;36(2):643-651.
7. Yang K, Gao ZY, Li TQ, *et al.* Anti-tumor activity and the mechanism of a green tea (*Camellia sinensis*) polysaccharide on prostate cancer. *Int J Biol Macromol*. 2019;122:95-103.

   doi: 10.1016/j.ijbiomac.2018.10.101
8. Wang Q, Yang X, Zhu C, Liu G, Sun Y, Qian L. Advances in the utilization of tea polysaccharides: Preparation, physicochemical properties and health benefits. *Polymers (Basel)*. 2022;14(14):2775.

   doi: 10.3390/polym14142775
9. Yoto A, Fukui N, Kaneda C, *et al.* Black tea aroma inhibited increase of salivary chromogranin-A after arithmetic tasks. *J Physiol Anthropol*. 2018;37(1):3.

   doi: 10.1186/s40101-018-0163-0
10. Formica ML, Real DA, Picchio ML, Catlin E, Donnelly RF, Paredes AJ. On a highway to the brain: A review on nose-to-brain drug delivery using nanoparticles. *Appl Mater Today*. 2022;29:101631.

    doi: 10.1016/j.apmt.2022.101631
11. Willard SS, Koochekpour S. Glutamate, glutamate receptors, and downstream signaling pathways. *Int J Biol Sci*. 2013;9(9):948-959.

    doi: 10.7150/ijbs.6426
12. Pal MM. Glutamate: The master neurotransmitter and its implications in chronic stress and mood disorders. *Front Hum Neurosci*. 2021;15:722323.

    doi: 10.3389/fnhum.2021.722323
13. Seo Y, Kim HS, Kang KS. Microglial involvement in the development of olfactory dysfunction. *J Vet Sci*. 2018;19(3):319-330.

    doi: 10.4142/jvs.2018.19.3.319
14. Ho CT, Zheng X, Li S. Tea aroma formation. *Food Sci Hum Wellness*. 2015;4(1):9-27.

    doi: 10.1016/j.fshw.2015.04.001
15. Parveen A, Qin CY, Zhou F, *et al.* The chemistry, sensory properties and health benefits of aroma compounds of black tea produced by *Camellia sinensis* and *Camellia assamica*. *Horticulturae*. 2023;9(12):1253.

    doi: 10.3390/horticulturae9121253
16. Rezaei-Seresht H, Cheshomi H, Falanji F, Movahedi-Motlagh F, Hashemian M, Mireskandari E. Cytotoxic activity of caffeic acid and gallic acid against MCF-7 human breast cancer cells: An *in silico* and *in vitro* study. *Avicenna J Phytomed*. 2019;9(6):574-586.
17. Daina A, Michielin O, Zoete V. SwissADME: A free web tool to evaluate pharmacokinetics, drug-likeness and medicinal chemistry friendliness of small molecules. *Sci Rep.* 2017;7:42717.

    doi: 10.1038/srep42717
18. Sharma C, Nigam A, Singh R. Computational-approach understanding the structure-function prophecy of fibrinolytic protease RFEA1 from Bacillus cereus RSA1. *PeerJ*. 2021;9:e11570.

    doi: 10.7717/peerj.11570
19. Trott O, Olson AJ. AutoDock Vina: Improving the speed and accuracy of docking with a new scoring function, efficient optimization and multithreading. *J Comput Chem*. 2010;31(2):455-461.

    doi: 10.1002/jcc.21334
20. Tian W, Chen C, Lei X, Zhao J, Liang J. CASTp 3.0: Computed atlas of surface topography of proteins. *Nucleic Acids Res*. 2018;46(W1):W363-W367.

    doi: 10.1093/nar/gky473
21. López-Blanco JR, Aliaga JI, Quintana-Ortí ES, Chacón P. iMODS: Internal coordinates normal mode analysis server. *Nucleic Acids Res*. 2014;42(W1):W271-W276.

    doi: 10.1093/nar/gku484
22. Lipinski CA, Lombardo F, Dominy BW, Feeney PJ. Experimental and computational approaches to estimate solubility and permeability in drug discovery and development settings. *Adv Drug Deliv Rev*. 1997;23(1-3):3-25.

    doi: 10.1016/S0169-409X(96)00423-1
23. Xu C, Cheng F, Chen L, *et al. In silico* prediction of chemical Ames mutagenicity. *J Chem Inf Model*. 2012;52(11):2840-2847.

    doi: 10.1021/ci300400a
24. Nobre AC, Rao A, Owen GN. L-theanine, a natural

constituent in tea, and its effect on mental state. *Asia Pac J Clin Nutr*. 2008;17 Suppl 1:167-168.

25. Gibson EL, Rycroft JA. Psychological and physiological consequences of drinking tea. In: Preedy VR, editor. *Handbook of Behavior, Food and Nutrition*. Berlin: Springer; 2011. p. 621-636.
26. Inoue-Choi M, Ramirez Y, Cornelis MC, *et al*. Tea consumption and all-cause and cause-specific mortality in the UK Biobank: A prospective cohort study. *Ann Intern Med*. 2022;175(9):1201-1211.

    doi: 10.7326/M22-0041
27. Gohain B, Borchetia S, Bhorali P, *et al*. Understanding Darjeeling tea flavour on a molecular basis. *Plant Mol Biol*. 2012;78(6):577-597.

    doi: 10.1007/s11103-012-9884-7
28. Huang SY. Comprehensive assessment of flexible-ligand docking algorithms: Current effectiveness and challenges. *Brief Bioinform*. 2018;19(5):982-994.

    doi: 10.1093/bib/bbw129
29. Royo M, Aznar Escolano B, Madrigal MP, Jurado S. AMPA receptor function in hypothalamic synapses. *Front Synaptic Neurosci*. 2022;14:833449.

    doi: 10.3389/fnsyn.2022.833449
30. Rijo-Ferreira F, Takahashi JS. Genomics of circadian rhythms in health and disease. *Genome Med*. 2019;11(1):82.

    doi: 10.1186/s13073-019-0704-0
31. Florent V, Baroncini M, Jissendi-Tchofo P, *et al*. Hypothalamic structural and functional imbalances in anorexia nervosa. *Neuroendocrinology*. 2020;110(6):552-562.

    doi: 10.1159/000503948
32. Herbert RP, Harris J, Chong KP, Chapman J, West AK, Chuah MI. Cytokines and olfactory bulb microglia in response to bacterial challenge in the compromised primary olfactory pathway. *J Neuroinflammation*. 2012;9:109.

    doi: 10.1186/1742-2094-9-109
33. Czapski GA, Strosznajder JB. Glutamate and GABA in microglia-neuron cross-talk in Alzheimer's disease. *Int J Mol Sci*. 2021;22(21):11677.

    doi: 10.3390/ijms222111677
34. Domercq M, Vázquez-Villoldo N, Matute C. Neurotransmitter signaling in the pathophysiology of microglia. *Front Cell Neurosci*. 2013;7:49.

    doi: 10.3389/fncel.2013.00049
35. Parellada E, Gassó P. Glutamate and microglia activation as a driver of dendritic apoptosis: A core pathophysiological mechanism to understand schizophrenia. *Transl Psychiatry*. 2021;11(1):271.

    doi: 10.1038/s41398-021-01385-9
36. Kim J, Choi Y, Ahn M, *et al*. Microglial and astroglial reaction in the olfactory bulb of mice after Triton X-100 application. *Acta Histochem*. 2019;121(5):546-552.

    doi: 10.1016/j.acthis.2019.04.010
37. Moseman EA, Blanchard AC, Nayak D, McGavern DB. T cell engagement of cross-presenting microglia protects the brain from a nasal virus infection. *Sci Immunol*. 2020;5(48):eabb1817.

    doi: 10.1126/sciimmunol.abb1817

ACCSCIENCE PUBLISHING

Innovative Medicines & Omics

ORIGINAL RESEARCH ARTICLE

Effects of exercise and *D*-ribose-*L*-cysteine supplements on neuroinflammation and oxidative stress in an aluminum chloride-induced rat model of Alzheimer's disease

Oluwafemi Abidemi Adedotun[1,2]*, Babatunde Ogunlade[1], Kingsley Afoke Iteire[3], and Adebanke Faith Balogun[1]

[1]Department of Human Anatomy, School of Basic Medical Sciences, Federal University of Technology, Akure, Ondo, Nigeria

[2]Department of Human Anatomy, Faculty of Allied Health Sciences, Elizade University, Ilara-Mokin, Ondo, Nigeria

[3]Department of Anatomy, Faculty of Basic Medical Sciences, University of Medical Sciences, Ondo, Nigeria

Abstract

Alzheimer's disease (AD) pathology involves several pathways, with oxidative stress and inflammation among the major drivers. This study employs an animal model to evaluate the effects of treadmill exercise and *D*-ribose-*L*-cysteine (DRLC) on aluminum chloride ($AlCl_3$)-induced AD. Seventy adult male Wistar rats (150–200 g) were randomized into seven groups (n=10), including a control and six experimental groups: (i) $AlCl_3$-only; (ii) $AlCl_3$ + DRLC; (iii) $AlCl_3$ + exercise; (iv) $AlCl_3$ + DRLC + exercise; (v) DRLC-only; and (vi) exercise-only. A modified rodent treadmill apparatus was used for the exercise regimen, and $AlCl_3$ and DRLC (100 mg/kg each) were prepared freshly for every administration. Y-maze and open field tests were used to evaluate the neurotoxic effects of $AlCl_3$ on working and spatial memory. Oxidative stress markers, neurotransmitter levels, neuroinflammatory markers, and immunohistochemical analysis were also conducted to assess the impact of $AlCl_3$ and the treatments on the hippocampus and prefrontal cortex. Results indicate that $AlCl_3$ administration led to a decrease in neurobehavioral performance, monoamine neurotransmitter levels, and antioxidant parameters, with a corresponding increase in oxidative stress and neuroinflammatory markers. The deleterious effects of $AlCl_3$ were also evident in the hippocampus and prefrontal cortex of the rats, contributing to AD-like pathology, as indicated by neurodegeneration. However, combined DRLC supplementation and treadmill exercise attenuated $AlCl_3$-induced behavioral, biochemical, and histopathological alterations, restoring several outcomes toward control levels. In conclusion, the combined approach of exercise and DRLC proved to possess multiple therapeutic benefits in relieving AD symptoms due to their neuroprotective properties.

Keywords: Alzheimer's disease; *D*-ribose-*L*-cysteine; Aluminum chloride; Treadmill exercise; Hippocampus; Prefrontal cortex

***Corresponding author:**
Oluwafemi Abidemi Adedotun (oluwafemi.adedotun@elizadeuniversity.edu.ng)

Citation: Adedotun OA, Ogunlade B, Iteire KA, Balogun AF. Effects of exercise and *D*-ribose-*L*-cysteine supplements on neuroinflammation and oxidative stress in an aluminum chloride-induced rat model of Alzheimer's disease. *Innov Med Omics*. 2026;3(1):48-65. doi: 10.36922/IMO025460060

Received: November 12, 2025

Revised: December 8, 2025

Accepted: January 26, 2026

Published online: February 12, 2026

1. Introduction

Alzheimer's disease (AD) is the most common cause of dementia and is characterized by cognitive decline, loss of independence in activities of daily living, and neurodegeneration.[1] The condition is linked with an increased risk of adverse events and death in older adults and is the primary cause of memory loss in the elderly.[2] According to the Alzheimer's Association, 33% of people over 65 years old will die from dementia or AD.[3] Consequently, AD is a significant health concern as people age, with 81% of AD patients being 75 years of age or older. Based on the estimates made by the Alzheimer's Association,[4] by 2050, there will be around one million new cases of AD annually, or one new diagnosis every 33 s. Depending on the stage of disease, symptoms, such as depression, apathy, difficulties in social interaction, poor decision-making, disorientation, motor and swallowing difficulties, and other behavioral changes can worsen, making daily activities increasingly challenging.[5] Factors, such as heredity, age, and sex influence the time course over which many of these symptoms manifest.[6]

The amyloid and cholinergic hypotheses are the two primary theories proposed as causes of AD, making it a multifactorial disease. Risk factors for AD include head trauma, vascular disorders, genetic susceptibility, infections, aging, and environmental exposures.[7] The accumulation of tau and amyloid-beta (Aβ) proteins is associated with the gradual cognitive deterioration observed in AD.[1] Beta- and gamma-secretases successively cleave the amyloid pre-cursor protein to create Aβ. Thus, when Aβ aggregates, harmful oligomers that impair neurons are formed.[8,9] Conversely, tau originates from the microtubule-associated protein tau gene by alternative splicing, which produces soluble protein isoforms.[9] Aβ and tau have been found to have several functional interactions in the damage of neuronal circuits and cognitive impairment associated with AD.[8] Unfortunately, there is presently no recognized treatment for the condition; however, present research focuses on understanding AD pathology by addressing several mechanisms, including aberrant tau protein metabolism, inflammatory responses, β-amyloid, cholinergic damage, and free radicals, to create prominent therapies that can put an end to or alter the course of the disease.[9]

Several studies have shown a strong correlation between heavy metals and neurodegenerative diseases, such as AD.[10,11] The onset of AD was directly linked to exposure to certain metal toxicants, such as aluminum (Al), which is absorbed by the body through occupational exposure, contaminated food, contaminated drinking water, and food cooked in Al cookware.[12,13] Given that Al directly affects many nervous system metabolic pathways, it is a key heavy metal linked with the onset and progression of neurodegenerative disorders.[13] Aluminum chloride ($AlCl_3$), found in many commercially made products, including food, toothpaste, medications, and packaged drinking water, has a highly diverse usage.[14] It ultimately accumulates in the brain and can alter the blood–brain barrier.[15] Consequently, Al brain poisoning is considered a contributing factor to neurological disorders and may impair the functioning of antioxidant enzymes, potentially harming neuronal DNA and altering brain chemistry.[15] In addition, Al has been demonstrated to cause oxidative stress, Aβ oligomer cross-linking and accumulation, as well as plaque development in the hippocampus and cortex, areas involved with memory and executive functions.[11,16] Consequently, the neuroprotective properties of different chemical substances and plant-based compounds against AD can be thoroughly investigated using the $AlCl_3$-induced AD rat model.[13,17]

According to Mahalakshmi *et al.*,[18] neuroprotection is the general term for preventing the death of neuronal cells through intervention and inhibition of the pathogenic process that results in cellular malfunction and death. In the quest for innovative treatments that may preserve neural tissue while improving the general outcome, the scientific community has shown great interest in the prospect of neuroprotection.[19] Kumar and Singh[20] stated several theories around AD pathogenesis, including increased phosphorylated tau and amyloid beta levels caused by age, a positive family history, Aβ deposition, genetic mutation in amyloid pre-cursor protein, decreased neuronal synaptic connections, and social and cognitive involvement. In addition, hippocampal degeneration, microglial activation, cerebral energy failure, neuroinflammation, and neuronal apoptosis appear to be associated with the pathogenesis of AD.[21] Conversely, research has indicated that there are preventable risk factors for AD, such as diabetes, high blood pressure, depression, smoking, obesity, and a sedentary lifestyle.[22] Given this, physical exercise might indirectly impact other disease-related characteristics and could be one of the most effective ways to combat various neurodegenerative diseases.[23] Regular exercise improves the health and function of the brain. Human and animal studies have revealed that exercise enhances cognitive function and speeds up the healing process after an injury.[24] The central noradrenergic, serotonergic, and dopaminergic systems are also impacted by physical exercise.[25] Exercise specifically causes the brain to release certain neurotransmitters that reduce physical and mental stress. It is also one of the few techniques for generating new neurons.[26] Although running has attracted a lot of attention in this area of study, all forms of aerobic exercise

have also shown neuroprotective advantages.[27] Based on a meta-analysis by Lin *et al.*,[28] exercise lowered dementia risk by 28% and AD risk by 45%, and increased daily physical activity is linked to a reduced risk of AD. Furthermore, recent research indicates that one of the major prominent risk factors for individuals with AD is inactivity;[22] further stating that exercise helps to improve neurogenesis, boosts cerebral blood flow, and enhances brain hippocampal and mitochondrial volumes. Therefore, exercise could improve daily living activities, minimize neuropsychiatric symptoms, and enhance cognitive performance in AD patients.[2] Compared to pharmacological interventions, exercise has also been shown to present fewer side effects and improve adherence.[22] Consequently, exercise appears to serve as a potential non-pharmacological approach to delay or slow down AD onset.[29] Lu *et al.*[30] and Tang *et al.*[31] reported that treadmill exercise increased angiogenesis and reduced hippocampal region neuronal apoptosis, protecting rats from cerebral ischemia.

The etiology of AD is also dependent on oxidative stress-mediated cellular damage.[32] The notion that oxidative stress is instrumental in AD pathophysiology is supported by the observed upsurge in lipid peroxidation and decrease in the endogenous level of antioxidants, which are present in the disease.[32,33] Reactive nitrogen and reactive oxygen species are typical oxidant molecules that contribute to lipid peroxidative tissue damage. These oxidant molecules then trigger a neuroinflammatory cycle, leading to the progressive degeneration of the neural pathways that control learning and memory.[34] However, Moreira *et al.*[33] and Mandal *et al.*[35] reported that glutathione (GSH) is the mammalian tissues' most significant intracellular antioxidant defense molecule, particularly in the brain, and the degree of alterations in its redox cycle appears to be correlated with the severity of any diseased condition. The neural circuits involved in the pathogenesis of AD exhibit substantial degeneration in GSH-deficient animals.[36] Accordingly, it has been suggested that increasing GSH levels in the brain might help protect the integrity of neurons and stop the gradual memory deterioration expressed in AD patients.[37] Riboceine, a synthetic antioxidant, helps cells generate glutathione when needed. Ogunlade *et al.*[38] describe *D*-ribose-*L*-cysteine (DRLC) as a potent antioxidant that helps cells produce glutathione when needed in the body. When cells require glutathione, ribose, which is a component of riboceine, effectively supplies and protects the delicate cysteine molecule.[39] DRLC is the active constituent of riboceine. Because it is derived from L-cysteine, a semi-essential amino acid produced from methionine, DRLC serves as a pre-cursor for GSH synthesis.[40] DRLC is a nutritional supplement designed to provide cysteine to the cells, increasing the GSH levels within them.[41] GSH exists throughout the body and plays significant antioxidative roles, but it can be readily depleted due to oxidative stress.[42] According to reports, people with AD may have modest cognitive improvement by elevating GSH levels.[27,37]

The present research aims to uncover the protective properties of treadmill exercise and DRLC supplementation on $AlCl_3$-induced AD in rats through the suppression of neuroinflammation, oxidative stress, and other neurodegeneration markers.

2. Materials and methods

2.1. Chemicals

DRLC and $AlCl_3$ were procured from Sigma Chemical Corporation (United States) and dissolved in distilled water. All other chemicals used in the study were of analytical grade.

2.2. Animal care and management

Seventy adult male Wistar rats (weighing 150–200 g) were obtained from the breeding stock at the Faculty of Agriculture and Agricultural Technology, Federal University of Technology, Akure (FUTA), Ondo State, Nigeria. The rats were kept in the Animal House Laboratory, Department of Human Anatomy, FUTA. They were housed in a wire gauze cage appropriately divided into four sections and large enough to allow sufficient airflow and free movement, promoting complete aeration, with a continuous 12-h light and dark schedule at room temperature (22 ± 3°C) for the duration of the study. The cage's floors were cushioned by coarse sawdust and lined with pieces of carpet. The rats were acclimatized for 7 days after being fed Growers Marsh (pellets), which were bought from a feed store at Agro Feeds, FUTA. The experimental animals were used in protocols that were approved by the Center for Research and Development, FUTA, and followed the Guide for the Care and Use of Laboratory Animals (FUTA/ETH/24/147).

2.3. Experimental design

The animals were randomized into seven groups (n=10). $AlCl_3$ (100 mg/kg body weight [BW])[11] and DRLC (100 mg/kg BW)[38] were freshly prepared before each administration. A treadmill apparatus modified for rodent exercise was used for the training regimen. The treadmill utilized shock grids to motivate the animals to keep running, and the speed was set at 0.5 m/s for 10 min/day.[43] This protocol was selected to provide a mild, non-exhaustive aerobic exercise regimen designed to minimize stress.[44,45] The animals were grouped as follows:

(i) Group A was the control group.
(ii) Group B was given 100 mg/kg BW of $AlCl_3$ only.
(iii) Group C was given 100 mg/kg BW of $AlCl_3$ and 100 mg/kg BW of DRLC.
(iv) Group D was given 100 mg/kg BW of $AlCl_3$ and 10 min of treadmill exercise at 0.5 m/s.
(v) Group E was given 100 mg/kg BW of $AlCl_3$, 100 mg/kg BW of DRLC, and 10 min of treadmill exercise at 0.5m/s.
(vi) Group F was given 100 mg/kg BW of DRLC only.
(vii) Group G was given 10 min of treadmill exercise at 0.5 m/s only.

For groups receiving more than one of the compounds and/or exercise regimen, administrations were performed sequentially with a 30-min interval. All animal-related procedures in this study were approved by the Departmental Committee on the Use and Care of Animals and conducted in accordance with the *Guide to the Care and Use of Laboratory Animals* (8th Edition).[46] All pharmacological administration was done through oral gavage once daily, and the experiment spanned 45 days. After the experiment, animals were sacrificed using cervical dislocation. The brain tissues of the rats were removed, purified, and rinsed with saline (0.9% sodium chloride).

2.4. Treadmill exercise protocol

An electric treadmill machine (JDB 1370, 6.0 HP, 12 km/h; SixBros® Electric Treadmill, United Kingdom) was used as the exercise apparatus, with some modifications[43] using a box of acrylic boards with eight compartments for the rats to run in, and a lid to keep them from escaping. In addition, copper wires were used to line the box, serving as panel terminals. To make contact with the rat's exposed rear end, the wires were bent into the shape of a hook, passing an electric shock with a tolerable voltage (132 V, 1.2 mA) through the wires to stop the rats from hanging back during the exercise session.[47] Before the exercise, all rats were acclimated to running on a treadmill for 10 min/day at a speed of 0.5 m/s for 1 week.[43] The rats in Group A were used as the control, and the animals in Groups D, E, and G were routinely exercised during the experiment.[48]

2.5. Behavioral parameters

Open field and Y-maze tests were performed to assess $AlCl_3$-induced neurobehavioral alterations, including locomotor/exploratory activity and spatial working memory, respectively, and to determine whether treadmill exercise combined with DRLC attenuates these deficits.

2.5.1. Open field test

The open field test was conducted according to the procedures outlined by Gould *et al.*[49] A wooden box measuring 100 cm × 100 cm with walls that are 50 cm high (open from the top) was used as the open field apparatus.[38,49] It was housed in a separate room with standard temperature and lighting conditions. The floor was marked with square grids, each 25 cm long, using a blue marker, and a central square of the same size was outlined with a red marker. An angled video recording device (EZVIZ H9c Dual, Hikvision, China) was set up to record the rats' movements inside the box arena. On day 0, following the acclimatization period before the experiment's commencement, the rats underwent neurobehavioral training, and after the final administration, they also went through behavioral testing. To prevent stress on the rats, each group was brought to the open field arena in its cage, with care taken to ensure no disturbance. Every rat was softly taken and placed in the center square, where it could explore for 5 min while the overhead camera recorded the video. For rats in each group, this process was repeated. To eliminate the smell of the previously tested rat, methylated spirit was used to wipe the apparatus before each test. In addition, during each test, a neutral observer steered clear of the apparatus.

Upon completing the test, the observer reviewed the video and tallied the number of squares each rat had explored. Two behavioral patterns (the frequency of rearing and the total lines crossed) were recorded. The number of times the rat crossed any of the grid lines with all four paws was recorded as the number of lines crossed; the times it crossed a red line into the central square with all four paws was noted as the center square entry; the total duration spent in the center square was labeled as the center square duration; the occurrences of the rat standing on its hind legs were counted as the rearing frequency; and the frequency of the rat showing forward extension of the head and shoulders before returning to the starting position was noted as the stretch attend posture.

2.5.2. Y-maze test

The Y-maze test was carried out following the methods outlined by Kraeuter *et al.*[50] to test the rats' working and cognitive memory. On day 0, following the acclimatization period before the experiment's commencement, the rats went through neurobehavioral training, and after the final administration, they also went through behavioral testing. The Y-maze was conducted from 9 a.m. to 3 p.m. in a calm, dimly lit room. An independent observer without knowledge of the experimental protocol scored each behavioral test after it was videotaped. A 10% ethanol solution was used to clean all test equipment to eliminate any potential bias from the previous animal's odor. The animals were placed in a Y-maze with arms that were 75 cm long, 15 cm wide, and angled at 120° from one another. The rats were given 5 min to explore the maze after being

placed on a pre-determined start arm. Arm entry was scored when the hind limbs were fully in the arm. When an animal successfully explored each of the maze's three arms per exploration triad (i.e., entering all three arms in the overlapping triplet sets is defined as correct alternation; for example, XYZ, ZXY, or YZX), the animal received a score. An alternation was deemed incorrect once two arms were explored per exploration triad (e.g., XYX, ZXZ, and YXY). The percentage of spontaneous alternation was calculated using Equation (1):

$$\text{Correct alternation}/(\text{total arm entries} - 2) \times 100 \quad (1)$$

2.6. Biochemical analysis

2.6.1. Tissue homogenization

Following the methods of Sun and Zigman,[51] the brain tissues (hippocampus and prefrontal cortex) were homogenized (Bead Ruptor Elite, OMNI International, United States of America [USA]) in ice-cold 0.25 M sucrose solution. The homogenates were transferred to 5-mL tubes and centrifuged (Model 90-1; Jiangsu Jinyi Instrument Tech, China) at 3,000 rpm for 15 min. Pasteur pipettes were used to collect the supernatant, which was then placed into sample bottles and kept in a freezer at −4°C until further use.

2.6.2. Superoxide dismutase (SOD) assay

SOD activity was measured using a spectrophotometric (NanoDrop, Thermo Fisher Scientific, USA) method. A reaction mixture (3 mL), including 0.02 mL of tissue homogenate, 2.95 mL of carbonate buffer, and 0.03 mL of 2 mM SOD substrate in 0.005 M hydrochloric acid was used to initiate the reaction. The reference cuvette contained 2.95 mL of buffer, 0.02 mL of water, and 0.03 mL of substrate. The absorbance was measured at 480 nm at regular intervals of 1 min for 5 min. Values were expressed as units per milligram of protein (U/mg protein).

2.6.3. Catalase (CAT) assay

CAT activity was determined according to the method described by Clairborne,[52] with slight modifications. Briefly, the reaction mixture contained 50 mM phosphate buffer (pH 7.0), tissue homogenate (100 µL), and 19 mM hydrogen peroxide in a final volume of 3 mL. The reaction was initiated by adding hydrogen peroxide and allowed to react for 1 min at room temperature. The decomposition of hydrogen peroxide was monitored by measuring the decrease in absorbance at 240 nm using the spectrophotometer. The reaction was terminated by adding 1 mL of a dichromate-acetic acid reagent (a mixture of 5% potassium dichromate in glacial acetic acid in a 1:3 ratio), followed by heating the tubes in a boiling water bath for 10 min to develop a stable color. CAT activity was expressed as µmoles of hydrogen peroxide decomposed per minute per mg of protein using the molar extinction coefficient for hydrogen peroxide (43.6/M/cm at 240 nm).

2.6.4. Reduced glutathione level

Reduced GSH levels were determined according to the method described by Jollow *et al.*,[53] with minor modifications. Briefly, 0.5 mL of tissue homogenate was mixed with 0.5 mL of 4% sulfosalicylic acid and centrifuged at 10,000 × g for 10 min at 4°C to precipitate proteins. The resulting supernatant (0.5 mL) was then added to 2.0 mL of 0.1 M phosphate buffer (pH 7.4) and 0.25 mL of 0.01 M 5,5'-dithiobis-(2-nitrobenzoic acid). The formation of the yellow-colored chromophore was measured spectrophotometrically at 412 nm against a reagent blank. GSH levels were calculated using a standard curve generated with known concentrations of reduced GSH and expressed as nmol of GSH per mg of protein.

2.6.5. Lipid peroxidation level

Lipid peroxidation was assessed by measuring the malondialdehyde (MDA) content in tissue homogenates, following the method of Farombi *et al.*,[54] with slight modifications. Briefly, 0.5 mL of tissue homogenate was mixed with 1.5 mL of 10% trichloroacetic acid, 1.5 mL of 0.75% thiobarbituric acid, and 0.5 mL of 5% (w/v) butylated hydroxytoluene in 0.1 M hydrochloric acid. The mixture was vortexed and then incubated in a boiling water bath at 95°C for 60 min. After cooling to room temperature, the tubes were centrifuged at 3,000 × g for 10 min, and the absorbance of the pink-colored supernatant was measured at 532 nm using a spectrophotometer. The concentration of MDA was calculated using an extinction coefficient (ε) of 1.56×10^5 L/mol/cm, and the results were expressed as nmol MDA per mg protein.

2.6.6. Determination of nitric oxide (NO) level

NO levels were determined as nitrite using the Griess reagent, following the method of Moshage *et al.*,[55] with slight modifications. Briefly, 100 µL of the tissue supernatant was mixed with 100 µL of freshly prepared Griess reagent, consisting of 1% sulfanilamide and 0.1% N-(1-naphthyl)ethylenediamine dihydrochloride in 2.5% phosphoric acid. The reaction mixture was incubated at room temperature for 20 min in the dark to allow color development. The absorbance was measured at 550 nm using an ultraviolet-visible spectrophotometer. A standard curve was generated using sodium nitrite solutions (0–100 µM), and the nitrite concentration in the samples was calculated accordingly. Results were expressed as µM nitrite per gram of tissue (µM/g).

2.7. Tissue collection and processing

A few hours after the behavioral tests concluded, the animals were sacrificed using cervical dislocation. Subsequently, the brain tissues were washed with cold phosphate-buffered saline and fixed in 4% paraformaldehyde for 24 h. After being removed from the fixed brain, the hippocampus and prefrontal cortex were dehydrated using ascending alcohol concentrations (50%, 70%, 90%, and 100%). The tissues were then cleared twice for 15 min each in xylene. Tissues were subsequently embedded in paraffin wax at similar orientations after infiltration, and embedding was completed using paraffin wax in a Leica (Germany) hot air oven at 56°C. A rotary microtome (Leica RM2245, Germany) was used to obtain tissue sections serially, which were subsequently mounted on glass slides.

For histology, 3 μm sections were used. Pearse[56] method, as amended by Fischer *et al.*,[57] was adopted in staining the brain sections. Hematoxylin and eosin staining was used to show the prefrontal cortex and hippocampal general cytoarchitecture. Immunohistochemistry was performed using primary antibodies against brain-derived neurotrophic factor (BDNF) and Aβ to assess BDNF expression and amyloid plaque burden, respectively. Sections underwent heat-induced antigen retrieval in 10 mM citrate buffer (pH 6.0) at 95°C for 15 min.[58] Endogenous peroxidase activity was blocked by incubating the sections with 3% hydrogen peroxide for 10 min. To prevent non-specific binding, sections were incubated in 5% normal goat serum for 30 min at room temperature.[59] The following primary antibodies were used: Anti-BDNF (rabbit polyclonal, ab108319; Abcam, United Kingdom) at 1:200 dilution and anti-Aβ (mouse monoclonal, ab11132; Abcam, United Kingdom) at 1:250 dilution. Sections were incubated with the primary antibodies overnight at 4°C. After phosphate-buffered saline washes, they were treated with biotinylated secondary antibodies. The secondary antibodies used were goat anti-rabbit immunoglobulin G (IgG) for BDNF (NB7160; Novus Biologicals, USA) and goat anti-mouse IgG for Aβ (11115-S; IBL-America, USA) at a 1:500 dilution for 1 h at room temperature. Immunoreactivity was visualized using an avidin-biotin complex method and 3,3'-diaminobenzidine as the chromogen.[60] Counterstaining was performed with Mayer's hematoxylin. Images were captured using a Leica® (Germany) DM5000B microscope and a Leica (Germany) EC3 digital camera.

2.8. Photomicrography and quantification

Immunostained slides were digitized with the Panoramic 250 Flash II slide scanner (3D Histech, Hungary). A complementary digital microscopy software, Caseviewer (version 2.5), was employed in the random capturing of 8–10 parallel photomicrographic fields of the hippocampus and prefrontal cortex regions. Thereafter, analysis of photomicrographs was conducted using Immunoratio and cell count plugins of the ImageJ software (version 1.54p). The ImmunoRatio plugin estimates the ratio of brown 3,3'-diaminobenzidine (positive immunoreactivity) to the hematoxylin counterstain by digital color deconvolution. The number of manually selected cell types was recorded using the cell counter plugin.[61] Data analysis was performed using the average scores of the analyzed photomicrographs.

2.9. Neurotransmitter analysis

2.9.1. Brain monoamine neurotransmitter analysis

Wet tissue was weighed and homogenized for about 1 min in 5 mL of hydrochloric acid in butanol to quantify the amount of monoamine neurotransmitters (serotonin, dopamine, and norepinephrine). The product was then centrifuged at 2,000 rpm for 10 min. A 1 mL aliquot of the supernatant phase was removed and placed in a centrifuge tube along with 2.5 mL of heptane and 0.31 mL of 0.1 M hydrochloric acid. Following 10 min of vigorous shaking, the tube was centrifuged under similar conditions to separate the two phases, and the organic layer on top was discarded. The aqueous phase (0.2 mL) was then extracted for the serotonin, dopamine, and norepinephrine assays. Every step was completed at 0°C.[62] To analyze dopamine and norepinephrine, 0.05 mL of 0.4 M hydrochloric acid and 0.1 mL of ethylenediaminetetraacetic acid/sodium acetate buffer (pH 6.9) were added to 0.2 mL of aqueous phase. For oxidation, 0.1 mL of iodine solution (0.1 M in ethanol) was added. After 2 min, the reaction was ended by adding 0.1 mL of sodium sulfite solution, followed by 0.1 mL of acetic acid after another 1.5 min. After the sample had recovered to ambient temperature, the solution was heated to 100°C for 6 min. The spectrofluorometer (FP-6500, JASCO Inc., Japan) was used to measure the excitation and emission spectra for norepinephrine and dopamine analysis. To analyze serotonin, 0.2 mL of aqueous extract was mixed with 0.25 mL of *o*-phthalaldehyde reagent and heated to 100°C for 10 min to allow fluorophore formation. Measurements were then taken using the spectrofluorometer once the samples had cooled to room temperature.

2.9.2. Determination of acetylcholinesterase (AChE) content

Using Ellman's method,[63] the level of AChE in the hippocampus and prefrontal cortex was determined by mixing 0.05 mL of supernatant with 0.1 mL of 5-dithio-bis-(2-nitrobenzoic acid) (Ellman's reagent), 3 mL of sodium phosphate buffer (pH 8), and 0.1 mL of acetylthiocholine iodide. Using the PerkinElmer (United States) Lambda 20

spectrophotometer, the absorbance change was measured at 30-s intervals for 2 min at 412 nm. The results were expressed in µmol of acetylthiocholine iodide hydrolyzed per minute per mg of protein.

2.10. Quantification of inflammatory markers

The levels of interleukin-6 (IL-6) and tumor necrosis factor-α (TNF-α) in the supernatants of the hippocampus and prefrontal cortex of control and treated animals were determined using the appropriate assay kits as per the manufacturer's instructions (Mybiosource, USA).[64]

2.11. Statistical analysis

Using GraphPad Prism® 8 Windows (GraphPad Software, USA), a one-way analysis of variance with Tukey's multiple comparisons test was used for the statistical analysis. Differences between means at $p<0.05$ were considered significant, and the results were expressed as mean ± standard error of mean.

3. Results

3.1. Effect of DRLC and treadmill exercise on the neurobehavior of rats

Locomotor/exploratory activity and spatial working memory were evaluated using the open field and Y-maze tests, respectively. In the open field test, activity was quantified as the number of lines crossed during a 5-min session (Figure 1A). In the Y-maze test, working memory was assessed using the percent correct alternation (Figure 1B). The result revealed that rats in Group B showed a significant decrease ($p<0.05$) in the number of lines crossed per 5 min and percentage correct alternation when compared to Group A (Figure 1). In addition, the rats in Groups C, D, and E showed a significant increase ($p<0.05$) in the number of lines crossed per 5 min and percentage correct alternation when compared with Group B. There was also no significant difference in the number of lines crossed per 5 min and percentage correct alternation when Group E was compared to the control group. In addition, no significant difference was observed in the number of lines crossed per 5 min and percentage correct alternation between Groups A, F, and G when compared to one another.

3.2. Effects of DRLC and treadmill exercise on antioxidant enzyme activities and oxidative stress markers

To evaluate the antioxidant activity in the brain (hippocampus and prefrontal cortex) of rats treated with DRLC and treadmill exercise against $AlCl_3$-induced neurodegeneration, the levels of SOD, CAT, and GSH were examined. MDA and NO, two indicators of oxidative stress, were also investigated (Figure 2). The findings demonstrated that the antioxidant enzyme activities (SOD, CAT, and GSH) of rats in Group B significantly decreased ($p<0.05$), accompanied by a corresponding increase ($p<0.05$) in oxidative stress markers (MDA and NO) when compared to Group A. Furthermore, when compared to Group B, Groups C, D, and E demonstrated a significant increase ($p<0.05$) in antioxidant enzyme activities (SOD, CAT, and GSH) and a consequent decrease ($p<0.05$) in oxidative stress markers (MDA and NO). Moreover, when Group E was compared to the control group, there was no significant difference in the levels of antioxidant enzyme activities (SOD, CAT, and GSH) or oxidative stress markers (MDA and NO). In addition, when compared to each other, there was no significant difference between Groups A, F, and G.

3.3. Effects of DRLC and treadmill exercise on brain monoamine neurotransmitters and acetylcholinesterase levels

This study examined the hippocampus and prefrontal cortex for the monoamine neurotransmitters (serotonin, dopamine, and norepinephrine). When compared to Group A, Group B had significantly lower ($p<0.05$) dopamine and serotonin levels and higher norepinephrine

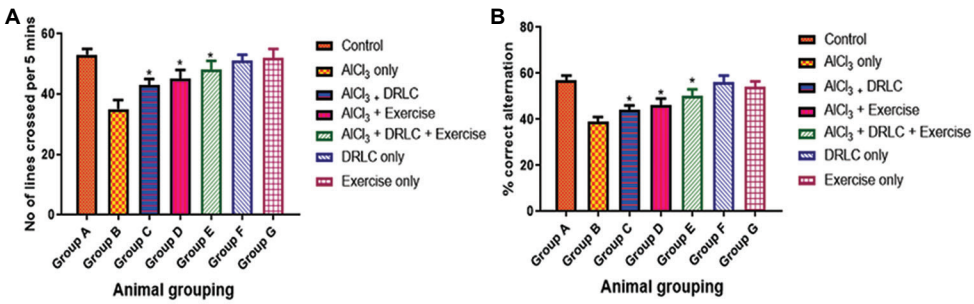

Figure 1. Effects of *D*-ribose-*L*-cysteine (DRLC) and treadmill exercise on neurobehavioral tests in aluminum chloride ($AlCl_3$)-induced neurodegeneration in normal and experimental rats. (A) Open field test. (B) Y-maze test. All data were analyzed using one-way analysis of variance followed by Tukey's multiple comparisons test. Data are expressed as mean ± standard error of mean (n=10). Group B differed significantly from Group A in all panels, indicating successful AD model induction. *$p<0.05$ versus Group B ($AlCl_3$-induced Alzheimer's disease model group).

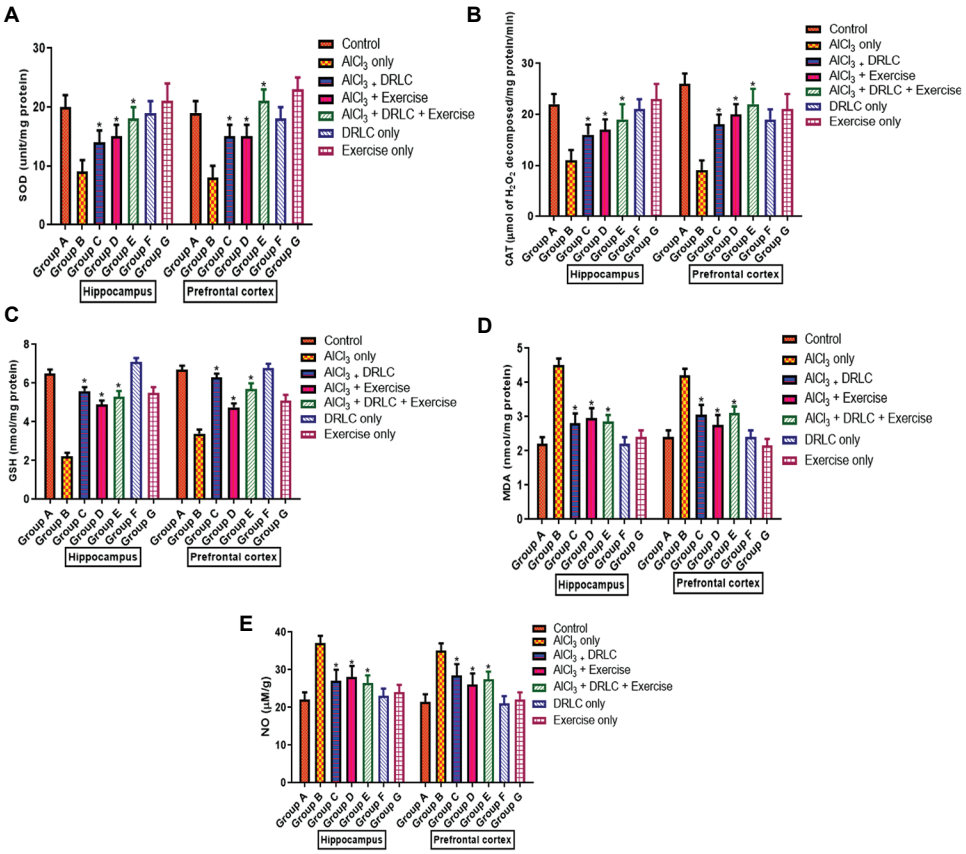

Figure 2. Effects of *D*-ribose-*L*-cysteine (DRLC) and treadmill exercise on antioxidant enzyme activities and oxidative stress markers in aluminum chloride ($AlCl_3$)-induced neurodegeneration in normal and experimental rats. (A) Superoxide dismutase (SOD), (B) catalase (CAT), (C) glutathione (GSH), (D) malondialdehyde (MDA), and (E) nitric oxide (NO). All data were estimated using one-way analysis of variance followed by Tukey's multiple comparisons test. Data are expressed as mean ± standard error of mean (n=10). Group B differed significantly from Group A in all panels, indicating successful AD model induction. *p<0.05 versus Group B ($AlCl_3$-induced Alzheimer's disease model group).

levels (Figure 3). However, when compared to Group B, Groups C, D, and E exhibited a significant increase (p<0.05) in dopamine and serotonin levels with a corresponding decrease in norepinephrine levels. Furthermore, when comparing Group B to Group A, a significant decrease (p<0.05) in AChE levels was observed in Group A. Similarly, Groups C, D, and E demonstrated a significant decrease (p<0.05) in the brain AChE levels as compared to Group B. However, when Group E was compared to the control group, there was no significant difference in the levels of monoamine neurotransmitters (serotonin, dopamine, and norepinephrine) or AChE in the brain. In addition, when compared to each other, there was no significant difference in these parameters between the control Groups A, F, and G.

3.4. Effects of DRLC and treadmill exercise on brain inflammatory markers

Inflammatory markers (TNF-α and IL-6) in the brain tissues (hippocampus and prefrontal cortex) were quantified in this study. Group B showed a significant increase (p<0.05) in brain inflammatory marker levels (IL-6 and TNF-α) when compared with Group A (Figure 4). Conversely, Groups C, D, and E showed a significant decrease (p<0.05) in the brain inflammatory marker levels (TNF-α and IL-6) when compared to Group B. However, there was no significant difference in the brain inflammatory marker levels (TNF-α and IL-6) in Group E when compared to the control group. Moreover, no significant difference was observed between Groups A, F, and G when compared to one another.

3.5. Effect of DRLC and treadmill exercise on hippocampal and prefrontal cortex histomorphology

The results of the histological assessment in this study showed normal hippocampal morphology in Group A (Figure 5A). Group B showed few pyramidal cells with vacuolated neuropil, distorted glial cells between the outer marginal layer and inner pyramidal layer (Figure 5B) when

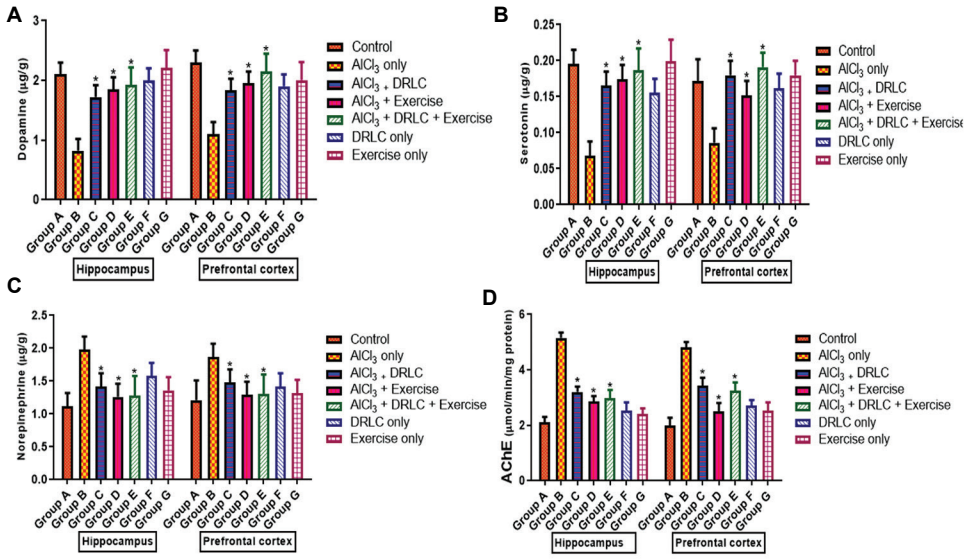

Figure 3. Effects of *D*-ribose-*L*-cysteine (DRLC) and treadmill exercise on brain monoamine neurotransmitters and acetylcholinesterase (AChE) levels in aluminum chloride ($AlCl_3$)-induced neurodegeneration in normal and experimental rats. (A) Dopamine, (B) serotonin, (C) norepinephrine, and (D) AChE. All data were estimated using one-way analysis of variance followed by Tukey's multiple comparisons test. Data are expressed as mean ± standard error of mean (n=10). Group B differed significantly from Group A in all panels, indicating successful AD model induction. *p<0.05 versus Group B ($AlCl_3$-induced Alzheimer's disease model group).

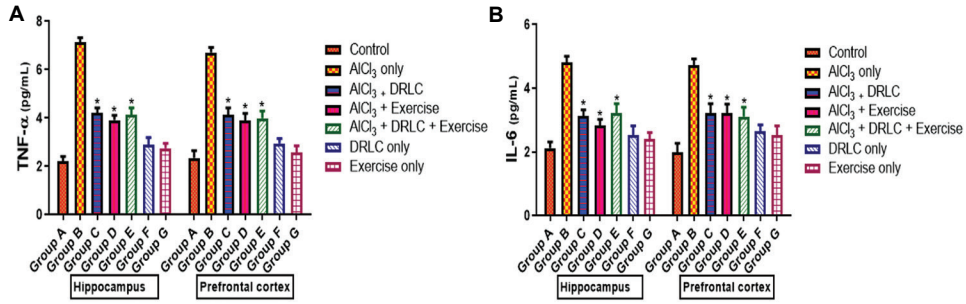

Figure 4. Effects of *D*-ribose-*L*-cysteine (DRLC) and treadmill exercise response on brain inflammatory markers in aluminum chloride ($AlCl_3$)-induced neurodegeneration in normal and experimental rats. (A) Tumor necrosis factor-alpha (TNF-α). (B) Interleukin-6 (IL-6). All data were estimated using one-way analysis of variance followed by Tukey's multiple comparisons test. Data are expressed as mean ± standard error of mean (n=10). Group B differed significantly from Group A in all panels, indicating successful AD model induction. *p<0.05 versus Group B ($AlCl_3$-induced Alzheimer's disease model group).

compared to the control group. Groups C (Figure 5C) and D (Figure 5D) showed a reduced glial proliferation between the outer marginal layer and inner pyramidal layer and fewer vacuolated neuropil areas than Group B. In addition, Group E (Figure 5E) showed a significant reduction in distorted glial cells in all hippocampal regions, as well as a low rate of neurodegeneration that is comparable to Group A. In Groups F (Figure 5F) and G (Figure 5G), there was normal orientation of glial cells similar to the control.

The photomicrograph representation of the prefrontal cortex in Group B showed distorted neuronal cells and vacuolated neuropils, indicating signs of neurodegeneration when compared to Group A, which displayed normal cortical architecture with intact neurons and glial cells (Figure 6A). Group B exhibited significant atrophy and cellular disorganization (Figure 6B). In addition, Group C demonstrated a noticeable reduction in neuronal distortion and vacuolation (Figure 6C) compared to Group B. A similar trend was observed in Group D, which showed improved neuronal morphology and reduced signs of neurodegeneration (Figure 6D). Groups E, F, and G exhibited cortical structures comparable to the control group, further confirming the protective effects of these treatments against $AlCl_3$-induced damage (Figure 6E-G, respectively).

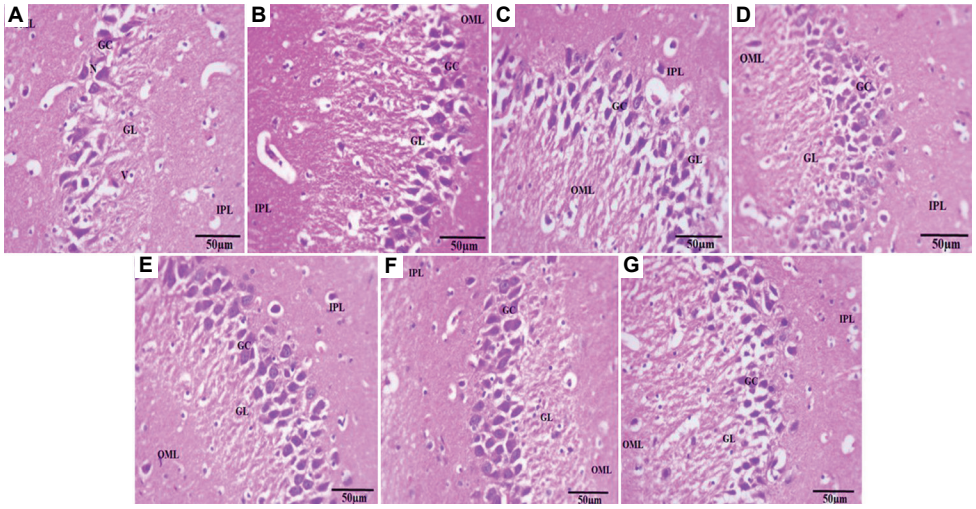

Figure 5. Photomicrographs of the CA3 region of the hippocampus showing the effect of *D*-ribose-*L*-cysteine (DRLC) and treadmill exercise against aluminum chloride ($AlCl_3$)-induced neurodegeneration in normal and experimental rats. (A) Control group; (B) $AlCl_3$-only group; (C) $AlCl_3$ + DRLC group; (D) $AlCl_3$ + exercise group; (E) $AlCl_3$ + DRLC + exercise group; (F) DRLC-only group; and (G) exercise-only group. Scale bar: 50 μm; magnification: 400×.
Abbreviations: GC: Glial cells; GL: Glial layer; IPL: Inner pyramidal layer; OML: Outer marginal layer; V: Vacuolated neuropil.

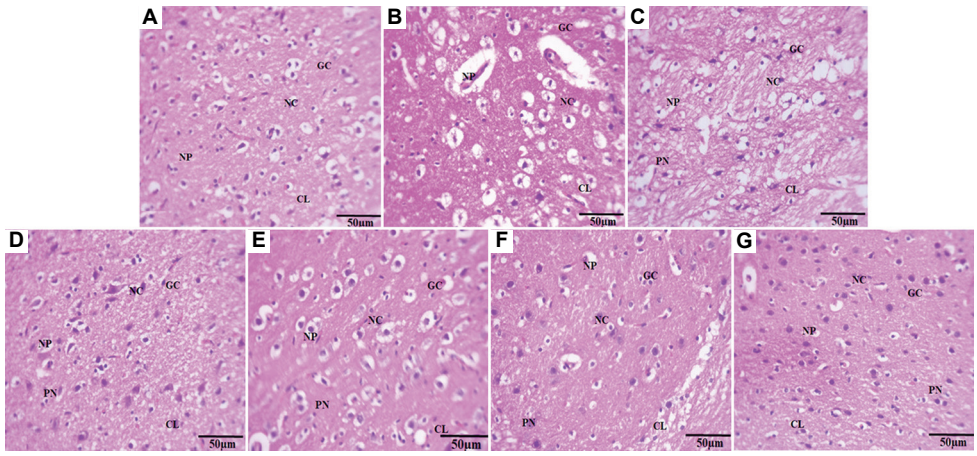

Figure 6. Photomicrographs of the prefrontal cortex showing the effect of *D*-ribose-*L*-cysteine (DRLC) and treadmill exercise against aluminum chloride ($AlCl_3$)-induced neurodegeneration in normal and experimental rats. (A) Control group; (B) $AlCl_3$-only group; (C) $AlCl_3$ + DRLC group; (D) $AlCl_3$ + exercise group; (E) $AlCl_3$ + DRLC + exercise group; (F) DRLC-only group; and (G) exercise-only group. Scale bar: 50 μm; magnification: 400×.
Abbreviations: CL: Cortical layer; GC: Glial cells; NC: Neuronal cells; NP: Neuropils; PC: Pyramidal cells.

3.6. Effects of DRLC and treadmill exercise on the immunohistochemical expressions and immunoreactivity of brain-derived neurotrophic factor and amyloid beta

The immunohistochemical expressions of BDNF and Aβ in the hippocampus of the rats in Group A revealed that the structural architecture of the hippocampus's pyramidal cells included normal neuronal cells devoid of any pathological features (Figure 7A). In the external pyramidal layer, the pyramidal neurons were arranged in a typically normal and structurally well-defined manner, with appropriate delineation and a normal cytoarchitectural assortment of the pyramidal cells. In contrast, Group B showed Aβ plaque deposition and neuronal degeneration, exhibiting characteristic pathological alterations indicative of hippocampal degeneration, including chromatolysis, distortion, and pyknotic changes in the pyramidal cells of the CA3 region and the external pyramidal layer of the hippocampus (Figure 7B). However, Group E showed normal immunohistochemistry and normal neuronal cells with notable improvement and restoration in the morphological integrity and cytoarchitectural appearance of the hippocampus, along with the absence of amyloid deposit (Figure 7C and D), as similarly observed in Groups

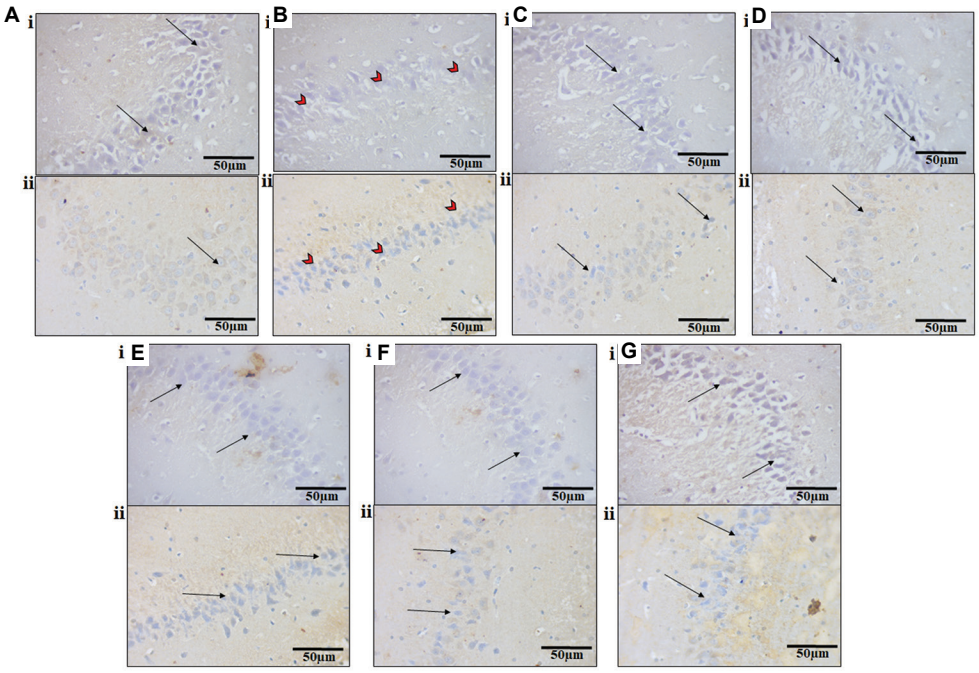

Figure 7. Immunohistochemical and immunoreactivity expressions of brain-derived neurotrophic factor (BDNF) and amyloid beta (Aβ) in the hippocampus. (A) Control group; (B) aluminum chloride ($AlCl_3$)-only group; (C) $AlCl_3$ + *D*-ribose-*L*-cysteine (DRLC) group; (D) $AlCl_3$ + exercise group; (E) $AlCl_3$ + DRLC + exercise group; (F) DRLC-only group; and (G) exercise-only group. Arrows indicate neuronal cells, and red arrowheads indicate neuronal degeneration with deposition of Aβ oligomers. Images labeled (i) show BDNF immunostaining, and images labeled (ii) show Aβ immunostaining. Scale bar: 50 μm; magnification: 400×.

E, F and G (Figure 7E to G).

The immunohistochemical evaluation of BDNF and Aβ expressions across the experimental groups demonstrated varying degrees of astrocytic activity in the prefrontal cortex. Group A displayed the baseline expression of BDNF and Aβ, with sparsely distributed astrocytes and faint processes (Figure 8A). In contrast, Group B showed a very low BDNF immunoreactivity, with a correspondingly high Aβ immunoreactivity, characterized by numerous astrocytes with elongated, densely stained processes, reflecting heightened neuroinflammation and neurodegeneration due to $AlCl_3$ exposure (Figure 8B). Groups C, D, and E exhibited an increase in BDNF, with a similar decrease in Aβ expressions compared to Group B, showing fewer astrocytes and less prominent processes, suggesting the treatment's potential role in attenuating the inflammatory response (Figure 8C-E). Groups F and G showed a moderate level of BDNF and Aβ expressions, indicating controlled astrocytic activation under experimental conditions (Figure 8F and G). In addition, the immunoreactivity and quantification of BDNF- and Aβ-positive cells, as well as the percentage of BDNF and Aβ immunoreactivities, were conducted in this study, and the results showed varying degrees of expression in the hippocampus and prefrontal cortex between the control and experimental groups (Figures 9 and 10).

4. Discussion

This study investigated the neuroprotective effects of exercise and DRLC supplementation on $AlCl_3$-induced AD pathology in rats. Our findings support the hypothesis that combined intervention can mitigate cognitive decline, oxidative stress, neuroinflammation, and neurodegeneration caused by $AlCl_3$ exposure.

In terms of behavior, rats treated with $AlCl_3$ exhibited significant impairments in working memory and locomotor activity, as demonstrated by reduced spontaneous alternation in the Y-maze test and fewer lines crossed in the open field test. These outcomes align with previous research showing the detrimental effects of Al on cognitive performance and anxiety-like behavior.[65,66] Exercise and DRLC treatments significantly improved these measures, supporting their role in enhancing hippocampal-dependent memory and exploratory behavior, likely through increased neurogenesis and synaptic plasticity.[67,68] This functional recovery suggests that interventions targeting oxidative damage and neuroinflammation can restore behavioral deficits associated with AD.

Oxidative stress is a key contributor to AD pathology,

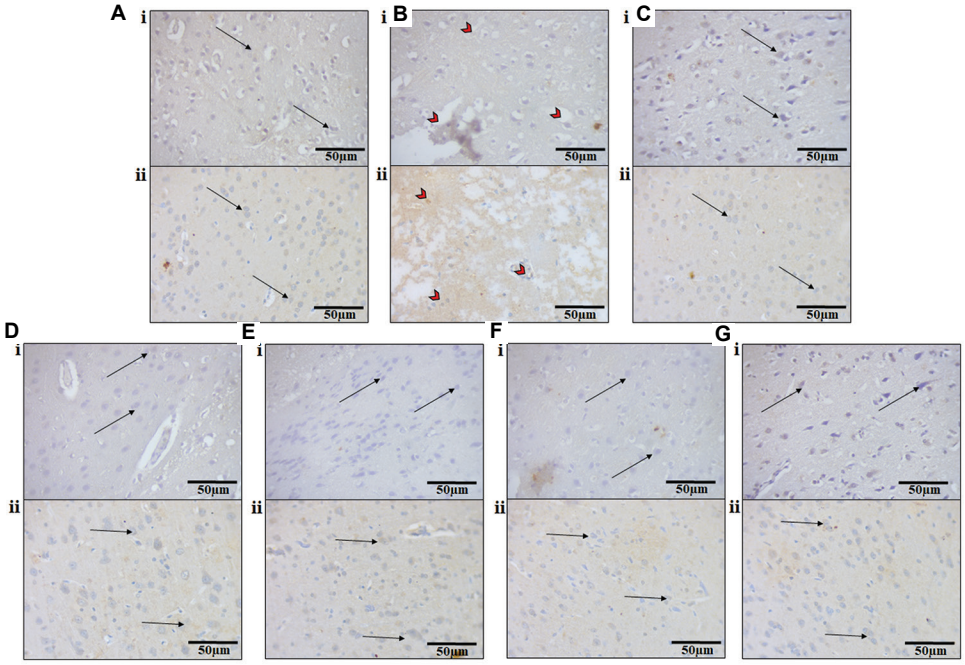

Figure 8. Immunohistochemical and immunoreactivity expressions of brain-derived neurotrophic factor (BDNF) and amyloid beta (Aβ) in the prefrontal cortex. (A) Control group; (B) aluminum chloride ($AlCl_3$)-only group; (C) $AlCl_3$ + *D*-ribose-*L*-cysteine (DRLC) group; (D) $AlCl_3$ + exercise group; (E) $AlCl_3$ + DRLC + exercise group; (F) DRLC-only group; and (G) exercise-only group. Arrows indicate cortical neurons, and red arrowheads indicate pathological changes, evident in neuronal degeneration and deposition of Aβ plaques. Images labeled (i) show BDNF immunostaining, and images labeled (ii) show Aβ immunostaining. Scale bar: 50 μm; magnification: 400×.

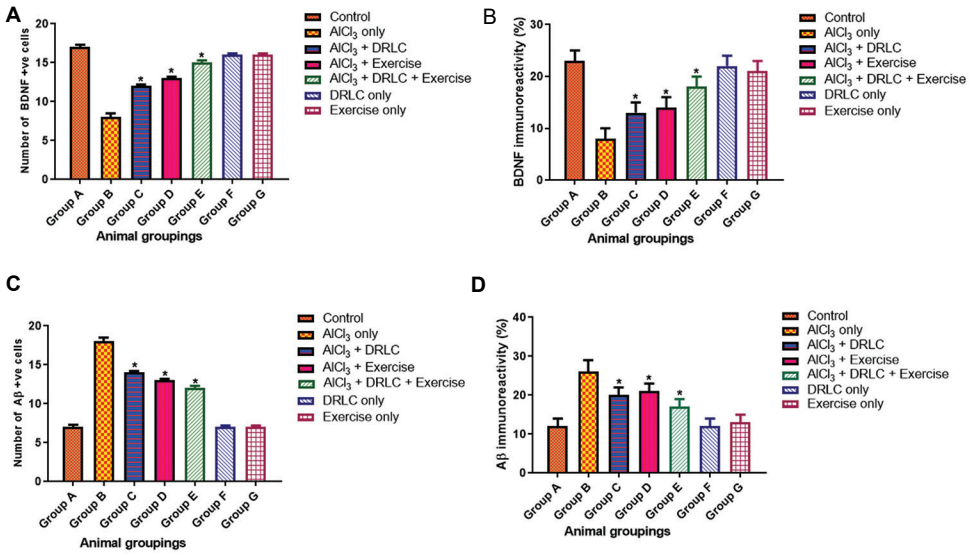

Figure 9. Immunohistochemical and immunoreactivity quantification of brain-derived neurotrophic factor (BDNF) and amyloid beta (Aβ) in the hippocampus. (A) Number of BDNF-positive cells and (B) BDNF immunoreactivity. (C) Number of Aβ-positive cells. (D) Aβ immunoreactivity. All data were estimated using one-way analysis of variance followed by Tukey's multiple comparisons test. Data are expressed as mean ± standard error of mean (n=10). Group B differed significantly from Group A in all panels, indicating successful AD model induction.*$p<0.05$ vs. Group B ($AlCl_3$-induced Alzheimer's disease model group).

driven by an imbalance between reactive oxygen species production and antioxidant defenses. Our data showed increased MDA and NO levels alongside decreased activities of key antioxidant enzymes (CAT, SOD, and reduced GSH) in the brains of $AlCl_3$-treated rats. These findings confirm earlier studies linking oxidative damage

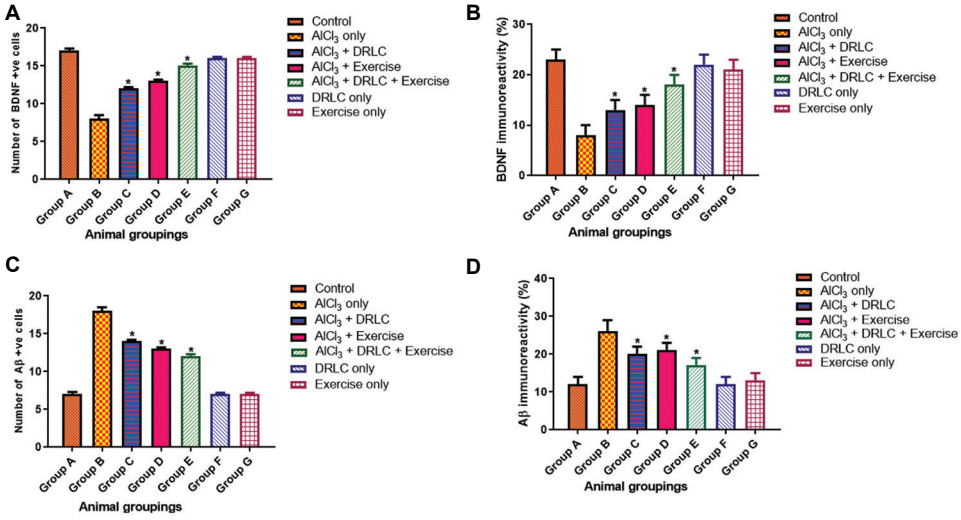

Figure 10. Immunohistochemical and immunoreactivity quantification of brain-derived neurotrophic factor (BDNF) and amyloid beta (Aβ) in the prefrontal cortex. (A) Number of BDNF-positive cells and (B) BDNF immunoreactivity. (C) Number of Aβ-positive cells. (D) Aβ immunoreactivity. All data were estimated using one-way analysis of variance followed by Tukey's multiple comparisons test. Data are expressed as mean ± standard error of mean (n=10). Group B differed significantly from Group A in all panels, indicating successful AD model induction.*$p<0.05$ vs. Group B ($AlCl_3$-induced Alzheimer's disease model group).

to neuronal dysfunction in AD.[69,70] Importantly, DRLC supplementation, which serves as a cysteine donor for GSH synthesis, alongside exercise, significantly restored antioxidant enzyme activities and reduced oxidative stress markers. This dual intervention likely enhanced endogenous antioxidant capacity, preventing oxidative damage to neural tissue and supporting cognitive function.[71,72]

This study also highlighted disruptions in key neurotransmitter systems. $AlCl_3$ exposure led to decreased dopamine and serotonin, alongside increased norepinephrine and AChE levels. These alterations reflect cholinergic dysfunction and monoaminergic imbalance characteristic of AD, which impair cognition and memory.[73,74] Combined DRLC and exercise treatment normalized these neurotransmitter levels, consistent with reports that physical activity modulates central dopaminergic and serotonergic pathways and that glutathione pre-cursors provide neuroprotection.[13,75] These neurochemical improvements likely contributed to the observed behavioral enhancements.

Neuroinflammation is another pathological hallmark of AD, with pro-inflammatory cytokines, such as TNF-α and IL-6 driving neuronal damage and cognitive decline.[13,76] Our findings revealed elevated TNF-α and IL-6 levels in $AlCl_3$-treated rats, indicative of heightened neuroinflammatory response, consistent with reports linking chronic inflammation to AD progression.[77,78] Notably, DRLC and exercise co-administration significantly suppressed these cytokines, suggesting anti-inflammatory effects, possibly mediated by antioxidant activity and exercise-induced modulation of the immune system.[79,80] This reduction in neuroinflammation likely plays a critical role in protecting neural tissues from ongoing degeneration.

Histological and immunohistochemical analyses further substantiated the biochemical and behavioral data. $AlCl_3$ exposure induced neuronal degeneration, Aβ plaque deposition, reduced BDNF expression, and astrocytic activation in the hippocampus and prefrontal cortex. These pathological changes mirror AD neuropathology and confirm Al's neurotoxic effects.[81,82] Conversely, DRLC and exercise treatment preserved neuronal architecture, prevented Aβ accumulation, enhanced BDNF expression, and reduced astrocytic activation, indicating attenuation of neurodegeneration and promotion of neuroplasticity. Exercise-induced increases of BDNF support neuronal survival and synaptic repair, which are critical mechanisms for cognitive recovery.[22,83]

5. Conclusion

The findings from this study provide compelling evidence that combined exercise and DRLC supplementation protect against $AlCl_3$-induced neurodegeneration by attenuating oxidative stress, neuroinflammation, and neurotransmitter imbalances while enhancing neurotrophic support. These effects culminate in improved cognitive and behavioral outcomes, supporting the therapeutic potential of integrating antioxidant supplementation with physical activity in AD management. Future studies should further explore the molecular mechanisms underlying these

benefits and their translational potential in clinical settings.

Acknowledgments

Special appreciation goes to the Department of Human Anatomy, Federal University of Technology, Akure, Ondo State, Nigeria, for providing the facilities and equipment needed to conduct this research seamlessly. A notable mention goes to Dr. Omamuyovwi Ijomone from the Laboratory of Experimental and Translational Neuroscience, whose lab access was monumental for the immunohistochemical findings in this study.

Funding

None.

Conflict of interest

The authors declare they have no competing interests.

Author contributions

Conceptualization: Babatunde Ogunlade
Data curation: Adebanke Faith Balogun
Formal analysis: Oluwafemi Abidemi Adedotun
Investigation: Babatunde Ogunlade
Methodology: Oluwafemi Abidemi Adedotun
Project administration: Adebanke Faith Balogun
Software: Oluwafemi Abidemi Adedotun
Supervision: Babatunde Ogunlade
Validation: Babatunde Ogunlade
Writing – original draft: Oluwafemi Abidemi Adedotun
Writing – review & editing: Kingsley Afoke Itiere

Ethics approval and consent to participate

Ethical approval was obtained from the Centre for Research and Development (CERAD) of The Federal University of Technology, Akure (FUTA/ETH/24/147).

Consent for publication

Not applicable.

Availability of data

Data will be made available upon request to the corresponding author.

Further disclosure

Part of the findings from this study have been presented at a 1st FUTA SBMS Conference of Biomedical Research "From Bench to Bedside: Translating Basic Science Research into Clinical Impact", under the title: "Neuroinflammatory and Oxidative Stress Responses of Exercise and DRLC Supplements on Aluminium Chloride-Induced Rat Model of Alzheimer's Disease," held on June 25–27, 2025, at the Federal University of Technology Akure, Ondo, Nigeria.

References

1. Breijyeh Z, Karaman R. Comprehensive review on Alzheimer's disease: Causes and treatment. *Molecules.* 2020;25:5789.
   doi: 10.3390/molecules25245789
2. Cass SP. Alzheimer's disease and exercise: A literature review. *Curr Sports Med Rep.* 2017;16:19-22.
   doi: 10.1249/JSR.0000000000000332
3. Barnes JN. Exercise, cognitive function, and aging. *Adv Physiol Educ.* 2015;39:55-62.
   doi: 10.1152/advan.00101.2014
4. Alzheimer's Association. 2015 Alzheimer's disease facts and figures. *Alzheimers Dement.* 2015;11:332-384.
   doi: 10.1016/j.jalz.2015.02.003
5. Alzheimer's Association. 2021 Alzheimer's disease facts and figures. *Alzheimers Dement.* 2021;17:327-406.
   doi: 10.1002/alz.12328
6. Vermunt L, Sikkes SA, Van Den Hout A, *et al.* Duration of preclinical, prodromal, and dementia stages of Alzheimer's disease in relation to age, sex, and APOE genotype. *Alzheimers Dement*. 2019;15:888-898.
   doi: 10.1016/j.jalz.2019.04.001
7. Selkoe DJ, Hardy J. The amyloid hypothesis of Alzheimer's disease at 25 years. *EMBO Mol Med.* 2016;8:595-608.
   doi: 10.15252/emmm.201606210
8. Haass C, Selkoe DJ. Soluble protein oligomers in neurodegeneration: Lessons from the Alzheimer's amyloid beta-peptide. *Nat Rev Mol Cell Biol.* 2007;8:101-112.
   doi: 10.1038/nrm2101
9. Abubakar MB, Sanusi KO, Ugusman A, *et al.* Alzheimer's disease: An update and insights into pathophysiology. *Front Aging Neurosci.* 2022;14:742408.
   doi: 10.3389/fnagi.2022.742408
10. Hussien HM, Abd-Elmegied A, Ghareeb DA, Hafez HS, Ahmed HE, El-moneam NA. Neuroprotective effect of berberine against environmental heavy metals-induced neurotoxicity and Alzheimer's-like disease in rats. *Food Chem Toxicol.* 2018;111:432-444.
   doi: 10.1016/j.fct.2017.11.025
11. Ogunlade B, Adelakun SA, Fidelis OP. Sulforaphane attenuates neuroinflammation, oxidative stress and cognitive impairment on aluminium-induced Alzeimer's disease in wistar rats. *J Neurosci Neuropharmaco.* 2020;6(2):13-22.
12. Exley C, Vickers T. Elevated brain aluminium and early onset

alzheimer's disease in an individual occupationally exposed to aluminium: A case report. *J Med Case Rep.* 2014;8(1):41.

doi: 10.1186/1752-1947-8-41

13. Chen SX, Zhang M, Ahmed M, Surapaneni KM, Veeraraghavan VP, Arulselvan P. Neuroprotective effects of ononin against the aluminium chloride-induced Alzheimer's disease in rats. *Saudi J Biol Sci.* 2021;28(8):4232-4239.

doi: 10.1016/j.sjbs.2021.06.031

14. Cao Z, Wang F, Xiu C, Zhang J, Li Y. Hypericum perforatum extract attenuates behavioral, biochemical, and neurochemical abnormalities in Aluminium chloride-induced Alzheimer's disease rats. *Biomed Pharmacother.* 2017;91:931-937.

doi: 10.1016/j.biopha.2017.05.022

15. Mirza A, King A, Troakes C, Exley C. Aluminium in brain tissue in familial Alzheimer's disease. *J Trace Elem Med Biol.* 2017;40:30-36.

doi: 10.1016/j.jtemb.2016.12.001

16. Hamdan AM, Alharthi FH, Alanazi AH, *et al.* Neuroprotective effects of phytochemicals against aluminium chloride-induced Alzheimer's disease through ApoE4/LRP1, Wnt3/β-catenin/GSK3β, and TLR4/NLRP3 pathways with physical and mental activities in a rat model. *Pharmaceuticals.* 2022;15(8):1008.

doi: 10.3390/ph15081008

17. Aalikhani M, Safdari Y, Jahanshahi M, Alikhani M, Khalili M. Comparison between hesperidin, coumarin, and deferoxamine iron chelation and antioxidant activity against excessive iron in the iron overloaded mice. *Front. Neurosci.* 2022;15:811080.

doi: 10.3389/fnins.2021.811080

18. Mahalakshmi B, Maurya N, Lee S, Bharath Kumar V. Possible neuroprotective mechanisms of physical exercise in neurodegeneration. *Int J Mol Sci.* 2020;21(16):5895.

doi: 10.3390/ijms21165895

19. Majid A. Neuroprotection in stroke: Past, present, and future. *ISRN Neurol.* 2014;2:515716.

doi: 10.1155/2014/515716

20. Kumar A, Singh A, Ekavali. A review on Alzheimer's disease pathophysiology and its management: An update. *Pharmacol Rep.* 2015;67(2):195-203.

doi: 10.1016/j.pharep.2014.09.004

21. Jin Y, Sumsuzzman D, Choi J, Kang H, Lee S, Hong Y. Molecular and functional interaction of the myokine irisin with physical exercise and Alzheimer's disease. *Molecules.* 2018;23(12):3229.

doi: 10.3390/molecules23123229

22. Pahlavani HA. Exercise therapy to prevent and treat Alzheimer's disease. *Front Aging Neurosci.* 2023;15(124):38-69.

doi: 10.3389/fnagi.2023.1243869

23. Barnes DE, Yaffe K. The projected effect of risk factor reduction on Alzheimer's disease prevalence. *Lancet Neurol.* 2011;10(9):819-828.

doi: 10.1016/S1474-4422(11)70072-2

24. Sutoo D, Akiyama K. Regulation of brain function by exercise. *Neurobiol Dis.* 2013;13(1):1-14.

doi: 10.1016/S0969-9961(03)00030-5

25. Schinder AF, Poo M. The neurotrophin hypothesis for synaptic plasticity. *Trends Neurosci.* 2020;23(12):639-645.

doi: 10.1016/S0166-2236(00)01672-6

26. Hosseini M, Alaei HA, Naderi A, Sharifib MR, Zahed R. Treadmill exercise reduces self-administration of morphine in male rats. *Pathophysiology.* 2019;16(1):3-7.

doi: 10.1016/j.pathophys.2008.11.001

27. Lu B, Chow A. Neurotrophins and hippocampal synaptic transmission and plasticity. *J Neurosci Res.* 2019;58(1):76-87.

28. Lin TW, Tsai SF, Kuo YM. Physical exercise enhances neuroplasticity and delays Alzheimer's disease. *Brain Plast.* 2018;4:95-110.

doi: 10.3233/BPL-180073

29. Ryan SM, Kelly ÁM. Exercise as a pro-cognitive, pro-neurogenic and anti-inflammatory intervention in transgenic mouse models of Alzheimer's disease. *Ageing Res Rev.* 2016;27:77-92.

doi: 10.1016/j.arr.2016.03.007

30. Lu Y, Dong Y, Tucker D, *et al.* Treadmill exercise exerts neuroprotection and regulates microglial polarization and oxidative stress in a streptozotocin-induced rat model of sporadic Alzheimer's Disease. *J Alzheimer Dis.* 2017;56(4):1469-1484.

doi: 10.3233/JAD-160869

31. Tang Y, Zhang Y, Zheng M, Chen J, Chen H, Liu N. Effects of treadmill exercise on cerebral angiogenesis and MT1-MMP expression after cerebral ischemia in rats. *Brain Behav.* 2018;8:e01079.

doi: 10.1002/brb3.1079

32. Kamat PK, Kalani A, Rai S, *et al.* Mechanism of oxidative stress and synapse dysfunction in the pathogenesis of Alzheimer's disease: Understanding the therapeutics strategies. *Mol Neurobiol.* 2016;53(1):648-661.

doi: 10.1007/s12035-014-9053-6

33. Moreira PI, Santos MS, Oliveira CR, *et al.* Alzheimer disease and the role of free radicals in the pathogenesis of the disease. *CNS Neurol Disord Drug Targets.* 2008;7:3-10.

doi: 10.2174/187152708783885156

34. Wojsiat J, Zoltowska KM, Laskowska-Kaszub K, Wojda U. Oxidant/antioxidant imbalance in Alzheimer's disease: Therapeutic and diagnostic prospects. *Oxid Med Cell Longev.* 2018;2018(1):1-16.

doi: 10.1155/2018/6435861

35. Mandal PK, Saharan S, Tripathi M, Murari G. Brain glutathione levels--a novel biomarker for mild cognitive impairment and Alzheimer's disease. *Biol Psychiatry.* 2015;78(10):702-710.

doi: 10.1016/j.biopsych.2015.04.005

36. Czerniawski J, Miyashita T, Lewandowski G, Guzowski JF. Systemic lipopolysaccharide administration impairs retrieval of context-object discrimination, but not spatial, memory: Evidence for selective disruption of specific hippocampus dependent memory functions during acute neuroinflammation. *Brain Behav Immun.* 2015;44:159-166.

doi: 10.1016/j.bbi.2014.09.014

37. Adair JC, Knoefel JE, Morgan N. Controlled trial of nacetylcysteine for patients with probable Alzheimer's disease. *Neurology.* 2001;57(8):1515-1517.

doi: 10.1212/WNL.57.8.1515

38. Ogunlade B, Fidelis OP, Afolayan OO, Agie JA. Neurotherapeutic and antioxidant response of D-ribose-L-Cysteine nutritional dietary supplements on Alzheimer-type hippocampal neurodegeneration induced by cuprizone in adult male wistar rat model. *Food Chem Toxicol.* 2021;147:111862.

doi: 10.1016/j.fct.2020.111862

39. Falana B, Adeleke O, Orenolu M, Osinubi A, Oyewopo A. Effect of D-ribose-L-cysteine on aluminium induced testicular damage in male sprague-dawley rats. *JBRA Assist Reprod.* 2017;21(2):94.

doi: 10.5935/1518-0557.20170023

40. Adelakun SA, Ogunlade B, Fidelis OP, Ajao AA. Nutritional supplementation of D-Ribose-L-Cysteine suppresses oxidative stress, spermatogenesis and steroidogenesis recovery in rats exposed to mercury chloride: Histomorphometry and biochemical evidence. *Endocr Metab Sci.* 2021;4:100105.

doi: 10.1016/j.endmts.2021.100105

41. Ojetola AA, Adedeji TG, Fasanmade AA. Changes in antioxidants status, atherogenic index and cardiovascular variables after prolonged doses of D-ribose-L-cysteine in male Wistar rats. *Heliyon.* 2021;7(2):e06287.

doi: 10.1016/j.heliyon.2021.e06287

42. Adedotun OA, Chukwunenye CC, Balogun AF, Olawale MA, Babatunde JO, Ogunlade B. Histomorphological response of D-ribose-L-cysteine to ketamine-induced testicular toxicity in adult male Wistar rats. *Redox Experiment Medicine.* 2023;1:20-23.

43. Ogunsuyi OB, Aro PO, Umar HI, Oboh G. Administration of curcumin plus treadmill exercise modulate some neuronal enzyme activities, redox markers and BDNF mRNA expression in pilocarpine-induced epileptic seizure in rats. *Neurochem J.* 2023;17(3):467-476.

doi: 10.1134/S1819712423030145

44. Alomari MA, Khabour OF, Alzoubi KH, Alzubi MA. Forced and voluntary exercises equally improve spatial learning and memory and hippocampal BDNF levels. *Behav Brain Res.* 2013;247:34-39.

doi: 10.1016/j.bbr.2013.03.007

45. Bayod S, Del Valle J, Lalanza JF, *et al.* Long-term treadmill exercise induces neuroprotective molecular changes in rat brain. *J Appl Physiol.* 2011;111(5):1380-1390.

doi: 10.1152/japplphysiol.00425.2011

46. National Research Council. *Guide to the Care and Use of Laboratory Animals*. 8th ed. Washington, DC: The National Academies Press; 2011. p. 246.

47. Bali A, Jaggi AS. Electric foot shock stress: A useful tool in neuropsychiatric studies. *Rev Neurosci*. 2015;26(6):655-677.

doi: 10.1515/revneuro-2015-0015

48. Bedford TG, Tipton CM, Wilson NC, Oppliger RA, Gisolfi CV. Maximum oxygen consumption of rats and its changes with various experimental procedures. *Appl Physiol Respir Environ Exerc Physiol.* 1979;47(6):1278-1283.

doi: 10.1152/jappl.1979.47.6.1278

49. Gould TD, Dao DT, Kovacsics CE. The open field test. In: *Mood and Anxiety Related Phenotypes in Mice*. Vol. 42. Totowa, NJ: Humana Press; 2009. p. 1-20.

doi: 10.1007/978-1-60761-303-9_1

50. Kraeuter AK, Guest PC, Sarnyai Z. The Y-maze for assessment of spatial working and reference memory in mice. *Methods Mol Biol.* 2019;1916:105-111.

doi: 10.1007/978-1-4939-8994-2_10

51. Sun M, Zigman S. An improved spectrophotometric assay for superoxide dismutase based on epinephrine autoxidation. *Anal Biochem.* 1978;90(1):81-89.

doi: 10.1016/0003-2697(78)90010-6

52. Clairborne A. Catalase activity. In: Greewald AR, editor. *Handbook of Methods for Oxygen Radical Research.* United States: CRC Press; 1995. p. 237-242.

53. Jollow DJ, Mitchell JR, Zampaglione N, Gillette JR. Bromobenzene-induced liver necrosis. Protective role of glutathione and evidence for 3,4-bromobenzene oxide as the hepatotoxic metabolite. *Pharmacology*. 1974;11(3):151-169.

doi: 10.1159/000136485

54. Farombi E, Tahnteng J, Agboola A, Nwankwo J, Emerole G. Chemoprevention of 2-acetylaminofluorene-

induced hepatotoxicity and lipid peroxidation in rats by kolaviron--a *Garcinia kola* seed extract. *Food Chem Toxicol.* 2000;38(6):535-541.

doi: 10.1016/S0278-6915(00)00039-9

55. Moshage H, Kok B, Huizenga JR, Jansen PL. Nitrite and nitrate determinations in plasma: A critical evaluation. *Clin Chem.* 1995;41(6):892-896.

doi: 10.1093/clinchem/41.6.892

56. Pearse AG. The role of histochemistry in increasing objectivity in histopathology. *Postgrad Med J.* 1975;51(600):708-710.

doi: 10.1136/pgmj.51.600.708

57. Fischer AH, Jacobson KA, Rose J, Zeller R. Hematoxylin and eosin staining of tissue and cell sections. *CSH Protoc.* 2008;2008(5):pdb.prot4986.

doi: 10.1101/pdb.prot4986

58. Shi SR, Key ME, Kalra KL. Antigen retrieval in formalin-fixed, paraffin-embedded tissues: An enhancement method for immunohistochemical staining based on microwave oven heating of tissue sections. *J Histochem Cytochem*. 1991;39(6):741-748.

doi: 10.1177/39.6.1709656

59. Burry RW. *Immunocytochemistry: A Practical Guide for Biomedical Research*. Berlin: Springer Science and Business Media; 2011.

60. Hsu SM, Raine L, Fanger H. Use of avidin-biotin-peroxidase complex (ABC) in immunoperoxidase techniques: A comparison between ABC and unlabeled antibody (PAP) procedures. *J Histochem Cytochem.* 1981;29(4):577-580.

doi: 10.1177/29.4.6166661

61. Erukainure OL, Ijomone OM, Sanni O, Aschner M, Islam MS. Type 2 diabetes induced oxidative brain injury involves altered cerebellar neuronal integrity and elemental distribution, and exacerbated Nrf2 expression: Therapeutic potential of raffia palm (*Raphia hookeri*) wine. *Metab Brain Dis.* 2019;34:1385-1399.

doi: 10.1007/s11011-019-00444-x

62. Pagel P, Blome J, Wolf HW. High-performance liquid chromatographic separation and measurement of various biogenic compounds possibly involved in the pathomechanism of Parkinson's disease. *J Chromatogr*. 2000;746(2):297-304.

doi: 10.1016/S0378-4347(00)00348-0.

63. Ellman GL. Tissue sulfhydryl groups. *Arch Biochem Biophys.* 1959;82(1):70-77.

doi: 10.1016/0003-9861(59)90090-6

64. Jain A, Jain R, Jain S. Quantitative determination of TNF alpha and interleukin-6. In: *Springer Protocols Handbooks*. United States: Springer; 2020. p. 87-89.

doi: 10.1007/978-1-4939-9861-6_27

65. Borsini F, Meli A. Is the forced swimming test a suitable model for revealing antidepressant activity? *Psychopharmacology.* 1998;94(2):147-160.

doi: 10.1007/BF00176837

66. Vlasak T, Dujlovic T, Barth A. Aluminum exposure and cognitive performance: A meta-analysis. *Sci Total Environ*. 2024;906:167453.

doi: 10.1016/j.scitotenv.2023.167453

67. Kandola A, Hendrikse J, Lucassen PJ, Yücel M. Aerobic exercise as a tool to improve hippocampal plasticity and function in humans: Practical implications for mental health treatment. *Front Hum Neurosci*. 2016;10:373.

doi: 10.3389/fnhum.2016.00373

68. De Sousa Fernandes MS, Ordônio TF, Santos GCJ, *et al.* Effects of physical exercise on neuroplasticity and brain function: A systematic review in human and animal studies. *Neural Plast*. 2020;2020:8856621.

doi: 10.1155/2020/8856621

69. Lovell MA, Ehmann WD, Butler SM, Markesbery WR. Elevated thiobarbituric acid-reactive substances and antioxidant enzyme activity in the brain in Alzheimer's disease. *Neurology.* 1995;45(8):1594-1601.

doi: 10.1212/WNL.45.8.1594

70. Tiwari SC, Soni RM. Alzheimer's disease pathology and oxidative stress: Possible therapeutic options. *J Alzheimers Dis Park*. 2014;04(05):162.

doi: 10.4172/2161-0460.1000162

71. Slitt AM, Dominick PK, Roberts JC, Cohen SD. Effect of ribose cysteine pretreatment on hepatic and renal acetaminophen metabolite formation and glutathione depletion. *Basic Clin Pharmacol Toxicol.* 2015;96(6):487-494.

doi: 10.1111/j.1742-7843.2005.pto_96613.x

72. Mattson MP. Energy intake and exercise as determinants of brain health and vulnerability to injury and disease. *Cell Metab.* 2022;16(6):706-722.

doi: 10.1016/j.cmet.2012.08.012

73. Zatta P, Ibn-Lkhayat-Idrissi M, Zambenedetti P, Kilyen M, Kiss T. *In vivo* and *in vitro* effects of aluminium on the activity of mouse brain acetylcholinesterase. *Brain Res Bull.* 2012;59(1):41-45.

doi: 10.1016/S0361-9230(02)00836-5

74. Amberla K, Nordberg A, Viitanen M, Winblad B. Longterm treatment with tacrine (THA) in Alzheimer's disease--evaluation of neuropsychological data. *Acta Neurol Scand Appl*. 2013;88(S149):55-57.

doi: 10.1111/j.1600-0404.1993.tb04257.x

75. Meeusen R, De Meirleir K. Exercise and brain

neurotransmission. *Sports Med*. 2005;20(3):160-188.

doi: 10.2165/00007256-199520030-00004

76. Cheng XJ, Gu JX, Pang YP, *et al.* Tacrine-hydrogen sulfide donor hybrid ameliorates cognitive impairment in the aluminium chloride mouse model of Alzheimer's disease. *ACS Chem Neurosci*. 2019;10(8):3500-3509.

doi: 10.1021/acschemneuro.9b00120

77. Ghosh S, Lertwattanarak R, Garduño JD, *et al.* Elevated muscle TLR4 expression and metabolic endotoxemia in human aging. *J Gerontol A Biol Sci Med Sci.* 2015;70(2):232-246.

doi: 10.1093/gerona/glu067

78. Uyar B, Palmer D, Kowald A, Murua-Escobar H, Barrantes I, Möller S. Single-cell analyses of aging, inflammation and senescence. *Ageing Res Rev*. 2020;64:101156.

doi: 10.1016/j.arr.2020.101156

79. Zagrodzki P, Joniec A, Gawlik M, *et al.* High fructose model of oxidative stress and metabolic disturbances in rats. Part I. Antioxidant status of rats' tissues. *Bull Vet Inst Pulawy.* 2019;51(3):407-412.

80. Valenzuela PL, Maffiuletti NA, Joyner MJ, Lucia A, Lepers R. Lifelong endurance exercise as a countermeasure against age-related VO_{2max} decline: Physiological overview and insights from masters athletes. *Sports Med.* 2020;50(4):703-716.

doi: 10.1007/s40279-019-01252-0

81. Cao Z, Yang X, Zhang H, *et al.* Aluminum chloride induces neuroinflammation, loss of neuronal dendritic spine and cognition impairment in developing rats. *Chemosphere.* 2016;151:289-295.

doi: 10.1016/j.chemosphere.2016.02.092

82. Zhang X, He Q, Huang T, *et al.* Treadmill exercise decreases deposition and counteracts cognitive decline in APP/PS1 mice, Possibly via hippocampal microglia modifications. *Front Aging Neurosci.* 2019;11:78.

doi: 10.3389/fnagi.2019.00078

83. Hosseini M, Alaei H, Reisi P, Radahmadi M. The effect of treadmill running on memory before and after the NBM-lesion in rats. *J Bodyw Mov Ther*. 2013;17(4):423-429.

doi: 10.1016/j.jbmt.2012.12.005

ACCSCIENCE PUBLISHING

Innovative Medicines & Omics

SHORT COMMUNICATION

Coculture of umbilical cord-derived mesenchymal stem cells for differentiation into chondrocytes and Schwann cells

Kyoko Baba[1,2]*, Yoshika Sugimoto[1], and Jumpei Wato[1]

[1]Department of Plastic Surgery and Aesthetic Surgery, Kitasato University School of Medicine, Kitasato, Minami-ku, Sagamihara, Kanagawa, Japan

[2]Department of Plastic Surgery, Kitasato University Medical Center, Arai, Kitamoto, Saitama, Japan

Abstract

Umbilical cord-derived mesenchymal stem cells (UC-MSCs) are reported to have features intermediate between those of fetal and adult mesenchymal cells. Hence, UC-MSCs were cocultured with chondrocytes and Schwann cells to induce differentiation because of their flexible differentiation potential. UC-MSCs were obtained from umbilical cords, and cells at the second passage were used in the experiments. Atelocollagen sponge was used as the scaffold for coculture; a horizontal, interactive coculture plate with a filter (pore size, 0.6 μm) was placed between the connected vessels. UC-MSCs were cocultured separately with chondrocytes and Schwann cells, and culture alone served as a control. Five weeks after induction of differentiation, each specimen was evaluated histologically. In the specimens cocultured with chondrocytes and the controls, cartilage tissues were detected using hematoxylin-eosin and toluidine blue staining. Cells positive for the S100 protein were detected in the specimens cocultured with Schwann cells, but not in the controls. UC-MSCs were easily induced to differentiate into chondrocytes and neural cells by coculture. This indicates that continuously shared humoral factors were effective in inducing differentiation of UC-MSCs. Thus, coculture may serve as a potentially useful technique for tissue regeneration using MSCs.

Keywords: Umbilical cord-derived mesenchymal stem cells; Coculture; Cell differentiation; Regenerative medicine; Chondrocytes; Schwann cells

***Corresponding author:**
Kyoko Baba
(kyokobaba@med.kitasato-u.ac.jp)

Citation: Baba K, Sugimoto Y, Wato J. Coculture of umbilical cord-derived mesenchymal stem cells for differentiation into chondrocytes and Schwann cells. *Innov Med Omics*. 2026;3(1):66-72.
doi: 10.36922/imo.4924

Received: September 24, 2024

Revised: October 27, 2024

Accepted: November 8, 2024

Published online: December 17, 2025

1. Introduction

In recent years, it has been recognized that the cellular kinetics of mesenchymal stem cells (MSCs) differ depending on their origin.[1] Umbilical cord-derived MSCs (UC-MSCs), one type of MSCs, are reported to have features intermediate between fetal and adult cells and have a flexible differentiation potential.[2] In a previous study, we verified the differentiation of UC-MSCs into adipocytes when using the same culture method as that described in this report.[3] Although our previous studies confirmed that UC-MSCs have the potential to differentiate into osteoblasts, we failed to generate mature bone tissues by culturing UC-MSCs under the same conditions as the culture of bone marrow-derived MSCs (BM-MSCs).[3,4] This suggested that the differentiation

potential of UC-MSCs might be affected by factors other than the differentiation potential of MSCs derived from tissues such as bone marrow and adipose tissue. We deduced that this result was attributed to the immaturity of UC-MSCs, based on the fact that UC-MSCs are primitive and resemble fetal cells that are likely to be affected by the surrounding environment.[5] Intercellular communication has been considered to involve the interaction of cells with their neighbors through interactions that are mediated by soluble molecules, such as cell-secreted cytokines. Recent studies have revealed that humoral factors, such as extracellular vesicles and exosomes, play an important role in cell–cell communication. If humoral factors can be sustained and shared, it may not be necessary to comprehensively elucidate the interactions. Coculture allows humoral factors to be shared continuously.[6] We hypothesized that UC-MSCs, which are likely to be affected by the surrounding environment, could be more easily induced to differentiate through the sharing of humoral factors with cocultured cells.

For the purpose of clinical application, it is meaningful to explore methods that are simple to operate, are less invasive to cells, and mimic the physiological process of tissue formation, in addition to considering ethics and safety.[7] These conditions can be met by coculture.[6] However, we did not find any reports on the differentiation potential of UC-MSCs that was evaluated using coculture techniques that were as simple as the technique performed in the present study. Coculture appears to be not only simple but also less stressful for cells because it seems to be more physiological and able to mimic the *in vivo* environment. Thus, UC-MSCs were cocultured with chondrocytes and Schwann cells, and the differentiation potential of UC-MSCs was evaluated. The present study is the first preliminary study investigating the potential of UC-MSC coculture. The examination of our hypothesis, which focuses on cell–cell interactions mediated by humoral factors, is expected to contribute to the realization of regenerative medicine using autologous tissues.

2. Materials and methods

The present study was conducted under the approval of the Ethics Committee of Kitasato University (B-07-13). This study was conducted in compliance with the "Ethical Guidelines for Medical and Health Research Involving Human Subjects." All materials used in this study were obtained from newborns at our institution. The samples of UC were collected from healthy full-term neonates during delivery. We obtained written informed consent from pregnant women and used the tissues that were normally discarded after delivery. The materials were collected under conditions ensuring the safety of neonates. The specimens provided were coded to prevent identification of individual donors.

2.1. Preparation of cells

UC-MSCs were obtained by the outgrowth method in accordance with our previous report.[3] The culture was continued until the moment when cells became subconfluent (Figure 1). The cells that became 80–90% subconfluent were subcultured, and the second-passage cells were used in the experiments. Commercially available chondrocytes (T0020-C, Cosmo Bio, Tokyo, Japan) were used. A mouse Schwann cell line (IMS32, Cosmo Bio, Tokyo, Japan) was used. They were cultured according to the respective recommended methods. The Schwann cells were used without subculturing.

2.2. Seeding on scaffolds and distribution of specimens

Atelocollagen sponge (Atelo Cell CSM-50, KOKEN Co., Ltd., Tokyo, Japan) was used as the scaffold (Figure 2). Each scaffold was seeded with 1×10^5 UC-MSCs, with each regarded as one specimen. Seeding was performed according to the procedure as described previously.[3] Subsequently, specimens were placed in each vessel of the coculture plate. The specimens were cultured in DMEM for 1 week to allow cell infiltration into the atelocollagen sponge. Six specimens were prepared. Three of them were used for the induction of differentiation into chondrocytes, and the other three were used for the induction of differentiation into neural cells.

2.3. Coculture and induction of differentiation

UC-MSCs that were seeded on scaffolds and cultured alone were used as the controls (control C: used for induction of differentiation into chondrocytes; control N, used for induction of differentiation into neural cells). Hence, the control condition was established to be free from the influence of humoral factors released by chondrocytes and Schwann cells. For coculture, a horizontal interactive coculture plate (NICO-1, Ginrei Lab, Ishikawa, Japan) was used (Figure 3). In this coculture condition, the soluble substances secreted by the cells in the medium are thought to move between vessels via diffusion.[6] Extracellular vesicles are also thought to move between vessels via Brownian motion due to their size.[6] These findings suggest that substances released by the cocultured chondrocytes and Schwann cells are shared with UC-MSCs at physiological concentrations and timing. In other words, rather than relying on artificially controlled conditions, physiological changes are continuously sustained. The specimens and controls were placed in the right and left vessels of the plate, and a necessary and sufficient amount of culture

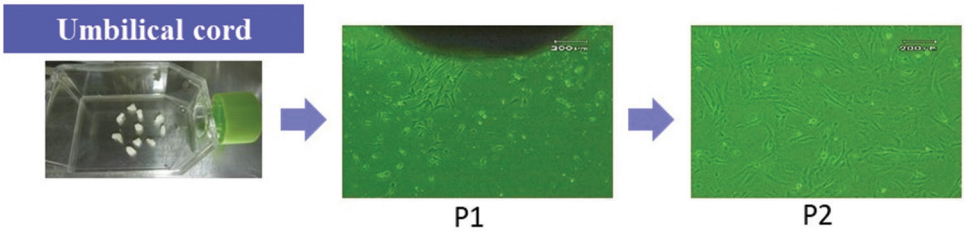

Figure 1. Preparation of umbilical cord-derived mesenchymal stem cells (UC-MSCs). UC-MSCs were obtained by the outgrowth method in accordance with our previous report.[3] The umbilical cord was washed of attached blood with phosphate-buffered saline, cut into approximately 5-mm sections, and used for culture. Following the emergence of adhesive spindle-shaped cells, the UC sections were removed. Cells that became 80–90% subconfluent were subcultured, and the second-passage UC-MSCs were used in the experiments. The images of P1 and P2 were observed under a phase-contrast microscope.

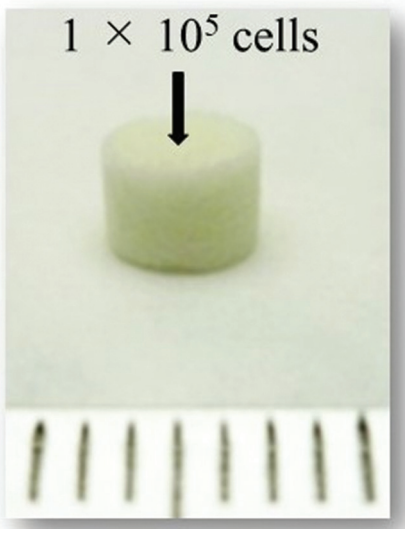

Figure 2. Atelocollagen sponge (Atelo Cell CSM-50, KOKEN Co., Ltd., Tokyo, Japan) was used as the scaffold. Each scaffold was seeded with 1×10^5 umbilical cord-derived mesenchymal stem cells (UC-MSCs).

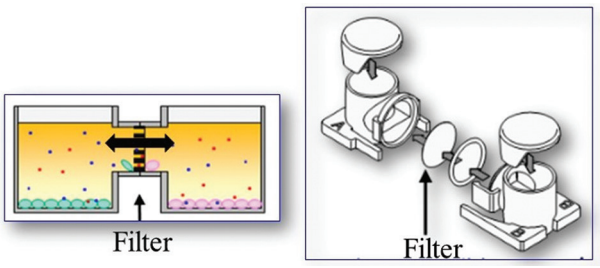

Figure 3. Horizontal interactive indirect coculture plate (NICO-1). The images are adapted from Ginreilab Inc. (https://nico-1.info/nico-1/, last accessed July 21, 2024); reprinted with permission of the copyright holder. A filter was placed between the vessels. This structure prevents cells from being mixed, but allows them to share humoral factors.

medium was added. A filter with a pore size of 0.6 μm was placed between these vessels to facilitate smooth and continuous passage of proteins and cytokines, including exosomes, from vessel to vessel. The filter precluded cross-contamination of the two distinct cell cultures.

This provided an environment where the culture medium could be shared without mixing the cells (Figure 4). The cells were also cultured at 37°C in 5% CO_2 during coculture and induction of differentiation. For the coculture of control specimens C with chondrocytes, the culture medium was changed to ChondroDiff Media (Miltenyi Biotec GmbH, Bergisch Gladbach, Germany), and the specimens were cocultured for 5 weeks to be induced to differentiate into chondrocytes. In these cocultures, no additional components—such as growth factors—were added to the differentiation induction medium.

For coculture of control specimens N (with Schwann cells), the culture medium was changed to MSCs Neurogenic Differentiation Medium® (PromoCell GmbH, Heidelberg, Germany), and the specimens were cocultured for 5 weeks to be induced to differentiate into Schwann cells. No substances other than the commercially available differentiation induction media were added for the induction of differentiation of either specimen. The flow of the experiments is shown in Figure 5.

2.4. Histological evaluation

Specimens removed from NICO-1 were fixed with 10% formalin. After washing, the samples were embedded in paraffin, cut to approximately 3-mm sections, stained with hematoxylin and eosin (H&E), and observed with an optical microscope. Specimens C and controls C were stained with toluidine blue O (Toluidine Blue O: CI 52040, Kanto Chemical CO., INK Tokyo, Japan). Specimens N and controls C were stained with polyclonal rabbit anti-S100 antibody (DAKO Agilent, CA, USA). The specimens were stained according to the respective manufacturer's methods and observed with an optical microscope.

3. Results

In specimens C and controls C, small elastic hard masses were formed outside the scaffolds. These small masses were cartilage matrices that were metachromatically stained with toluidine blue. H&E staining also showed findings

consistent with those of cartilage tissue (Figure 6). In H&E staining of the controls, cartilage-like tissues detected in the controls were smaller than those in the specimens.

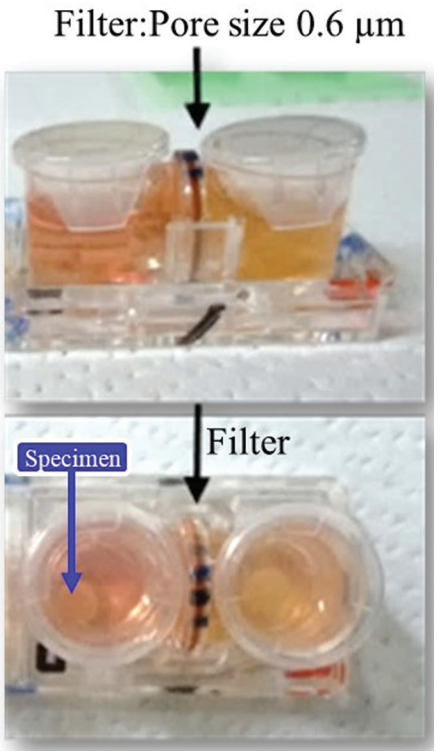

Figure 4. Indirect horizontal coculture. The filter has a defined pore size of 0.6 μm, precluding the cross-contamination of the two distinct cell cultures. This facilitates the smooth and continuous passage of proteins and cytokines, including exosomes, from vessel to vessel.

In toluidine blue staining, metachromatically stained cartilage matrices were also detected in a smaller area of the controls than that of the specimens. Controls N showed no cells stained with anti-100 antibody, whereas specimens N showed cells positive for S100 staining. H&E staining revealed that the morphology of S100 protein-positive cells in specimen N was consistent with that of Schwann cells (Figure 7). In H&E staining of the controls N, no cells showed morphology specific to Schwann cells.

4. Discussion

The availability of autologous tissues as biomedical materials for regenerative medicine suggests that they may be safe for use in patients. The number of pregnant women attending our department for prenatal consultations about their fetuses diagnosed with an alveolar cleft is not rare. As a consequence, we have focused on the umbilical cord as a source of autologous regenerative medicine. Collecting these autologous tissues at birth poses no difficulty. Recent studies have revealed the presence of MSCs in many tissues, including the umbilical cord. The presence of UC-MSCs has become well known in recent years, and attention is paid to their usefulness. In this study, we focused on the umbilical cord, which has the following advantages: (i) it is autologous tissue; (ii) it can be non-invasively collected; and (iii) it provides an abundant volume of tissue. The purpose of this study was to obtain autologous tissues for tissue regeneration in the form of UC-MSCs.

Currently, investigators are conducting studies to determine the process of tissue regeneration. However,

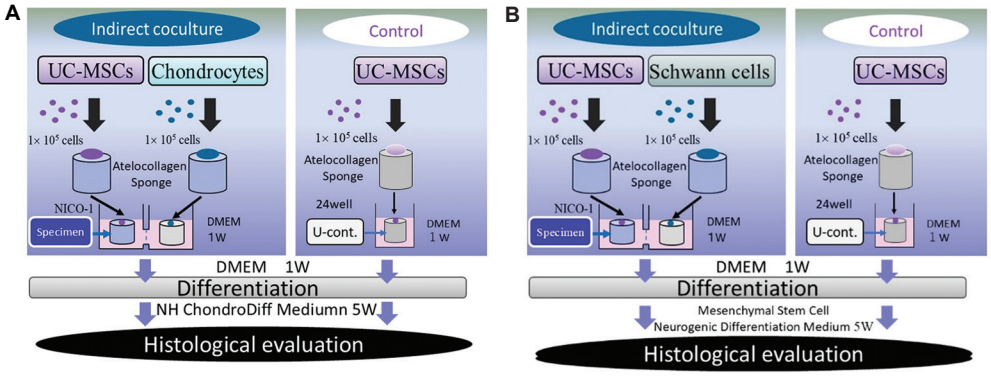

Figure 5. The flow of the coculture experiments. (A) Induction of differentiation into chondrocytes. The atelocollagen sponge was seeded with 1×10^5 UC-MSCs. The specimens were placed in each vessel of the coculture plate and cultured in DMEM for 1 week to allow cell infiltration into the atelocollagen sponge. For coculture of control specimens with chondrocytes, the culture medium was changed to ChondroDiff Media (Miltenyi Biotec GmbH, Bergisch Gladbach, Germany), and the specimens were cocultured for 5 weeks to be induced to differentiate into chondrocytes. Subsequently, specimens removed from NICO-1 (a horizontal interactive coculture plate) were evaluated histologically. (B) Induction of differentiation into neural cells. The atelocollagen sponge was seeded with 1×10^5 UC-MSCs. The specimens were placed in each vessel of the coculture plate and cultured in DMEM for 1 week to allow cell infiltration into the atelocollagen sponge. For coculture of control specimens N (with Schwann cells), the culture medium was changed to Mesenchymal Stem Cell Neurogenic Differentiation Medium® (PromoCell GmbH, Heidelberg, Germany), and the specimens were cocultured for 5 weeks to be induced to differentiate into Schwann cells. Subsequently, specimens removed from NICO-1 were evaluated histologically.
Abbreviations: DMEM: Dulbecco's modified Eagle medium; UC-MSCs: Umbilical cord-derived mesenchymal stem cells.

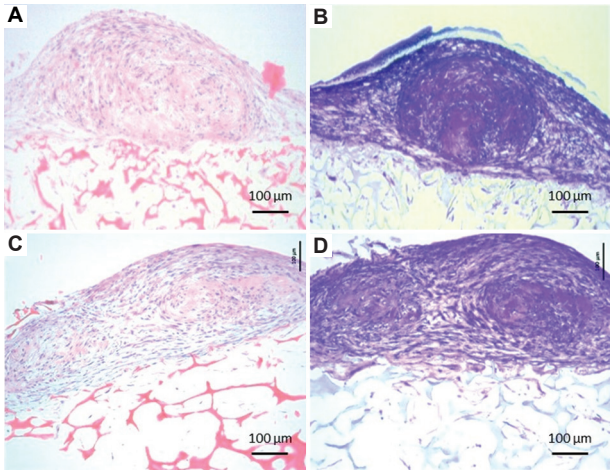

Figure 6. Results of the histopathological examination of the specimens and controls that were induced to differentiate into chondrocytes. (A) Hematoxylin-eosin (H&E) staining of the cocultured specimens. Cartilage-like tissues were detected. The cartilage-like tissue matrix appeared eosinophilic following H&E staining. (B) Toluidine blue staining of the cocultured specimens. Metachromatically-stained cartilage matrices were detected. With toluidine blue staining, the cartilage-like tissue displayed metachromasia, staining reddish-purple rather than the dye's original color (black arrow). (C) H&E staining of the controls. Cartilage-like tissues detected in the controls were smaller than those in the specimens. The cartilage-like tissue matrix appeared eosinophilic following H&E staining. (D) Toluidine blue staining of the controls. Metachromatically-stained cartilage matrices were detected in a smaller area in the controls than in the specimens. With toluidine blue staining, the cartilage-like tissue displayed metachromasia, staining reddish-purple rather than the dye's original color (black arrow).

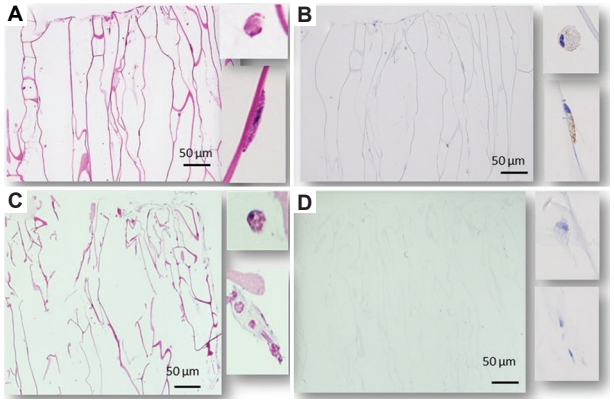

Figure 7. Results of the histopathological examination of the specimens and controls that were induced to differentiate into Schwann cells. (A) Hematoxylin–eosin (H&E) staining of the cocultured specimens. Cells that morphologically appeared to be Schwann cells were detected. (B) S100 protein staining of the cocultured specimens. Schwann cell-like cells were positive for S100 protein. (C) H&E staining of the controls. No cells showed morphology resembling the Schwann cells. (D) S100-protein staining of the controls. No cells positive for S100 protein were detected.

not all elements of the process, such as timing, substances, concentrations, and combinations and ratios of substances, have been elucidated. When tissues are formed in the body, cells continuously release various factors, such as exosomes, and interact to regenerate tissues. In the case of *in vitro* tissue formation, essential operations that have been reported are performed. However, the *in vitro* operations may not necessarily mimic the physiological tissue formation in the body. For example, adding bone morphogenic protein (BMP) to BM-MSCs induces BM-MSCs to differentiate into osteoblasts so that bone tissues can be obtained. Nevertheless, this is achieved in an environment different from the complex *in vivo* environment.[8] As a means to solve this issue, we focused on coculture. The advantage of coculture is that the factors released from cocultured cells can continuously be used at physiological timing and concentrations during coculture.[6,9] This outcome is achievable regardless of whether the details are known. Because UC-MSCs are more primitive and more likely to be affected by the surrounding environment than adult tissue-derived MSCs,[2] we hypothesized that coculture would benefit tissue regeneration with UC-MSCs and facilitate tissue formation compared to tissue formation by culturing UC-MSCs alone. Horizontal coculture vessels were employed in our study, as they are believed to facilitate more efficient and continuous exchange of humoral factors between cell types. This configuration optimizes the interaction between cells by promoting a stable and consistent environment for factor diffusion, which may enhance the overall coculture system's performance and reliability.[10] Considering the results of the differentiation assays, indirect horizontal coculture appears to have been beneficial for the continuous exchange of humoral factors observed in this study. In recent years, investigators have studied the importance of the actions of humoral factors, such as exosomes, on cells. In the present study, US-MSCs in the control N, which were induced to differentiate only in the commercially available differentiation induction medium, did not differentiate into Schwann cells. UC-MSCs in control N differentiated into Schwann cells, suggesting that humoral factors shared through the filter in coculture might have contributed to the induction of differentiation into neural cells. As for the induction of differentiation into cartilage, the histological evaluation revealed cartilage-like tissues in both control C and specimen C. However, specimen C showed more mature and larger cartilage-like tissues that were macroscopically detectable. In conventional exosome research, liquid biopsy is commonly used to analyze exosomes extracted from various disease states. However, exosomes are only one of the many critical components involved in cellular communication. To fully elucidate their role, replicating *in vivo* conditions and investigating these interactions in a comprehensive manner are essential. Previous studies suggest that coculture techniques, which do not require

exosome extraction, may serve as an effective alternative for observing natural cellular interactions.[10]

In the present study, we did not specifically measure factors such as exosomes or cytokines. In the future, a longitudinal evaluation of humoral factors, such as exosomes, may further elucidate the mechanisms underlying tissue formation in greater detail. In the present study, we were able to induce differentiation into both chondrocytes and Schwann cells with similar culture techniques using commercially available differentiation induction media without any special manipulation of cells or inventive additives to the culture media. The results of the present study suggest that coculture is useful for the induction of differentiation of UC-MSCs.

Currently, we are working on developing an innovative therapeutic approach that employs UC-MSCs as an autologous tissue-based material for regenerative medicine. For clinical applications, the transplantation of genetically modified cells raises safety concerns. In contrast, coculture techniques involve minimal manipulation, allowing for tissue regeneration through a simpler process. In addition, depending on the type of cells cocultured with UC-MSCs, it may be possible to induce differentiation into a diverse range of cell types. Coculturing strategies with UC-MSCs are anticipated to be versatile, potentially enabling not only the regeneration of transplantable tissues but also the generation of cells involved in diseases for which directed differentiation has been challenging. This approach suggests potential contributions to disease modeling and therapeutic drug development. Currently, research on UC-MSCs is not as extensively reported as studies on adipose-derived or bone marrow-derived stem cells. Given that UC-MSCs exhibit unique properties distinct from adult somatic stem cells, the authors believe that further research in this area holds considerable promise for future development.

5. Conclusion

This study demonstrates that indirect coculture enhances UC-MSC differentiation into chondrocytes and Schwann cells through sustained humoral factor exchange, supporting its potential as a simple and physiologically relevant strategy for regenerative applications.

Acknowledgments

The authors would like to thank Honyaku Center Inc. for their assistance with English language editing.

Funding

This research was funded by a grant-in-aid for scientific research (C) 20K09871 from the Ministry of Education, Culture, Sports, Science and Technology, Japan.

Conflict of interest

The authors declare they have no competing interests.

Author contributions

Conceptualization: Kyoko Baba
Data curation: Kyoko Baba
Investigation: Yoshika Sugimoto, Jumpei Wato
Methodology: Kyoko Baba
Writing–original draft: Kyoko Baba
Writing–review & editing: Kyoko Baba

Ethics approval and consent to participate

The study was conducted in accordance with the Declaration of Helsinki and approved by the Ethics Committee of Kitasato University (B-07-13). Informed consent was obtained from the parents or legal guardians of all neonates enrolled in the study.

Consent for publication

Written informed consent has been obtained from the parents or legal guardians of neonates to publish this paper.

Availability of data

The original contributions presented in the study are included in the article; further inquiries should be directed to the corresponding author.

Further disclosure

This paper has been uploaded to or deposited in a preprint server (doi: 10.20944/preprints202407.2505.v1). The findings reported in this paper have been presented at several conferences:

(i) Kyoko Baba, Yasuharu Yamazaki, Yumiko Sone, Yoshika Sugimoto, Kazuno Moriyama, Takayuki Sugimoto, Kenichi Kumazawa, Akira Takeda. Coculture of Umbilical Cord-derived MSCs (UCMSCs) and Chondrocytes Improved Chondrogenic Differentiation. 11th WORLD BIOMATERIALS CONGRESS. 2020 WEB.

(ii) Kazuno Moriyama, Kyoko Baba, Yasuharu Yamazaki, Yumiko Sone, Yoshika Sugimoto, Takayuki Sugimoto, Kenichi Kumazawa, Akira Takeda. Coculture of Umbilical Cord-derived MSCs (UCMSCs) and Schwann cells Improved Neurogenic Differentiation. 15th Japan-Korea PRS 2023.

References

1. Sarugaser R, Lickorish D, Baksh D, Hosseini MM, Davies JE. Human umbilical cord perivascular (HUCPV) cells: A source of mesenchymal progenitors. *Stem Cells*. 2005;23(2):220-229.

doi: 10.1634/stemcells.2004-0166

2. Kern S, Eichler H, Stoeve J, Klüter H, Bieback K. Comparative analysis of mesenchymal stem cells from bone marrow, umbilical cord blood, or adipose tissue. *Stem Cells*. 2006;24(5):1294-1301.

   doi: 10.1634/stemcells.2005-0342

3. Baba K, Yamazaki Y, Ikemoto S, Aoyagi K, Takeda A, Uchinuma E. Osteogenic potential of human umbilical cord-derived mesenchymal stromal cells cultured with umbilical cord blood-derived autoserum. *J Craniomaxillofac Surg*. 2012;40(8):768-772.

   doi: 10.1016/j.jcms.2012.02.006

4. Baba K, Yamazaki Y, Ishiguro M, *et al*. Osteogenic potential of human umbilical cord-derived mesenchymal stromal cells cultured with umbilical cord blood-derived fibrin: A preliminary study. *J Craniomaxillofac Surg*. 2013;41(8):775-782.

   doi: 10.1016/j.jcms.2013.01.025

5. Li X, Bai J, Ji X, Li R, Xuan Y, Wang Y. Comprehensive characterization of four different populations of human mesenchymal stem cells as regards their immune properties, proliferation and differentiation. *Int J Mol Med*. 2014;34(3):695-704.

   doi: 10.3892/ijmm.2014.1821

6. Shimasaki T, Yamamoto S, Omura R, *et al*. Novel platform for regulation of extracellular vesicles and metabolites secretion from cells using a multi-linkable horizontal co-culture plate. *Micromachines (Basel)*. 2021;12(11):1431.

   doi: 10.3390/mi12111431

7. Ohgushi H, Kitamura S, Kotobuki N, *et al*. Clinical application of marrow mesenchymal stem cells for hard tissue repair. *Yonsei Med J*. 2004;45 Suppl:61-67.

   doi: 10.3349/ymj.2004.45.Suppl.61.

8. Baba K, Yamazaki Y, Sone Y, *et al*. An *in vitro* long-term study of cryopreserved umbilical cord blood-derived platelet-rich plasma containing growth factors-PDGF-BB, TGF-β, and VEGF. *J Craniomaxillofac Surg*. 2019;47(4):668-675.

   doi: 10.1016/j.jcms.2019.01.020

9. Shimasaki T, Yamamoto S, Arisawa T. Exosome research and co-culture study. *Biol Pharm Bull*. 2018;41(9):1311-1321.

   doi: 10.1248/bpb.b18-00223

10. Sumi S, Kawagoe M, Abe R, Yanai G, Yang KC, Shirouzu Y. A multiple-funnels cell culture insert for the scale-up production of uniform cell spheroids. *Regen Ther*. 2017;7:52-60.

    doi: 10.1016/j.reth.2017.08.003

ACCSCIENCE PUBLISHING

Innovative Medicines & Omics

COMMENTARY

Addressing the burden of obesity: Commentary to *"Obesity management: An update on the available pharmacotherapy"*

Amedeo Lonardo[1]* and Ralf Weiskirchen[2]*

[1]Department of Internal Medicine, Azienda Ospedaliero-Universitaria of Modena, Modena, Italy

[2]Institute of Molecular Pathobiochemistry, Experimental Gene Therapy and Clinical Chemistry (IFMPEGKC), RWTH University Hospital Aachen, Aachen, Germany

Abstract

Obesity is a complex systemic condition with significant sexual dimorphism, increasing the risks of disorders such as type 2 diabetes mellitus, arterial hypertension, dyslipidemia, metabolic dysfunction-associated steatotic liver disease, chronic kidney disease, premature cardiovascular disease, and certain types of cancers. A recent publication by Christaki *et al.* on the comprehensive overview of obesity management in *Innovative Medicines* and *Omics* highlights the multifactorial nature of obesity, as well as the importance of lifestyle changes, alongside pharmacological treatments and bariatric surgery. This commentary advocates for precision medicine strategies to effectively address the challenges posed by obesity. By highlighting the potential health and economic benefits of reducing obesity, we call for a holistic approach that integrates behavioral, medical, and policy interventions. We also identify research gaps, suggesting that future studies explore endocrine connections in obesity and assess endoscopic techniques targeting the duodenum as adjunct therapies in the context of tailored care.

Keywords: Endocrine connections; Endoscopy; Lifestyle interventions; Metabolic disorders; Pharmacotherapy; Precision medicine approaches

***Corresponding authors:**
Amedeo Lonardo
(a.lonardo@libero.it)
Ralf Weiskirchen
(rweiskirchen@ukaachen.de)

Citation: Lonardo A, Weiskirchen R. Addressing the burden of obesity: Commentary to "*Obesity management: An update on the available pharmacotherapy.*" *Innov Med Omics*. 2026;3(1):73-76. doi: 10.36922/IMO025290033

Received: July 15, 2025

Revised: August 12, 2025

Accepted: September 1, 2025

Published online: September 29, 2025

1. Background

Pragmatically defined based on classes of body mass index (BMI), obesity is a systemic condition with complex pathogenic determinants and significant sexual dimorphism.[1,2] Alarmingly, obesity often acts as the precursor of a cluster of self-aggregating metabolic disorders, including type 2 diabetes mellitus (T2DM), arterial hypertension (HTN), atherogenic dyslipidemia, metabolic dysfunction-associated steatotic liver disease (MASLD; previously known as nonalcoholic fatty liver disease, NAFLD), and chronic kidney disease (CKD).[3-5] These metabolic conditions are interrelated and collectively impact cardio-metabolic health, the risk of hepato-renal failure, and certain types of cancer.[3,6-8] Over the past few decades, the burden of T2DM and obesity has rapidly increased, while the rise in HTN and dyslipidemia has slowed, and the burden of MASLD burden has remained stable.[9]

According to a recent survey, from 1990 to 2021, global deaths and disability-adjusted life years (DALYs) attributed to high BMI have more than doubled in both sexes.[10] The

age-standardized death rates remained steady for females, increased by 15.0% for males, and the age-standardized DALY rates increased by 21.7% for females and 31.2% for males.[10] In 2021, the six leading causes of high BMI-attributable DALYs were T2DM, ischemic heart disease, hypertensive heart disease, CKD, low back pain, and stroke.[10] From 1990 to 2021, the highest annual percentage changes in age-standardized DALY rates were observed in countries of low-middle socio-demographic index (SDI), with high SDI countries showing the lowest changes.[10]

To combat obesity, a wide range of therapeutic interventions are available, including lifestyle changes, pharmacological approaches, and, ultimately, endoscopic techniques and bariatric surgery.[11-14] Lifestyle changes are affordable and easily accessible, but they can be difficult to sustain over long periods of time.[11] Pharmacological treatment, although usually effective and safe for most patients, may cause financial burdens and potential side effects for a small group of individuals.[12] Endoscopic techniques are less invasive than bariatric surgery, but their availability and risk-benefit profile are still uncertain.[13] Metabolic bariatric surgery results in long-term weight loss and improvement in certain obesity-related conditions, but it necessitates lifelong lifestyle changes and comes with risks of complications and potential weight regain.[14]

2. Summary of the paper by Christaki *et al.*

With this complex background, Christaki *et al.*[15] recently published a comprehensive overview of drug therapy for obesity management in *Innovative Medicines and Omics*. The review provides a thorough analysis of childhood obesity, a growing concern exacerbated by the COVID-19 pandemic due to its long-term health and psychosocial impacts, lifestyle interventions, and supplements. Christaki *et al.*, highlight the global prevalence of obesity, its socioeconomic consequences, and the economic burden it places on healthcare systems. The authors emphasize the multifactorial nature of obesity, influenced by genetic, behavioral, and hormonal factors, which pose significant health risks such as cardiovascular diseases, diabetes, and certain cancers. They also note that while BMI is commonly used to classify obesity severity, alternative metrics such as waist-to-hip ratio and body fat percentage provide more detailed insights.

Reducing obesity can yield significant health, social, and economic benefits, including lower healthcare costs, improved quality of life, and enhanced productivity. Various strategies are available to achieve this goal, such as lifestyle changes, including dietary modifications, physical activity, behavioral therapy, stress management, and sleep optimization. While these are foundational options, they are often challenging to sustain in the long run in most cases.

According to Christaki *et al.*,[15] pharmacological treatments include food and drug administration-approved drugs such as orlistat, liraglutide, semaglutide, phentermine/topiramate, naltrexone/bupropion, metreleptin, setmelanotide, and tirzepatide. These medications act through suppression of appetite, inhibition of fat absorption, and metabolic regulation, with each individual drug having a specific profile of safety, efficacy, mechanisms, and dosages. Supplements such as L-carnitine, conjugated linoleic acid, ginseng, glucomannan, psyllium, melatonin, and cannabidiol are also being explored for their potential in weight management. The chapter on supplements adds to the accuracy of the review article, although additional clinical data are needed before utilizing these drugs in clinical practice. Bariatric surgery is recommended for more advanced cases of obesity, particularly in the presence of comorbidities and if other treatments have failed.

Ongoing research into genetic and metabolic factors promises more targeted and effective treatments. Obesity management requires a multifaceted approach that combines lifestyle changes, pharmacotherapy, and, in severe cases, surgical interventions.[15]

3. Strengths and limitations

This review provides a comprehensive overview of obesity pharmacotherapy, covering established treatments like orlistat and newer to emerging options like tirzepatide. One of its strengths is recognizing that obesity is a complex issue that requires a combination of behavioral, medical, and policy interventions. The wide range of therapies discussed allows clinicians and researchers to understand the ongoing advancements in personalized obesity management. However, a limitation is the focus on weight-centric outcomes, while future studies should consider including "visceral endpoints," such as biomarkers of hepatic health and renal function, to better understand the impact of obesity on multiple organs. This would provide more accurate evaluations of treatment effectiveness and safety. In addition, while the review effectively summarizes current interventions, there is a need for systematic comparisons of cost-effectiveness and real-world adherence, considering genetic, cultural, and socioeconomic factors.

4. Research agenda

Further investigation should focus on the mutual and bi-directional endocrine connections in obesity. These connections can range from obesity resulting from primary endocrine deficiencies, such as those seen in hypothalamic

obesity,[16] to hypogonadism resulting from primary obesity.[17] In addition, the potential role of concurrent endoscopic techniques, such as duodenal mucosa resurfacing,[18] as an add-on option to pharmacological treatment should be explored further through randomized controlled trials. Moreover, the significant role of sex differences,[19] as well as the various genetic and metabolic forms of MASLD in determining the progression from healthy to unhealthy obesity and its complications,[19,20] needs to be more thoroughly investigated. This includes examining the impact of obesity treatment on crucial visceral outcomes such as MASLD and CKD.[2,21,22]

5. Conclusion

In conclusion, this paper lays a solid foundation for expanding obesity research to include holistic endpoints and precision medicine approaches.

Acknowledgments

None.

Funding

None.

Conflict of interest

The authors declare that they have no competing interests.

Author contributions

Conceptualization: All authors
Writing–original draft: All authors
Writing–review & editing: All authors

Ethic approval and consent to participate

Not applicable.

Consent for publication

Not applicable.

Availability of data

Not applicable.

Further disclosure

The author, Amedeo Lonardo retired from Azienda Ospedaliero-Universitaria of Modena, Modena, Italy in 2023.

References

1. Chandrasekaran P, Weiskirchen R. The signaling pathways in obesity-related complications. *J Cell Commun Signal*. 2024;18(2):e12039.

   doi: 10.1002/ccs3.12039

2. Lonardo A, Weiskirchen R. Liver and obesity: A narrative review. *Explor Med*. 2025;6:1001334.

   doi: 10.37349/emed.2025.1001334

3. Lonardo A, Ballestri S, Marchesini G, Angulo P, Loria P. Nonalcoholic fatty liver disease: A precursor of the metabolic syndrome. *Dig Liver Dis*. 2015;47(3):181-190.

   doi: 10.1016/j.dld.2014.09.020

4. Ndumele CE, Rangaswami J, Chow SL, *et al*. Cardiovascular-kidney-metabolic health: A presidential advisory from the American Heart Association. *Circulation*. 2023;148(20):1606-1635.

   doi: 10.1161/CIR.0000000000001241

5. Leith D, Lin YY, Brennan P. Metabolic dysfunction-associated steatotic liver disease and type 2 diabetes: A deadly synergy. *touchREV Endocrinol*. 2024;20(2):5-9.

   doi: 10.17925/EE.2024.20.2.2

6. Kanwal F, Kramer JR, Li L, *et al*. Effect of metabolic traits on the risk of cirrhosis and hepatocellular cancer in nonalcoholic fatty liver disease. *Hepatology*. 2020;71(3):808-819.

   doi: 10.1002/hep.31014

7. Bilson J, Hydes TJ, McDonnell D, *et al*. Impact of metabolic syndrome traits on kidney disease risk in individuals with MASLD: A UK Biobank Study. *Liver Int*. 2025;45(4):e16159.

   doi: 10.1111/liv.16159

8. Standl E, Schnell O. Increased risk of cancer-An integral component of the cardio-renal-metabolic disease cluster and its management. *Cells*. 2025;14(8):564.

   doi: 10.3390/cells14080564

9. Zhang H, Zhou XD, Shapiro MD, *et al*. Global burden of metabolic diseases, 1990-2021. *Metabolism*. 2024;160:155999.

   doi: 10.1016/j.metabol.2024.155999

10. Zhou XD, Chen QF, Yang W, *et al*. Burden of disease attributable to high body mass index: An analysis of data from the Global Burden of Disease Study 2021. *EClinicalMedicine* 2024;76:102848.

    doi: 10.1016/j.eclinm.2024.102958

11. Roomy MA, Hussain K, Behbehani HM, *et al*. Therapeutic advances in obesity management: An overview of the therapeutic interventions. *Front Endocrinol* (*Lausanne*). 2024;15:1364503.

    doi: 10.3389/fendo.2024.1364503

12. Weiskirchen R, Lonardo A. How "miracle" weight-loss semaglutide promises to change medicine but can we afford the expense? *Br J Pharmacol*. 2025;182(8):1651-1670.

    doi: 10.1111/bph.70003

13. Chung Y, Paik B, Jeon D, Kim YJ. Obesity, kidney and metabolic bariatric surgery: A surgeon's narrative review. *Metab Target Organ Damage*. 2024;4:38.

doi: 10.20517/mtod.2023.51

14. Basa ML, Cha DS, Mitchell DP, Chan DL. Metabolic bariatric surgery, alcohol misuse and liver cirrhosis: A narrative review. *Metab Target Organ Damage*. 2024;4:29.

doi: 10.20517/mtod.2024.22

15. Christaki E, Protopapa C, Siamidi A, Vlachou M. Obesity management: An update on the available pharmacotherapy. *Innov Med Omics*. 2025;2(2):1-19.

doi: 10.36922/imo.8316

16. Lonardo A, Weiskirchen R. From hypothalamic obesity to metabolic dysfunction-associated steatotic liver disease: Physiology meets the clinics via metabolomics. *Metabolites*. 2024;14(8):408.

doi: 10.3390/metabo14080408

17. Di Vincenzo A, Crescenzi M, Granzotto M, Vettor R, Rossato M. Relationship between sex hormones, markers of adiposity and inflammation in male patients with severe obesity undergoing bariatric surgery. *Metab Target Organ Damage*. 2023;3:12.

doi: 10.20517/mtod.2023.13

18. Lonardo A, Singal AK. Duodenal mucosa resurfacing: The endoscopic silver bullet against metabolic disorders? *Metab Target Organ Damage*. 2025;5:13.

doi: 10.20517/mtod.2024.130

19. Lonardo A, Mantovani A, Lugari S, Targher G. Epidemiology and pathophysiology of the association between NAFLD and metabolically healthy or metabolically unhealthy obesity. *Ann Hepatol*. 2020;19(4):359-366.

doi: 10.1016/j.aohep.2020.03.001

20. Lonardo A, Targher G. Not all fat is alike in MASLD. *J Hepatol*. 2025;82(5):e271-e272.

doi: 10.1016/j.jhep.2024.12.025

21. European Association for the Study of the Liver (EASL), European Association for the Study of Diabetes (EASD), European Association for the Study of Obesity (EASO). EASL-EASD-EASO Clinical Practice Guidelines on the management of metabolic dysfunction-associated steatotic liver disease (MASLD). *J Hepatol*. 2024;81(3):492-542.

doi: 10.1016/j.jhep.2024.04.031

22. Lonardo A. Association of NAFLD/NASH, and MAFLD/MASLD with chronic kidney disease: An updated narrative review. *Metab Target Organ Damage*. 2024;4:16.

doi: 10.20517/mtod.2024.07

Our Journals

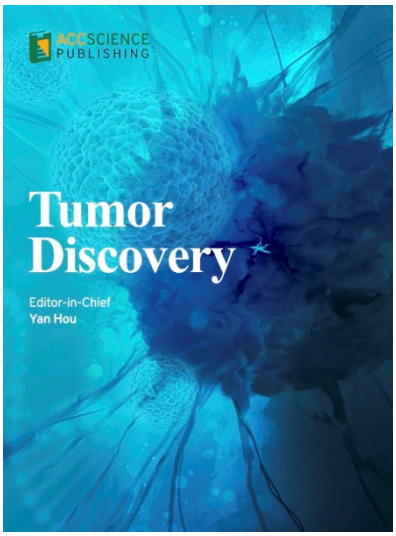

Tumor Discovery is a peer-reviewed and open-access journal that aims to present new cancer research with strong emphasis on fundamental and translational studies. *Tumor Discovery* covers topics, including but not limited to the following:

- Etiology and pathogenesis of cancer
- Mechanisms and molecular pathways underlying cancer initiation and progression
- Tumor metastasis
- Tumor evolution and heterogeneity
- Tumor microenvironment and tumor-host interactions
- Cancer genetics and genomics
- Cancer characterization using omics approaches
- Discovery and validation of cancer biomarker
- Discovery of new therapeutic targets
- New approaches of diagnostic and treatment modalities
- Statistical methods in cancer research

Artificial Intelligence in Health is an online open-access, multidisciplinary journal dedicated to publishing high-quality peer-reviewed research in all areas of Artificial Intelligence in health and medicine science. By publishing high-quality research papers, reviews, and case studies, the journal seeks to contribute to the scientific community's understanding of the potential, challenges, and impact of AI and its applications on health delivery, patient outcomes, and population health.

Artificial Intelligence in Health covers topics, including but not limited to the following: AI-based medical diagnosis and prognosis, AI clinical decision support systems, AI-driven drug discovery and development, AI-enabled healthcare operations and management, and the research and application in telemedicine, AI-assisted electronic health records and clinical informatics, AI-based research and application of wearable devices for diagnosis and treatment and social implications of AI in health.

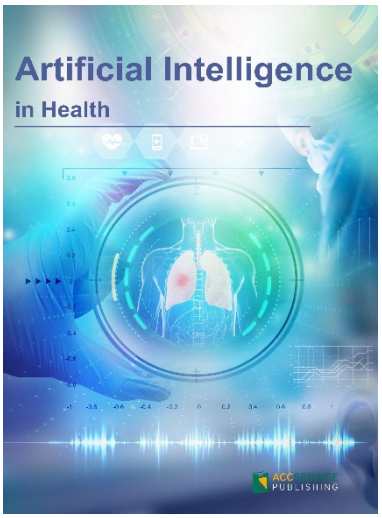

Start a new journal

Write to us via email if you are interested to start a new journal with AccScience Publishing. Please attach your CV, professional profile page and a brief pitch proposal in your email. We shall inform you of our decision whether we are interested to collaborate in starting a new journal.

Contact: info@accscience.com

https://accscience.com/journal/IMO

Access Science Without Barriers

Contact

www.accscience.com
9 Raffles Place, Republic Plaza 1 #06-00 Singapore 048619
Email: editorial@accscience.com
Phone: +65 8182 1586